

Structure-Guided Design of Novel Therapeutics Targeting

Translesion DNA Synthesis and Lipid A Biosynthesis

by

Javaria Najeeb

Department of Biochemistry
Duke University

Approved:

Pei Zhou, Supervisor

Maria Schumacher

Kenneth Kreuzer

Raphael Valdivia

Ronald Venters

Dissertation submitted in partial fulfillment of
the requirements for the degree of Doctor
of Philosophy in the Department of
Biochemistry in the Graduate School
of Duke University

2019

ABSTRACT

Structure-Guided Discovery of Novel Therapeutics Targeting

Translesion DNA Synthesis and Lipid A Biosynthesis

by

Javaria Najeeb

Department of Biochemistry
Duke University

Approved:

Pei Zhou, Supervisor

Maria Schumacher

Kenneth Kreuzer

Raphael Valdivia

Ronald Venters

An abstract of a dissertation submitted in partial
fulfillment of the requirements for the degree of Doctor
of Philosophy in the Department of
Biochemistry in the Graduate School
of Duke University

2019

Copyright by
Javaria Najeeb
2019

Abstract

Cancer is one of the most devastating diseases in modern society, with over 1.6 million new cancer cases occurring in the US alone each year. DNA-damaging agents are often the first line of defense against rapidly dividing cancer cells. However, cancer cells can become resistant to chemotherapy by up-regulating an error-prone DNA-repair process called translesion DNA synthesis (TLS). The Rev1 polymerase orchestrates this pathway by recruiting one of three inserter polymerases and the extender polymerase (Pol ζ) to bypass the lesion. Here we report the discovery and characterization of an inhibitor of the protein-protein interaction between Rev1 and Rev7, a subunit of Pol ζ , using biochemical and biophysical techniques. Our X-ray crystallographic structural analysis of the Rev1 and the inhibitor (JH-RE-06) complex reveals that the inhibitor blocks Rev7 binding by inducing Rev1 dimerization. Such an unexpected observation is confirmed by an *in vitro* crosslinking assay. *In vitro* cell-killing assays show that JH-RE-06 enhances sensitivity of a variety of cancer cell lines to a wide range of chemotherapeutic agents; furthermore, co-administration of JH-RE-06 with cisplatin significantly suppresses melanoma growth in mice and prolongs the survival time of tumor bearing mice, highlighting the therapeutic potential of translesion synthesis inhibitors as a novel class of cancer adjuvant therapeutics to enhance the outcome of chemotherapy currently available to cancer patients.

Due to their compromised immune systems, cancer patients are particularly susceptible to opportunistic bacterial infections, many of which are becoming rapidly resistant to current antibiotic therapies. We describe the combined use of X-ray crystallography and NMR spectroscopy to delineate a cryptic inhibitor envelope for optimization of a small molecule inhibitor of LpxC, an enzyme essential to the survival of Gram-negative bacteria. The resulting inhibitor shows vast improvement over its parent compound over a wide range of bacterial orthologs.

In summary, we demonstrate successful structural characterization and structure-guided design and optimization of lead compounds in two different systems. These studies have profound implications for drug discovery and lead optimization in other disease-relevant systems as well.

Dedication

This work is dedicated to my parents: Zakia Najeeb, and Najeeb-ur-Rab Ansari.

Contents

Abstract	iv
List of Tables	x
List of Figures	xi
List of Abbreviations	xiii
Acknowledgements	xvi
Chapter 1. Introduction.....	1
Chapter 2. DNA-damaging Agents as Chemotherapeutics and Mechanisms of Resistance	22
2.1 Translesion DNA Synthesis as an Error-prone DNA Repair Process	23
2.2 Rev1- POL ζ Mediated TLS as a Mechanism of Resistance to Chemotherapy	26
2.3 Important Protein-protein Interactions in the Rev1- POL ζ - POL κ Translesionsome Complex	27
Chapter 3. Discovery and Characterization of An Inhibitor of the Rev1-Rev7 Interaction	30
3.1 Small Molecule Inhibitor Identification and Validation	30
3.2 Molecular Basis of Inhibition of Rev1 by JH-RE-06	34
3.3 In Vitro Validation of Rev1 Dimer Induction in the Presence of JH-RE-06.	41
3.4 JH-RE-06 Enhances Tumor Sensitivity to Cisplatin and other DNA-damaging Agents in Tumor Cells and Mouse Xenograft Model.	42
3.4 Discussion.....	48
3.5 Methods	51
3.5.1 Genetic Cloning and Protein Purification.....	51

3.5.2 High-throughput ELISA Screen	51
3.5.3 Chemical Synthesis of JH-RE-06.....	53
3.5.4 AlphaScreen Assay for Dose-Dependent Inhibition of the Rev1-Rev7 Interaction.....	54
3.5.5 X-ray Crystallography	54
3.5.6 <i>In Vitro</i> DSS Cross-linking Experiment	56
3.5.7 Cell Culturing	57
3.5.8 Clonogenic Survival Assay	57
3.5.9 Cell Viability Assay	58
3.5.10 HPRT Mutagenesis Assay	59
3.5.11 Mouse Xenograft Tumor Model.....	60
Chapter 4. Risk of multidrug-resistant Bacterial Infections in Cancer Patients.....	61
4.1 The Lipid A Biosynthesis Pathway and LpxC in Gram-negative Bacteria	62
4.2 Targeting LpxC for Antibiotic Development	66
Chapter 5. Optimization and Characterization of an LpxC Inhibitor using Static and Dynamic Information	70
5.1 The χ_1 Angle of the Threonyl Head Group of CHIR-090 and LPC-011 Favors the Trans Conformation but can Sample other Conformations	70
5.2 Triple Substitution at C β Position of Threonyl Side-chain Yields Enhanced Inhibitors.....	76
5.3 Expansion of the Inhibitor Envelope is a Successful Strategy for Improving LpxC Inhibitor in the γ Position.....	77
5.4 LPC-058 Exhibits Enhanced Inhibition and Antibiotic Activity in Comparison to LPC-011 and CHIR-090.....	83

5.5 Discussion.....	84
5.6 Methods	88
5.6.1 Crystallographic Studies	88
5.6.2 NMR Measurements	92
5.6.3 Enzymatic Assays.....	93
5.6.4 Minimum Inhibitory Concentration (MIC) Measurements	95
Chapter 6. Conclusions	97
References	103
Biography.....	118

List of Tables

Table 1: X-ray Data Collection and Refinement Statistics for the Rev1-JH-RE-06 Complex Structure.	36
Table 2: Chemical Structures of LpxC Inhibitors.....	67
Table 3: Characteristic 3J coupling Values for Threonine Sidechain.....	72
Table 4: C δ 1 Chemical Shift, Depending on χ 2 Rotameric Angle.....	80
Table 5: Inhibition Constants for LpxC Inhibitors.....	86
Table 6: X-ray data collection and refinement statistics for LpxC inhibitors	91

List of Figures

Figure 1: DNA-Damaging Therapeutic Agents.....	23
Figure 2: Translesion DNA synthesis.....	25
Figure 3: The Translesionsome Complex (PDBID 4FJO).....	28
Figure 4: The Hydrophobic Pocket at the Rev1/Rev7Interface.....	29
Figure 5: High-throughput ELISA Assay	31
Figure 6: Structure of JH-RE-06.....	32
Figure 7: Alpha Screen Assay.....	33
Figure 8: Diffraction Quality Inhibitor-bound Protein Crystals were obtained by Sitting-drop Vapor Diffusion	35
Figure 9: The Rev1-JH-RE-06 Complex.....	37
Figure 10: Monomer 1 C-terminal Tail Pushed Out.....	38
Figure 11: JH-RE-06 Fits Snugly in Pocket.....	39
Figure 12: Rev1-JH-RE-06 Interactions.....	39
Figure 13: Rev1 Dimerization Blocks Rev7 Interaction.	40
Figure 14: JH-RE-06 Enhances Rev1-CTD Dimerization In Vitro.	41
Figure 15: JH-RE-06 Enhances Cisplatin Chemosensitivity in Different Cancer Cell Lines.	44
Figure 16: JH-RE-06 Suppresses Cisplatin Induced Mutagenesis in HT1080 Cells.....	45
Figure 17: JH-RE-06 Sensitizes <i>Kras^{mut}P53^{-/-}</i> Cells to Various DNA-Damaging Agents. ...	46
Figure 18: JH-RE-06 Enhances Cisplatin Sensitivity in Murine Xenograft Tumor Model.	47
Figure 19: The Rev1-Rev7 Interface.....	50

Figure 20: The Structure of Lipopolysaccharide.....	64
Figure 21: Kdo ₂ Lipid A Biosynthesis.....	64
Figure 22: AaLpxC in Complex with Substrate Analog Inhibitor.....	65
Figure 23: LpxC Inhibitors Often Feature a Hydroxamate Head Group	68
Figure 24: Threonyl Head Group of LPC-011 Features <i>Trans</i> χ^1 Angle	71
Figure 25: LPC-011 and CHIR-090 Access Minor Conformations in Solution, Defining an Inhibitor Envelope	74
Figure 26: LPC-40 in Complex with PaLpxC	75
Figure 27: LPC-037 and LPC-040 are Better Inhibitors than LPC-011	77
Figure 28: Optimization of LPC-023 with Help of Extended Inhibitor Envelope.....	81
Figure 29: LPC-058 Forms Optimal Interactions with LpxC Active Site Residues.....	82
Figure 30: LPC-058 is a Better Antibiotic at a Broad Spectrum Level than CHIR-090 and LPC-011	87
Figure 31: LPC-058 is a Potent Inhibitor Compared to Parent Compound	88

List of Abbreviations

3D – Three-dimensional

4-NQO - 4-Nitroquinoline 1-oxide

6-TG – 6-thioguanine

AaLpxC - *Aquifex aeolicus* LpxC

ATP – adenosine triphosphate

BPDE - Benzo[a]pyrene-7,8-dihydrodiol-9,10-epoxide

BSA – Bovine serum albumin

CCC – Clear cell carcinoma

Cryo EM – Cryogenic electron microscopy

CTD – C-terminal domain

CTX – Cyclophosphamide

DMSO - dimethylsulfoxide

DNA – Deoxyribonucleic acid

DSS - Disuccinimidyl suberate

DTT - dithiothreitol

E.coli – *Escherichia coli*

EcLpxC - *Escherichia coli* LpxC

ELISA – Enzyme linked immunosorbent assay

HIV – Human immunodeficiency virus

HORMA – Hop1, Rev7, Mad2

HPRT - hypoxanthine phosphorybosyl transferase

HRP - Horseradish peroxidase

LC-MS – liquid chromatography-mass spectrometry

LPS – Lipopolysaccharide

MALDI-TOF - matrix-assisted laser desorption/ionization–time of flight mass spectrometry

MMS - Methylmethane sulfonate

MPD - 2-methyl-2,4-pentanediol

NCCLS - National Committee for Clinical Laboratory Standards

NMR - Nuclear magnetic resonance

NMNG - N-methyl-N-nitro-N-nitrosoguanidine

ORF – open reading frame

PaLpxC – *Pseudomonas aeruginosa* LpxC

PBS – Phosphate-buffered saline

PCNA – Proliferating cell nuclear antigen

PDB - Protein Data Bank

POL ι – DNA Polymerase iota

POL η - DNA Polymerase eta

POL κ - DNA Polymerase kappa

POL ζ - DNA Polymerase zeta

PPI - protein-protein interface

RIR – Rev1-interacting region

S. cerevisiae - *Saccharomyces cerevisiae*

TAP – tandem affinity purification

TCEP – Tris (2-carboxyethyl) phosphine

TEV – Tobacco etch virus

TLS – Translesion bypass synthesis

TMB – 3, 3', 5, 5' tetramethylbenzidine

UDP - Uridine diphosphate- N-acetylglucosamine

Acknowledgements

I would like to thank my advisor, Pei Zhou, for his steady guidance throughout graduate school, his patience with me and his accessibility in general. He has honed me as a scientist and given me the tools to think independently and critically.

I would like to thank my lab mates, current and former, for making me feel at home all these years and for making the lab such a comfortable and happy place to be in. This includes CJ, Su, Jess, Ali, Hayley, Josh, Jinshi, Qinglin, Shivesh, Jennifer, Jae, Ben and Chin.

I would like to thank my committee members; Maria Schumacher, Kenneth Kreuzer, Raphael Valdivia and Ronald Venters, for their valuable feedback and support over the years.

Finally, I would like to thank my family and friends for their support over the years and for helping me follow my passions.

Chapter 1. Introduction

With the development of X-ray crystallography, nuclear magnetic resonance (NMR) spectroscopy, Cryo- electron microscopy (EM), and computational modeling leading to an exponential increase in available 3D structures of protein targets, structure-guided drug design has become a vital part of lead compound discovery, generation and optimization.

Despite this, there is no one size fits all strategy. Each relevant biological pathway has its own characteristics, intricacies, and varying degrees of interconnectedness with other pathways. It is essential to understand the system at a molecular level, including protein-protein interactions that regulate it, in order to develop effective inhibitors.

The first step to structure-guided drug design is target identification. One of the ways in which this can be done is with genome analysis. In 1985, when rational drug design was still in its infancy, Mellor et al.¹ identified a yeast transposon that produces a fusion protein by fusing two out-of-phase open reading frames (ORFs) via frame-shifting. The authors noted that this was remarkably similar to a process used by retroviruses. Toh et al.² used this information to identify the gene for the retroviral protease, bringing it on the radar of several groups, who almost simultaneously solved the crystal structures of the homologous Rous Sarcoma Virus and Human Immuno-

deficiency Virus (HIV) proteases in 1989.³⁻⁶ Analysis of the retroviral and HIV genome was thus critical to the discovery of a protease that was essential to AIDS antiviral development.⁷ Since then, computational genomic techniques have become much more powerful and many whole genome sequences are readily available, and homologs both close and distant are relatively easily identifiable.⁸ However, this approach is now increasingly considered “reductionist” as target proteins rarely act alone, so many target identification trials now focus on a more “holistic approach”. Since many powerful small molecule inhibitors were discovered as a result of chemical genetics, “phenotype-based drug discovery,” which is the retrospective identification of the molecular targets responsible for phenotypic responses, is now considered the more powerful approach to target discovery. This “target deconvolution” strategy involves the investigation of signaling pathways in a systems-based manner for elucidating biological mechanisms of disease and, it is argued, is more conducive to the development of structure–activity relationship studies by allowing optimization of target-specific assays.⁹ Examples of this approach include proteomics analysis, yeast-two hybrid, phage display and tandem affinity purification (TAP).

Proteomics analysis is a powerful and emerging tool for target identification. For example, the global protein composition of a healthy cell can be compared to that of a diseased one to identify the molecular basis of disease. This has been especially useful in

identifying protein networks involved in cancer progression for novel therapeutic target discovery.¹⁰

As stable protein complexes are often vital for cellular function, finding important protein-protein interaction networks is a useful tool in target discovery. High-throughput experimental techniques are used to map protein-protein interaction networks, most notably the yeast two-hybrid system, created in 1989 by Fields and Song.¹¹ Another method to map important interactions is TAP followed by mass spectrometry. Krogan and colleagues used TAP, followed by matrix-assisted laser desorption/ionization–time of flight, and liquid chromatography-mass spectroscopy (MALDI-TOF, LC-MS), and machine learning, to undertake the massive task of analyzing 4,562 different tagged proteins of *Saccharomyces cerevisiae* (*S. cerevisiae*), to identify protein-protein interactions with high confidence, leading to a core dataset of 7,123 protein–protein interactions involving 2,708 proteins.¹² Phage display can also be used for high-throughput screening of protein interactions. It involves the insertion of gene fragments into capsid-encoding genes. The resulting fusion gene encodes a capsid protein displayed on the phage surface and exposed to a library of proteins or peptides. This strategy has also shown success in identifying specific targets of small molecules, as in the discovery of a calmodulin antagonist that was shown to inhibit cell cycle progression in colon cancer cells.¹³

Finally, there are emerging network-alignment algorithms that employ global and local network alignment methods to compare homologous protein networks that could serve as powerful tools in identification of disease-related sub networks for target discovery in the future.¹⁴

Once a target is identified, and protein-protein interactions validated with *in vitro* direct binding studies, it is essential to obtain structural information to further the structure-based drug design campaign. Most structures are determined by x-ray crystallography, and, to a lesser degree, by NMR spectroscopy. Of the almost 150,000 structures available on the protein data bank, more than 130,000 were determined by crystallography, with about a tenth (~13000) determined by nuclear magnetic resonance (NMR) spectroscopy and about a fourth of that by EM (~3000 structures), with the rest solved with a combination of different structural biology techniques (rscb.org).¹⁵ The first success stories utilizing structural information for drug design started appearing in the early 90's, with a good example being the use of the HIV protease crystal structure in the development of a "potent and orally bioavailable" retroviral protease inhibitor.¹⁶

At the early stage, even low-resolution structures (worse than 3-4 Å) can provide valuable information, such as overall architecture and existence of potential binding pockets and their composition, and critical protein-protein interactions. These low-resolution structures can be used for "virtual" screening using *in silico* docking and

design, which can be used for identification of desired epitopes or pharmacophores and important interactions-which can then be incorporated with binding, activity and pharmacological assays to aid in lead compound discovery.¹⁷ Virtual docking can also be done for fragment-based screening, in which simple and small fragments are used to identify a scaffold that can be used as a starting point for lead compound development. Of course, this must be validated with experimentally derived X-ray or NMR structures. An example of a successful campaign led by this approach is the identification of a methylpyridine-derived inhibitor of bromodomains, which are involved in many malignant cancers.¹⁸ In the absence of a structure, homology modeling can be used to determine important structural information. Powerful search tools allow the detection of homologs on the basis of both sequence and structure. Malhotra and colleagues demonstrated the usefulness of this approach by modeling an adenosine triphosphate (ATP)-dependent mycobacterium enzyme purC from a homologous *S. cerevisiae* structure and validated the modeled ATP-binding pocket by superposition with the known ATP-bound crystal structure.¹⁹ Lower resolution structures can be used in molecular dynamics simulations, computational structure minimization, calculations of probable loop or rotamer configurations, or in identification of the position of chemically relevant waters.²⁰⁻²¹ Cryo-EM has recently emerged as an accessory tool to crystallography and NMR in structure-guided drug design. Its biggest limitation is

resolution, although it is improving every day. In its current state, EM can be used to get initial low-resolution structures, especially for large macromolecular complexes and potentially provide information on different conformations experienced by the complex, even within the same sample. This can give valuable insight into protein function.

However, this information is not enough to expose atom-atom interactions, changes in atom positions, or main chain or side chain motions, which occur on as small a scale as 0.5-1.5 Å. This is essential to structure-based drug design.²² For example, Tordai and colleagues noted that the pioneering structures of cystic fibrosis transmembrane conductance regulator, though impressive, are not enough at below 8 Å to understand the effects of mutations, prohibiting studies for lead compound development. However, they showed that molecular dynamics simulations can prove to be a useful tool in analyzing these low-resolution structures which can potentially aid in structure-guided drug design in the future.²³ The combination of low-resolution experimental structures and computational modeling can become a powerful tool for rational drug design, especially when independent validation techniques are available.

Armed with initial structural information (by experimental or homology modeling techniques), high-throughput screening can commence using compound libraries with specific chemical properties, or even diverse small molecule compound libraries aimed at an observed binding pocket. An increasingly popular approach is

fragment-based screening, where small molecules that are an average of half the size of traditional libraries can be used for screening, and initial hit scaffold can be modified and expanded to increase affinity with crystallography or NMR.²⁴ Primary high throughput screening can use high-density arrays of microreaction wells and employ various techniques such as fluorescence resonance energy transfer or homogenous time resolved fluorescence. NMR-based screening techniques such as measuring of chemical shift perturbation or saturation transfer difference NMR can be extremely useful as they can detect even weak interactions (in the mM range), which is helpful in the case of the small scaffolds in fragment-based screening, with the added advantage of providing information on the location of binding, as well as epitope mapping.²⁵

An initial hit must be validated with secondary screening using adopted biological or biochemical tests. For example, an assay testing the abrogation of a known protein-protein interaction vital for function can be used in this regard. Some of the most reliable and sensitive assays are multi-protein assays or functional cell-based assays, which measure the change in protein function in response to a potential inhibitor.²⁶ An example is the discovery of a class of benzimidazolinone compounds that were found to open small conductance potassium ion channels, which are associated with a range of diseases such as cancer and hypertension, in whole-cell patch-clamp ion current assays.²⁷

With a compound identified and validated, high resolution structural information is essential for the elucidation of molecular details of inhibition, such as contacts responsible for binding, and conformational changes in the protein such as sidechain or main chain movement. This is to understand the basis of inhibition as well as to optimize receptor-ligand interactions with chemical modification to improve affinity for the target. This is an iterative process that involves several rounds of inhibitor modification and structure-activity relationship studies. High-quality inhibitor-bound crystal structures at each step are useful in validating the modifications made to an inhibitor. NMR spectroscopy is particularly useful at this step of the process, termed “lead compound optimization,” as it can be used to assess the following parameters: ligand quality (such as solubility and integrity using 1D spectra), protein quality in the presence of ligand (aggregation, degradation, etc.), and binding ability (both protein-observed through experiments measuring chemical shift changes with HSQC experiments, and ligand-observed-such as changes in rotational tumbling measured by relaxation experiments such as R_2 and NOE).²⁸

The overall aim is to improve “drug-like” qualities, such as strong inhibition, high stability and solubility, specificity (to minimize off-target effects and toxicity), and good bioavailability. The drug must be validated *in vitro* in cellular models and *in vivo* in animal models to exhibit its ability to affect disease outcomes. There are many examples,

and the following are two instances of successful campaigns. The first case involves the development of an inhibitor of the BCL-2/BCL-xL interaction, which is frequently upregulated in tumor cells. Fragment based screening was used to identify simple chemical scaffolds that blocked BCL-2 interaction with BCL-xL and x-ray crystallography used to validate the mode of binding. The inhibitor was improved by expanding the scaffold with linkers for higher affinity to the target and better solubility and stability in solution. The mode of binding was validated again by crystallography. The inhibitor was tested functionally in cellular models to assess its ability to induce apoptosis. It was tested *in vivo* in an animal model to assess its anti-tumor ability. Several rounds of optimizing for affinity, solubility, stability, selectivity and anti-tumor activity, using crystallography, chemical modification, *in vitro* and *in vivo* validation resulted in a potent, orally bioavailable anti-cancer drug, ABT-263, which is currently in clinical trials.²⁹⁻³⁰

The second example tells the story of the discovery and characterization of an inhibitor of the BCR-ABL1 fusion oncoprotein, known to be a factor in chronic myeloid leukemia. Wylie and colleagues performed fragment-based NMR screening, and optimized hits using virtual docking, crystallography and NMR analysis. Using previous knowledge that auto-inhibited kinases have a “bent” conformation, they developed a conformational NMR assay to further narrow down the list of candidates.

The bent conformation was cross-validated with crystallography. Several rounds of optimization were carried out to improve specificity, affinity and *in vivo* potency. The resulting compound (ABL001) showed tight binding in NMR and other biophysical assays, lack of activity against all other kinases tested (high specificity), anti-proliferative activity in tumor cell lines, and *in vivo* efficacy in a mouse xenograft model. The inhibitor was also tested against tumors resistant to an older drug targeting the same kinase and showed a 100-fold slower increase in resistance and also a completely independent resistance profile; thus it was shown to be a truly novel inhibitor. It is currently in clinical trials in lymphomas, leukemia and myeloma.³¹⁻³²

The two major challenges facing structure-based drug discovery are two factors that are essential to the obtaining of a bigger picture and better understanding of protein function, i.e. protein movement, and protein interaction with other protein.

It is challenging to visualize or account for movement/dynamics using current structural methods for drug development. Information on protein flexibility can be vital to understanding its function, or understanding how drugs exert their biological effects. This information can be crucial for developing increased affinity between drug and target. One way to address this is to “freeze” the target in certain conformations to obtain snapshots of it in different stages of it performing its function, such as when bound to substrate or product. For example, several crystal structures of the ATP-

binding cassette transporters suggested a mechanism of substrate export (important to drug extrusion in drug resistant bacteria and cancer cells). The ATP-bound structure of a bacterial drug exporter (*Staphylococcus aureus* Sav1866) had an “outward facing conformation,” whereas the nucleotide-free structure of a different transporter (*Escherichia coli* MalK) suggested an “inward-facing conformation,” hinting at a propagation of conformational changes driven by ATP.³³ A follow-up study used crystallographic snapshots of a transporter, P-glycoprotein, in complex with several rationally-designed ligands to investigate how it can recognize diverse substrates and couple their binding to ATP hydrolysis and subsequent helical movement to transport the substrates across. The study acted as a structure-activity relationship analysis, showing how altering size and hydrophobicity in functional groups can impact the interaction with this clinically important exporter, by, for example, binding to the transporter but inhibiting propagation of conformational change to the outer side, which has implications for future drug design.³⁴ However, this type of information with “indicated movement”, while important, does not show true movement and certain conformations can be “enriched” in these frozen structures. Additionally, these structures cannot be used in the visualizing of flexible regions of protein, which are often important to function.³⁵

One might intuit that NMR studies would be widely used to address these concerns in drug development campaigns, as NMR has the ability to reveal atomic motions on a wide range of time scales, and has clearly shown many times that clinically relevant proteins require internal movements for function and drug binding.³⁶⁻³⁸ Despite this, NMR “flexibility-function” studies are rare in rational drug design. One reason is the “lower throughput” quality of NMR, and the limitation of meaningful data extracted from larger proteins. Many therapeutic targets have large molecular weights and exhibit crowded and broad signals, leading to a difficulty in signal interpretation and long acquisition times. Additionally, protein dynamic metrics like exchange rates and correlation times do not translate easily to pharmaceutical optimization, whereas fixed structural coordinates can be used to rationalize addition or removal of functional groups.³⁹ Of course, there are examples of innovative use of NMR to extract dynamic information relevant to drug design. For example, Mauldin et al. used backbone ¹⁵N dispersion experiments for dihydrofolate reductase bound to cofactor nicotinamide adenine dinucleotide phosphate and observed collective motion of loops surrounding the cofactor and substrate binding sites, corresponding to exchange between known closed and open states, representing communication between the cofactor and substrate pockets. When two known drugs that bind to the substrate site were added, distant conformational exchange with the cofactor site was eliminated. Additionally, fast

exchange along the backbone was affected between the substrate binding pockets and residues important for catalysis. Further, there was localized exchange detected in the substrate pocket but at a much slower pace. Thus, the experiments showed a “dynamic dysfunction” and a breakdown of communication within the protein network as a mechanism of inhibition. Such studies highlight the importance of dynamic studies to reveal novel inhibition modes and to expand on traditional strategies of drug design.⁴⁰ It is important to note, additionally, that structure-based drug design is the iterative modification of inhibitors, but very few studies have focused on the dynamics of the ligand. A study used natural abundance ^{13}C relaxation NMR to characterize the conformational dynamics of a ligand in its free and receptor bound states, suggesting new possibilities for the use of ligand flexibility profiles to analyze the effect of dynamics on potency or pharmacokinetic properties. However, this strategy has not been successfully demonstrated for tight-binding inhibitors or the identification of minor conformations.⁴¹ Thus, the incorporation of both receptor and ligand dynamics is an outstanding problem in rational drug design but one that has the potential to add significantly to inhibitor optimization.

A second major challenge in rational drug design is that of targeting protein-protein interactions. Proteins do not work alone, and their interactions with other proteins are essential to their function, making protein-protein interfaces (PPI) attractive

targets. For a time, PPI's were considered undruggable, due to the large buried surface area involved. However, a critical development in understanding PPIs was the realization that interactions driving affinity between proteins are not evenly distributed across the entire surface. Rather, certain residues or areas, within the PPI, that are generally evolutionarily conserved, provide the majority of the energy of binding. These residues or clusters are called "hot spots" and can be experimentally determined by alanine scanning, a sequential mutational analysis, also known as hot spot analysis.⁴²⁻⁴³ Where experimental analysis is infeasible due to the time-consuming nature of alanine scanning and difficulty in purifying each protein component, *in silico* hotspot analysis approaches may be used. These techniques are becoming increasingly powerful at predicting hot spots as we gather more and more information about known PPIs. Predicted hot spots can be verified with orthogonal validation methods,⁴⁴ such as with mutational analysis done with the help of co-immunoprecipitation.

Knowledge of hot spot regions made the targeting of PPI more tractable but still challenging. Some of the challenges are briefly described here. When the PPI is that of two globular proteins, the task of targeting them with a small molecule is still a formidable one. The interaction surface appears generally flatter on average and potentially less amenable to the binding of a small molecule.⁴⁵ There are very few examples of successful targeting of globular-globular interaction. A clever approach was

used by researchers at Sunesis pharmaceuticals to target interleukin-2 (IL-2), a cytokine important for immune response. IL-2 interacts with its associated cell-surface receptors, which are expressed by activated T cells, and together trigger an immune response. IL-2 residues at the perimeter of its hot spot were mutated to cysteines and screened against a library of disulfide-containing fragments. This “tethering” fragment-based screening strategy led to the identification of compounds containing aromatic carboxylic acids, which were shown by crystallography to bind at the end of a conserved hydrophobic channel. *In silico* modeling with the help of the crystal structure was used to optimize the fragments and obtain a powerful inhibitor (SP4206), with an IC_{50} of 60 nM for the inhibition of the IL-2-IL-2R α (associated receptor) interaction. These studies also showed that while no binding pocket is visible in the absence of inhibitor, “cryptic” binding pockets can appear on flat surfaces upon inhibitor binding.⁴⁶⁻⁴⁷

By contrast, PPIs involving a globular protein and a peptide (peptidic region on another protein) have been proposed to be more druggable, as the interface is “simpler” and usually includes an easily identifiable “groove” to target with small molecules.⁴⁸ An example is the interaction of caspase 9 (apoptotic protein) with XIAP (apoptosis inhibitor upregulated in tumor cells) via a tetrapeptide motif. Using the knowledge that a natural inhibitor of this interaction exists (DIABLO), small molecule inhibitors were derived based on the natural tetrapeptide inhibitory motif, which exhibited low

nanomolar affinity.⁴⁹ Other inhibitors have been developed using fragment based methods with lower affinity but better bioavailability.⁵⁰ The problem with targeting an interaction like that where binding is based on an epitope without other interactions improving affinity to a specific protein is the lack of selectivity- indeed, while some of these inhibitors are in clinical trials, most are not selective for XIAP and recent studies have shown toxic side effects of these inhibitors such as activation of tumor-necrosis factor.⁵¹ Achieving better selectivity is more feasible when the peptide partner binds via multiple epitopes, as is the case with Bcl-2 and Bcl-xL. As outlined earlier, researchers used a fragment-based approach to identify suitable chemotypes/epitopes and used linkers to combine these epitopes, followed by extensive optimization to obtain a selective, orally bioavailable inhibitor ABT-263, which currently in clinical trials.²⁹⁻³⁰ The major drawback of multi-valent inhibitors with linkers is the difficulty in making them bioavailable due to their larger size.

Most PPI inhibitor design is aimed at disrupting the interactions between proteins. This is challenging for the aforementioned reasons: difficulty in targeting pairs of globular proteins, achieving selectivity for a specific PPI to minimize side-effects, and designing inhibitors that are small enough to be bioavailable and potent in cells. Additionally, obligate PPIs are exceptionally difficult to target because obligate/tight

interactions are dominated by hydrophobic interactions, similar to the core of globular proteins. The penalty of exposing those residues is high.⁵²

A promising future approach may be to stabilize PPIs, rather than to disrupt them. The following arguments endeavor to make a case for such an approach. A compelling argument in favor of PPI stabilization is the existence of numerous natural compounds that have been in use for years, which, through recent advances, have been revealed to act by stabilizing specific PPIs.⁵³ An example of this is Swinholide A, a compound that inhibits actin polymerization. Since actin remodeling is associated with malignant phenotypes, it has anti-cancer properties. It has a macrocyclic structure with a 2-fold axis of symmetry, and is found in marine sponges. It disrupts actin polymerization by freezing G-actin in a homo-dimer complex. The protomers have no contacts with each other, with each half of the inhibitor making hydrophobic contacts with both protomers.⁵⁴⁻⁵⁶

There are also synthetic inhibitors that were retrospectively found to act by stabilizing certain PPIs, either by stabilizing interfaces that prevent the binding of a different binding partner (e.g. RO2443, which prevents p53 binding to anti-apoptotic MDM2 and MDMX by promoting dimerization),⁵⁷ or stabilizing inactive conformations of a protein (e.g. ICRF-187, which locks topoisomerase II in its inactive or “closed clamp” dimer conformation to reduce oxidative stress induced by chemotherapeutics).⁵⁸

Despite the promising potential of PPI stabilizers, there are scarce examples of their *ab initio* discovery. This is because the idea of targeting PPI for stabilization and not disruption is still very new and not a generally considered strategy during rational drug design. Additionally, most compound libraries consist of traditional “drug-like chemicals” whereas the bulk of PPI stabilizers have scaffolds derived from “natural compounds” with very different shapes and chemical properties.⁵³ An example of successful intentional design of a PPI stabilizer is Compound 24 (Bosch pharmaceuticals). Researchers did *in silico* screening of possible molecules that could stabilize the interaction between an aldolase and a transmembrane adhesion in *Plasmodium falciparum*, which would prevent pathogen gliding on the host membrane and inhibit cellular invasion. Candidates were tested with biochemical assays and *in vitro* parasite assays. Compound 24 reduced liver cell invasion by 95% and a crystal structure confirmed the mode of inhibition as being PPI stabilization, although a very high concentration of inhibitor was used (500µM).⁵⁹ As very little is known about PPI stabilizers, and current chemical libraries belong to a specific type of chemical space, it is currently challenging to target PPIs for stabilization; however, focusing on motifs that are known for their dimerization properties (e.g. 14-3-3 proteins, that are known for their homo- and hetero- dimerization properties, and, additionally, are known to be stabilized by fusicoccin A, a fungal product)⁶⁰ and screening with *in silico* docking to

expand the chemical space, as well as expanding current chemical libraries by including natural compound mimetics such as symmetric macrocyclic compounds, could help increase the likelihood of discovery and design of PPI stabilizers.

In this thesis, I address two of the challenges described above that are faced during structure-guided drug design: use of ligand dynamics for finer iterative modification of ligands, and the targeting of a featureless PPI of two globular partners. I describe my research on two pathways relevant to the treatment of cancer patients: the translesion DNA synthesis pathway in human cells, and the Lipid A biosynthesis pathway in bacterial cells.

The translesion DNA synthesis pathway is of interest, particularly with respect to tumors that are resistant to chemotherapy, as genetic ablation of key proteins in the translesion DNA synthesis pathway sensitizes cancer cells to DNA-damaging chemotherapeutics. Translesion DNA synthesis is dependent on the interaction between the Rev1 polymerase and Rev7, an accessory subunit of polymerase ζ . We report the discovery of a small molecule inhibitor of this interaction (JH-RE-06), and the crystal structure of JH-RE-06 in complex with Rev1. We show that the compound acts by forcing Rev1 to dimerize, converting the ostensibly shallow binding pocket at the Rev1-Rev7 interface into a deep cavity that engulfs the small molecule. We also show that JH-RE-06 enhances the chemosensitivity of various tumor cell lines to different types of

chemotherapeutic agents, thus validating it as a promising adjuvant to traditional chemotherapy.

Another challenge to successful treatment of cancer patients is the opportunistic bacterial infection, as patients frequently become immunocompromised due to chemotherapy. Infections caused by Gram-negative bacteria pose the most serious health threat as these bacteria are becoming increasingly multi-drug resistant, posing life-threatening risks to cancer patients. There is an urgent need for novel antibiotics to overcome existing resistance mechanisms. The Lipid A biosynthetic pathway is of special interest, as it is essential to the survival of Gram-negative bacteria. The enzyme that catalyzes the first committed step in this pathway is the metal-dependent deacetylase LpxC. It is an excellent target for antibiotic development as it is essential for bacterial viability, has a unique structure, and has no similarity with any other metalloenzymes, including human deacetylases. While many high-resolution crystal structures of inhibitors in complex with LpxC exist, and have been used in lead compound optimization, these static structures overlooked the conformational flexibility of both the inhibitor and the enzyme. In this work we combine the technique of X-ray crystallography with solution NMR spectroscopy to reveal minor conformations and utilize it to delineate a solvent-accessible inhibitor envelope. Using this strategy, we

have developed an inhibitor that exhibits significant improvement in binding affinity and antibiotic activity over its parent compound.

Taken together, my thesis research has revealed two strikingly different strategies for the development of novel therapeutics against challenging targets. In the first case, we show that seemingly intractable protein-protein binding interfaces (such as a the shallow binding pocket at the Rev1-Rev7 interface) can be viable targets for lead compound development through compound-induced dimerization, strengthening the case for PPI stabilization as a mechanism of inhibition. In the second case, we show that by combining static and dynamic information obtained using X-ray crystallography and solution NMR spectroscopy, we can gain insight on the dynamics of ligand binding, and delineate a hidden, dynamically accessible envelop to guide lead compound optimization.

Chapter 2. DNA-damaging Agents as Chemotherapeutics and Mechanisms of Resistance

Based on the statistics from the International Agency for Research on Cancer (IARC), there were ~17 million new cancer cases and ~9.5 million cancer deaths in 2018. Due to population growth and aging, projected annual cancer cases and death will reach 27.5 million and 16.3 million by 2040, respectively, highlighting the urgent need for more effective cancer therapeutics.⁶¹

Tumor cells are often treated with DNA-damaging agents. Different DNA-damaging agents can inflict varying types of DNA damage, such as double-stranded breaks (DSB) induced by the UV-mimetic 4-Nitroquinoline 1-oxide (4-NQO), inter- and intra-strand cross-links induced by cisplatin and cyclophosphamide (CTX), aberrant methylation induced by alkylating agents such as methylmethane sulfonate (MMS) and N-methyl-N-nitro-N-nitrosoguanidine (NMNG), and oxidative damage induced by drugs such as methotrexate (Figure 1).⁶²⁻⁶⁴ Such DNA-damage will result in stalling of replication, which will lead to cellular dysfunction and, eventually, cell death.^{63, 65}

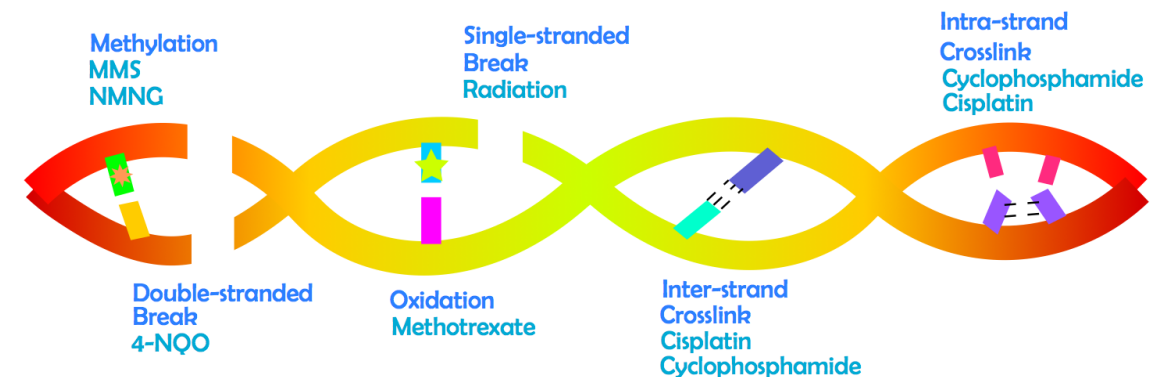


Figure 1: DNA-Damaging Therapeutic Agents.

Many cancer drugs kill cancer cells by inducing DNA damage, leading to cellular dysfunction and activation of apoptotic signaling.

However, tumor cells can become resistant to chemotherapy by dysregulating different cellular pathways, such as suppression of apoptotic proteins, inhibiting drug uptake, enhancing secretion or metabolism of drugs, and upregulating DNA repair pathways, including the translesion DNA synthesis.^{66,67}

2.1 Translesion DNA Synthesis as an Error-prone DNA Repair Process

Replicative polymerases are high fidelity and seldom make mistakes. Their catalytic pocket is small and fits undamaged DNA snugly. Since damaged DNA bases usually lead to distortion of DNA strands, nearly all types of DNA damage or lesions halt replication. On the contrary, Y family polymerases, though low fidelity, have a

solvent-exposed catalytic pocket that can accommodate DNA damage with even bulky lesions.⁶⁸ When a replication fork is stalled in normal cells, it is preferable to bypass it in a potentially mutagenic way than to let the fork collapse, turning it into a double-stranded break, which triggers cell death. To initiate bypass, a replicative switch happens, whereby the processivity factor, PCNA, gets monoubiquitinated, increasing its affinity to Y-family polymerases.⁶⁹ The Y-family polymerase, Rev1, which has catalytic ability but functions primarily as a scaffold, recruits one of three inserter Y polymerases- POL ι , POL κ , or POL η , to insert a base opposite the lesion. It then recruits POL ζ , via its accessory subunit, Rev7. The catalytic subunit, Rev3, adds additional nucleotides past the lesion and extends beyond it to a point where the correct base-pairing is restored, and the replicative polymerase is able to take over, continuing replication (Figure 2).⁶⁹⁻⁷⁴

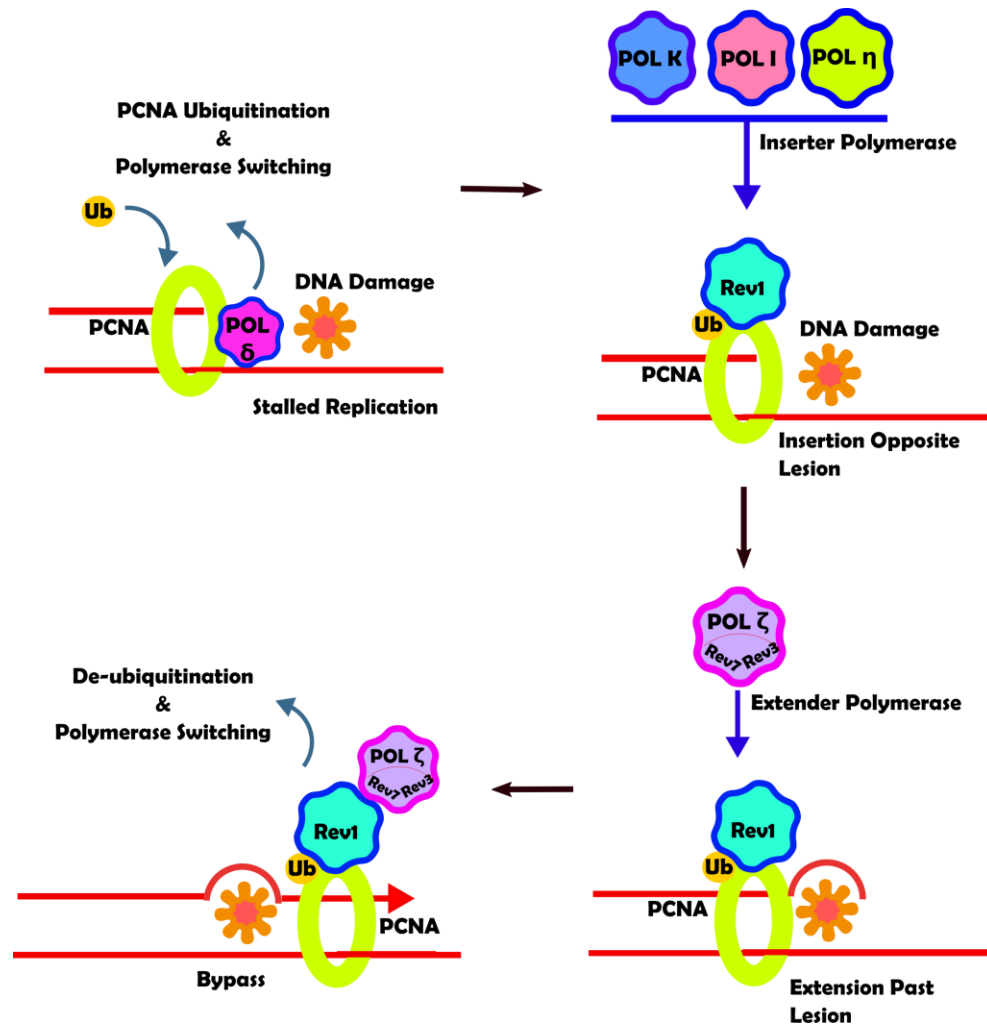


Figure 2: Translesion DNA synthesis.

PCNA gets ubiquitinated at the stalled replication fork, resulting in the replicative polymerase being switched out. Translesion bypass is dependent on the Rev1 polymerase and its function as a scaffold that recruits other insertase polymerases, and the extender polymerase, POL ζ . Once the lesion is bypassed, the replicative polymerase is switched back in and replication proceeds as normal.

2.2 Rev1- POL ζ Mediated TLS as a Mechanism of Resistance to Chemotherapy

A wealth of evidence points towards the involvement of the Rev1-mediated TLS in cancer progression and developing resistance to chemotherapy. Elevated levels of Rev1 protein are a predictor of unfavorable prognosis and poor response to treatment in patients with prostate cancer.⁷⁵ Genetic missense mutations in the *Rev1* gene are associated with increased risk for cervical carcinoma.⁷⁶ Ovarian carcinoma cells engineered to express higher levels of Rev1 (2.7 to 6.2 fold higher), showed marked increase in resistance to killing by cisplatin and enhanced cisplatin-induced mutagenesis.⁷⁷ Lung adenocarcinoma cells resistant to cisplatin treatment were re-sensitized when Rev3 expression was suppressed using short-hairpin RNA. These cells also displayed reduced levels of cisplatin-induced mutagenesis.⁷⁸ B cell lymphoma tumors transplanted into mice were more sensitive to cyclophosphamide treatment in Rev3 knockdown cells.⁷⁹ Ovarian clear cell carcinoma (CCC) cells were more sensitive to cisplatin treatment when Rev7 expression was suppressed. Additionally, CCC tumors xenografted into mice showed enhanced reduction in volume upon cisplatin treatment in Rev7 knockdown cells compared to control cells.⁸⁰

Additionally, B-cell lymphoma cells that survived chemotherapy were much more likely to become resistant in subsequent rounds of chemotherapy in the presence

of Rev1 as opposed to when Rev1 expression was suppressed. This indicates that not only does Rev1- POL ζ mediated TLS promote chemoresistance by bypassing normally destructive DNA damage, but also helps the acquiring of new cancer drug resistance.⁷⁹

Taken together, these compelling pieces of evidence show that Rev1-mediated TLS is a key factor in promoting chemoresistance and is therefore an important pathway to target for the development of novel cancer adjuvant therapeutics.⁸¹

2.3 Important Protein-protein Interactions in the Rev1- POL ζ - POL κ Translesionsome Complex

The interactions between Rev1 and the inserter and extender polymerases occur at the C-terminal domain of Rev1. Each of the inserter polymerases interacts with Rev1 via a Rev1-interacting-region (RIR). The extender polymerase ζ interacts with Rev1 via its accessory subunit, Rev7. The quaternary structure of Rev1, a fragment of POL ζ (Rev7 with a peptide of Rev3) and the RIR region of POL κ shows that the flexible N-terminal region of the Rev1 C-terminal domain (CTD), as well as the alpha helices 1, 2 and the loop connecting them, forms hydrophobic and some polar interactions with the POL κ RIR. The alpha-helices 2,3 and 4, as well as the flexible loop between helices 2 and 3 and the flexible C-terminal tail of the Rev1 C-terminal domain (CTD) form the majority of the interface between Rev1 and Rev7 (Figure 3), forming a conserved, shallow hydrophobic pocket.⁸²⁻⁸⁵

Since the Rev1-Rev7 binding interface has only one interacting partner (Rev7) and is evolutionarily conserved, we focused our efforts on targeting this interface for lead compound discovery (Figure 4).

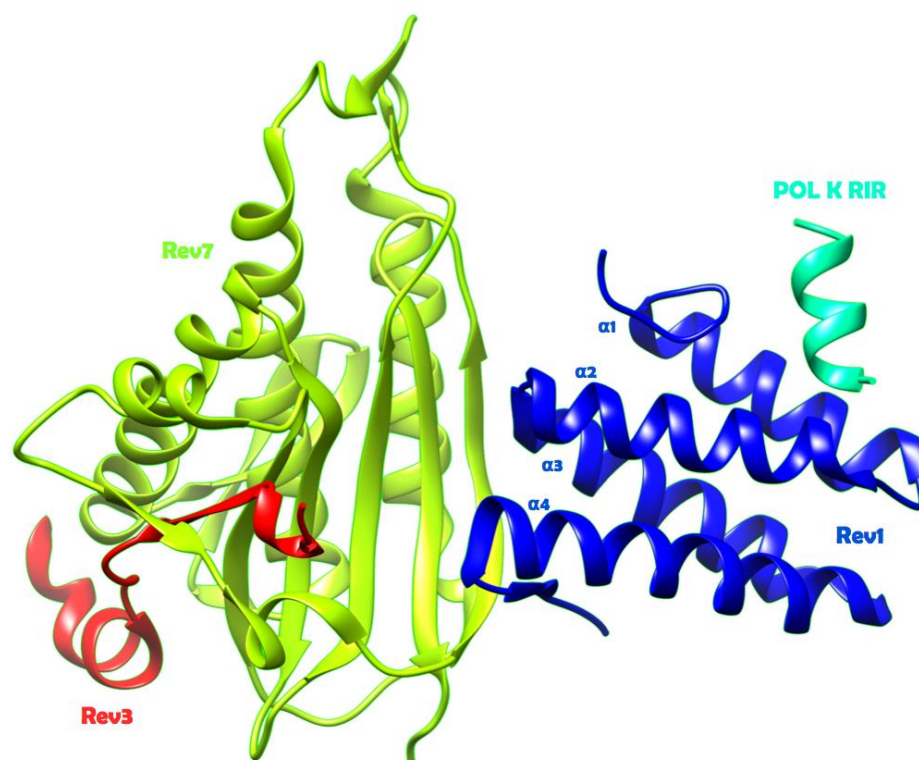


Figure 3: The Translesionsome Complex (PDBID 4FJO).

The quaternary complex structure shows that the C-terminal end of Rev1 CTD interacts with Rev7, while the N-terminal end interacts with the RIR of POL K.

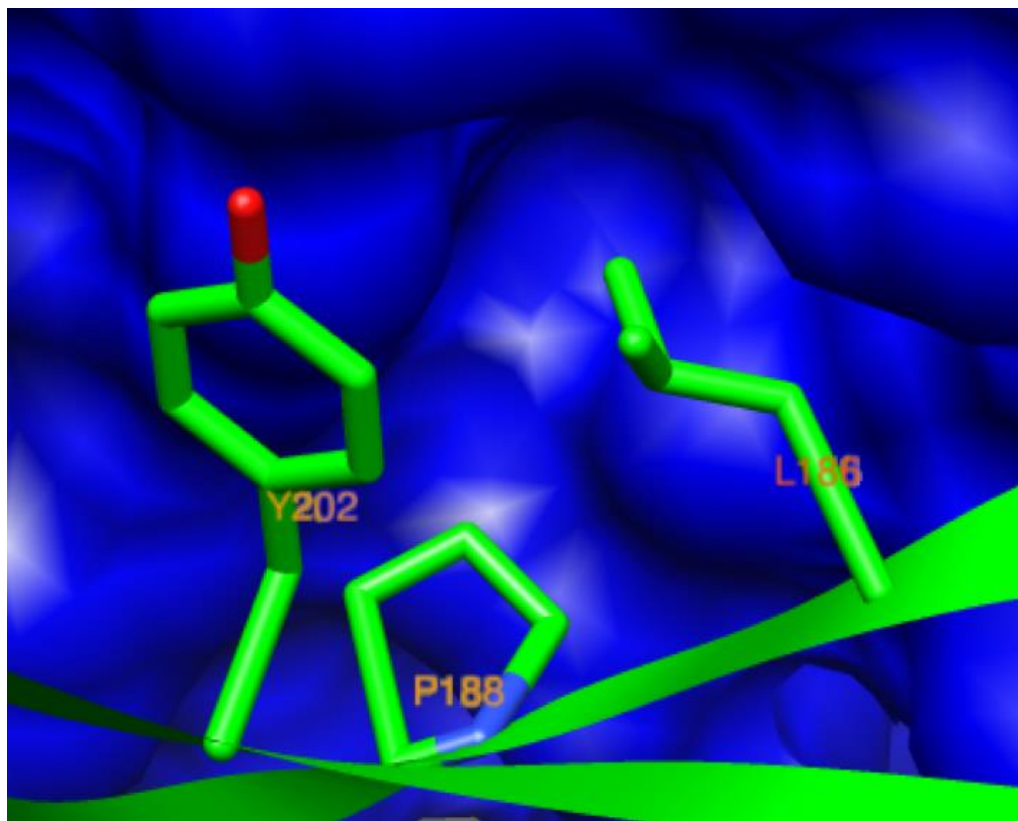


Figure 4: The Hydrophobic Pocket at the Rev1/Rev7Interface.

At its interface with Rev7, Rev1 forms a shallow hydrophobic pocket which interacts favorably with hydrophobic residues on Rev7. We aimed to target this pocket for lead compound development.

Chapter 3. Discovery and Characterization of An Inhibitor of the Rev1-Rev7 Interaction

Using a high-throughput Enzyme-linked immunosorbent (ELISA) assay (described below), we screened about 10,000 compounds in the LOPAC, PRESTWICK and Korean Chemical Bank libraries and identified a promising small molecule inhibitor.

3.1 Small Molecule Inhibitor Identification and Validation

In our ELISA assay, the His₈-tagged Rev7 co-expressed with a Rev3 fragment (His.Rev7/3) was immobilized onto Ni²⁺-NTA-coated wells. We then probed whether a construct with the FLAG-tagged Rev1-CTD chimerically fused with a POL κ RIR fragment (FLAG. κ .Rev1) could stay attached to His.Rev7/3 in the presence of a potential inhibitor after vigorous washing, using a horseradish peroxidase (HRP) conjugated antibody (Figure 5). Using this strategy, we identified a dihydroquinolone compound, JH-RE-06 (Figure 6). This work was done by Dr. Jessica Wojtaszek and a former Duke Undergraduate Yaohua Xue. JH-RE-06 was synthesized at a large scale through our collaboration with Dr. Jiyong Hong's group in the Department of Chemistry at Duke University. The synthesis was done by Dr. Minhee Lee.

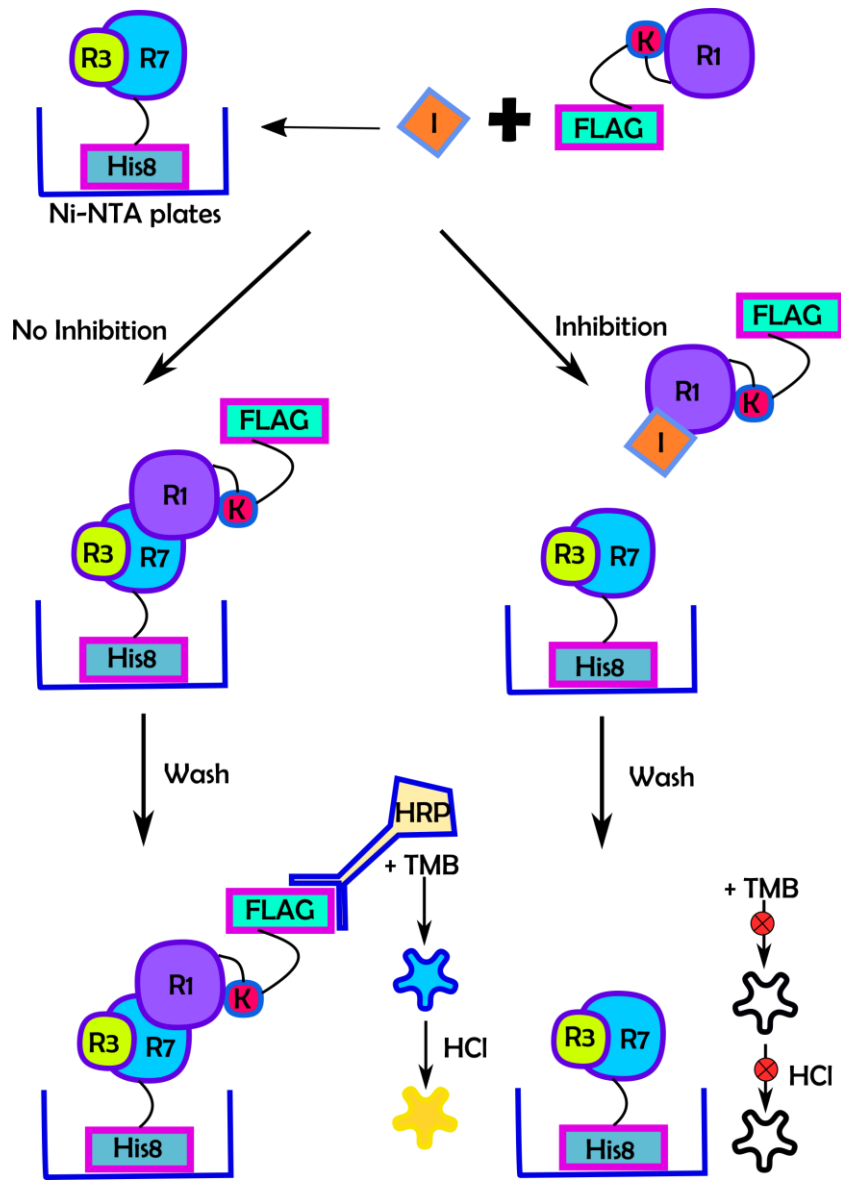


Figure 5: High-throughput ELISA Assay

His₈-tagged Rev7 co-expressed with a Rev3 peptide was attached to Ni²⁺-NTA wells and incubated with a mixture of a potential inhibitor and FLAG-tagged Rev1-CTD with a POL κ peptide. After vigorous washing, the wells were probed with an anti-FLAG HRP-conjugated antibody, which could convert its substrate TMB blue, which could then be treated with acid to yield a yellow color that could be read at 420nm.

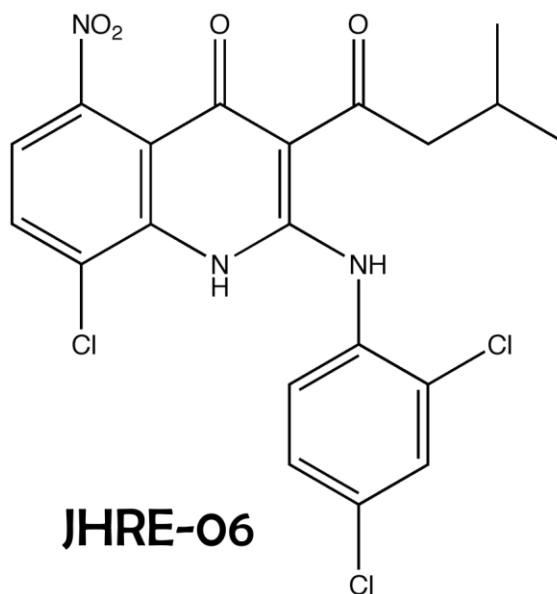


Figure 6: Structure of JH-RE-06.

(8-chloro-2-((2,4-dichlorophenyl)amino)-3-(3-methylbutanoyl)-5-nitroquinolin-4(1*H*)-one), or JH-RE-06 was identified as a potential inhibitor of the Rev1-Rev7 interaction.

To independently validate the hypothesis that JH-RE-06 was inhibiting Rev1 binding to Rev7 *in vitro*, and to extract a value of the IC₅₀ of inhibition, we performed an AlphaScreen assay, in which an anti-FLAG-coated donor bead attached to FLAG.κ.Rev1 could transfer energy via an unstable oxygen species to an anti-His₆-coated acceptor bead attached to His.Rev 7/Rev 3, unless the interaction was abrogated by JH-RE-06 (Figure 7). Analysis of the dose-dependent inhibition curve yielded an IC₅₀ value of 0.78 +/- 0.15 μM.

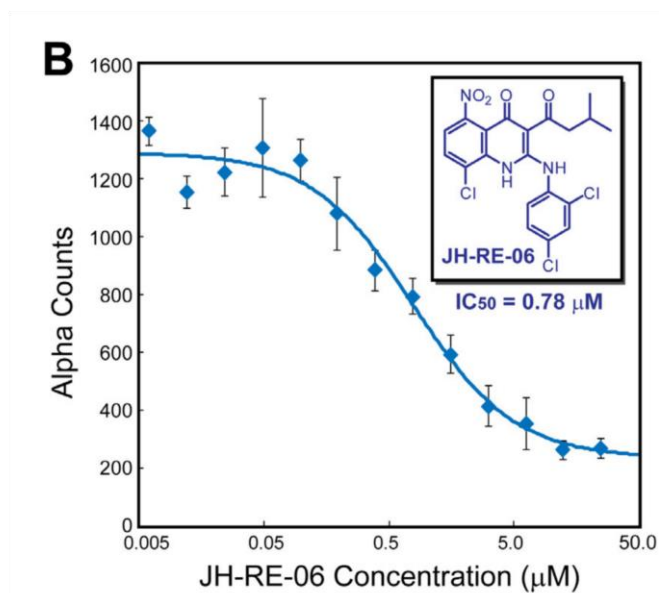
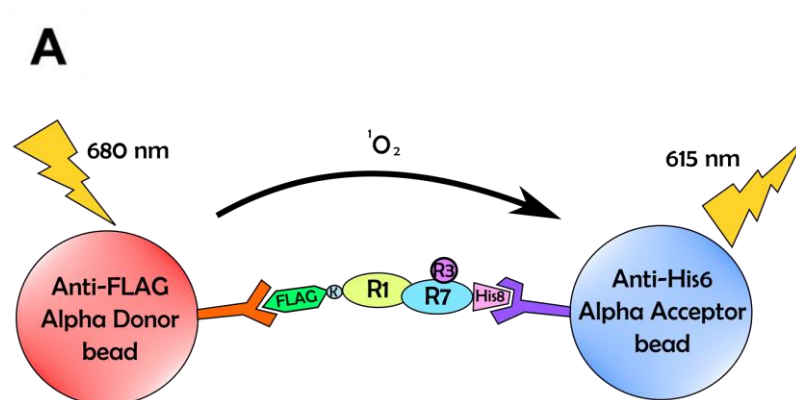


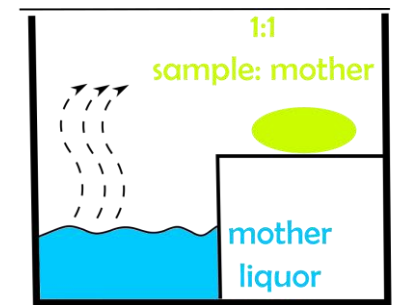
Figure 7: Alpha Screen Assay

JH-RE-06 was titrated into a mixture of donor beads attached to FLAG. κ .Rev1 and acceptor beads attached to His.Rev7/3. An increase in JH-RE-06 concentration corresponded to a decrease in signal as the interaction between the protein partners, and, as a result, the beads was interrupted. Using this strategy, we were able to obtain an IC_{50} value of $0.78 \pm 0.15 \mu\text{M}$

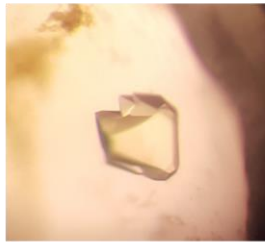
3.2 Molecular Basis of Inhibition of Rev1 by JH-RE-06

To probe the molecular details of the inhibition of Rev1 by JH-RE-06, we used X-ray crystallography to visualize the inhibitor-protein interaction. We obtained diffraction quality crystals through sitting-drop vapor diffusion (Figure 8, Table 1). With these crystals, we were able to obtain a high-resolution picture of the interaction between Rev1 and JH-RE-06. Unexpectedly, the inhibitor is bound to not one but two molecules of Rev1. Two Rev1 monomers form a tail-to-tail asymmetric dimer with the flexible C-terminal tails forming an anti-parallel beta sheet at the interface, stabilizing the structure further (Figure 9). To accommodate the inhibitor, one of the C-terminal tails is pushed outward by $\sim 16^\circ$ (Figure 10). Together, the two monomers completely engulf the inhibitor, with different residues involved in favorable hydrophobic and polar interactions with the inhibitor (Figure 11 and 12). The previously identified hydrophobic pocket on one monomer is effectively doubled in size as a result of the induced dimerization process.

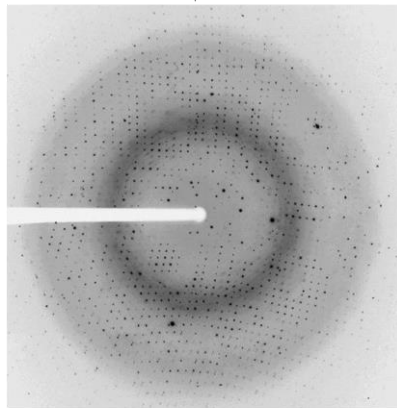
Superimposing the inhibitor-bound Rev1-CTD structure with the translesionsome structure gives a further indication about the mechanism of inhibition: by forcing Rev1 to dimerize, the inhibitor effectively blocks the Rev1 interface at which Rev7 would bind (Figure 13).



sitting-drop vapor diffusion



protein-inhibitor complex
crystal



crystal diffraction pattern

Figure 8: Diffraction Quality Inhibitor-bound Protein Crystals were obtained by Sitting-drop Vapor Diffusion

Table 1: X-ray Data Collection and Refinement Statistics for the Rev1-JH-RE-06 Complex Structure.

Data collection		Refinement	
Wavelength (Å)	0.9778	R_{work}/R_{free}	0.164/0.191
Space group	P 21 21 21	No. of atoms	2396
Cell dimensions		Protein	1938
a,b,c (Å)	48.55, 51.02, 98.92	Ligand/ion	30
α, β, γ (°)	90, 90, 90	Water	428
	(35.17-1.50	Avg. B-factors	19.25
Resolution (Å)	(1.55-1.50)	Protein	16.55
R_{sym} or R_{merge}	0.07146 (0.3938)	Ligand/ion	15.79
Mean $I/\sigma I$	16.54 (4.06)	Water	31.71
Completeness (%)	99.84 (99.85)	R.m.s. deviation	
Redundancy	7.7 (5.6)	Bond length (Å)	0.007
Total reflections	309510 (21842)	Bond angle (°)	1.1
Unique reflections	40047 (3914)	Ramachandran	
		Favored (%)	99.12
Values in parentheses are for high resolution shells		Allowed (%)	0.88
		Outliers (%)	0

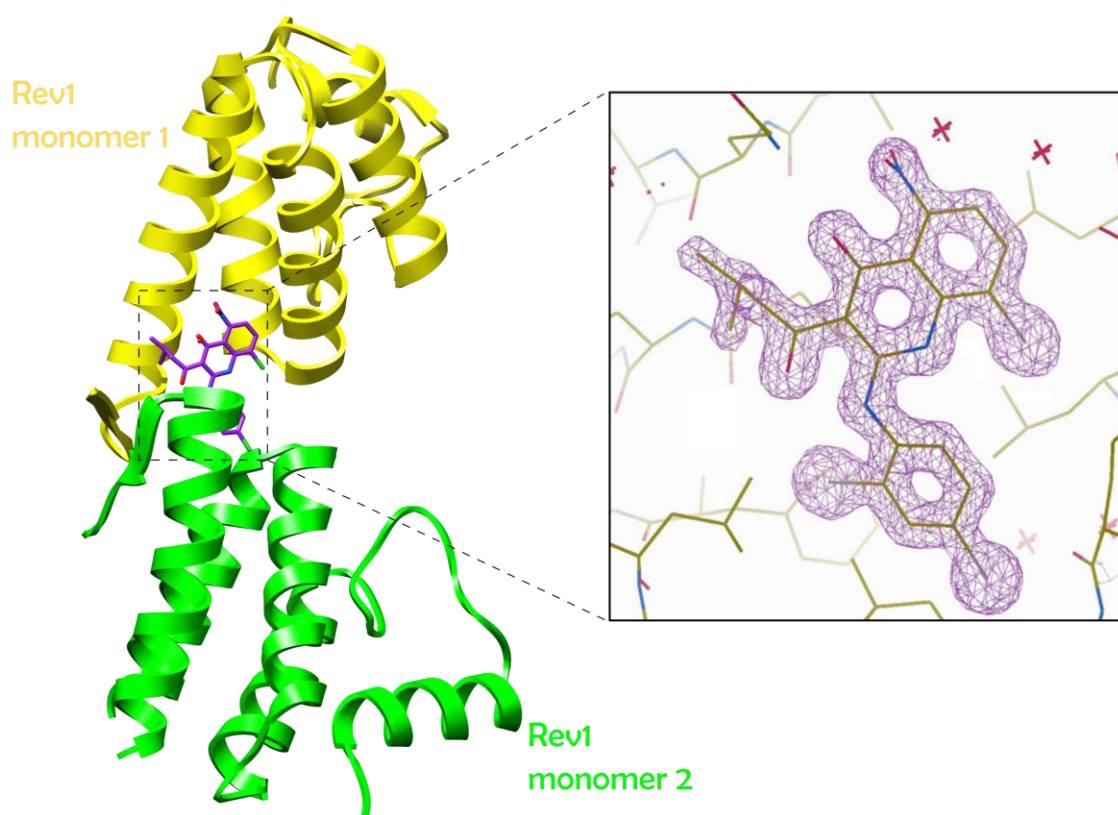


Figure 9: The Rev1-JH-RE-06 Complex.

This crystallographic model shows that the inhibitor is bound to two molecules of Rev1, with the C-terminal tails forming an anti-parallel beta sheet. The monomers are shown in ribbon form, the inhibitor in stick form, with an enlarged model showing an omit map ($2mF_o-DF_c$) at 1σ .

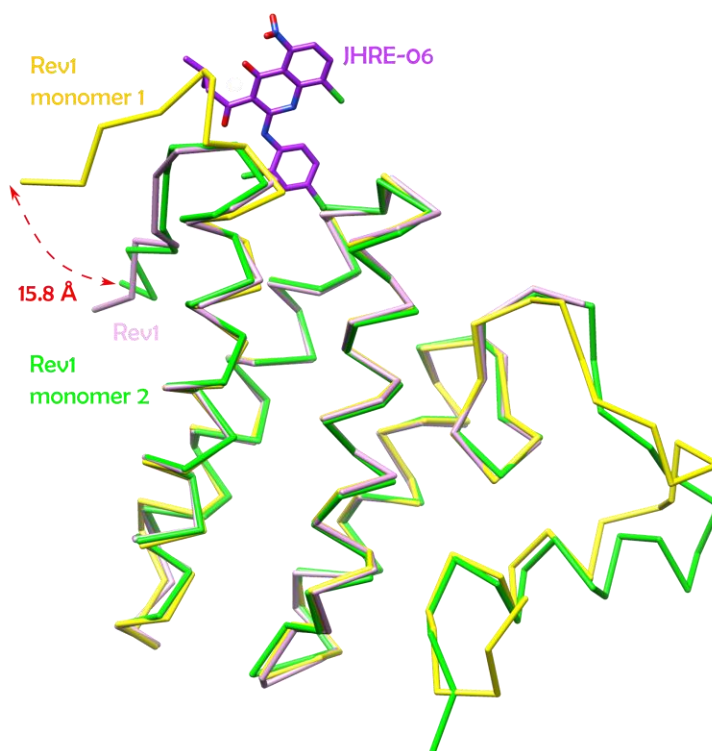


Figure 10: Monomer 1 C-terminal Tail Pushed Out.

This superimposition between monomer 1 and 2 of the inhibitor-bound structure and Rev1 from the translesionsome complex shows that while one monomer is almost exactly like in the translesionsome complex, in the other the C-terminal tail is pushed out by ~16 degrees to accommodate the inhibitor.

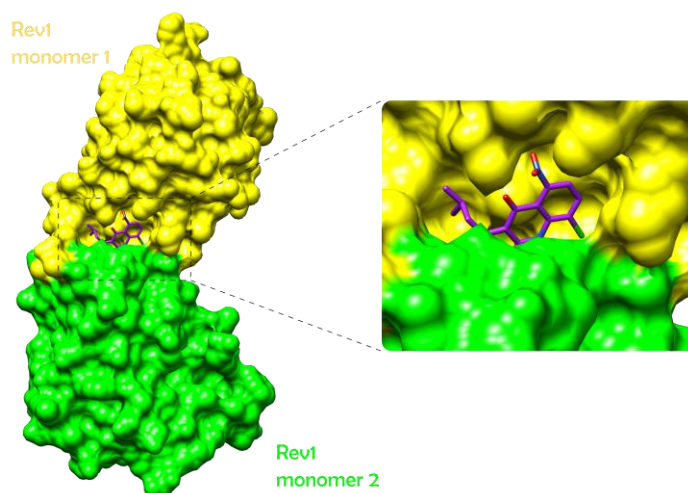


Figure 11: JH-RE-06 Fits Snugly in Pocket.

A surface-filling model shows that the interface of the Rev1 monomers forms a pocket ideally suited for the shape of JH-RE-06

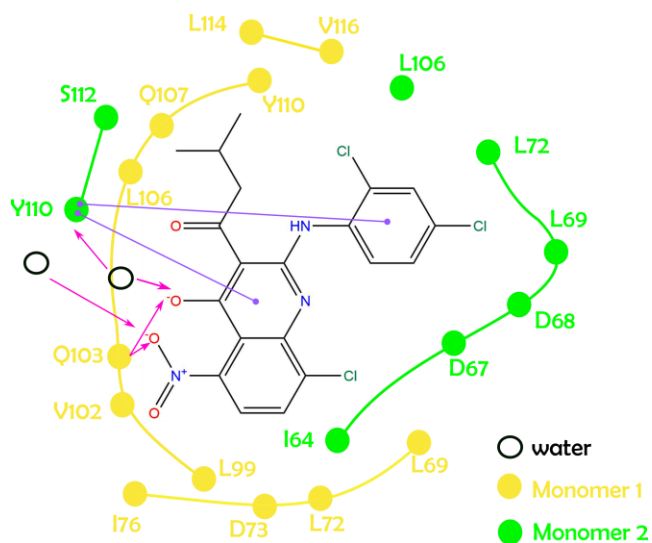


Figure 12: Rev1-JH-RE-06 Interactions.

The residues from both monomers form favorable hydrophobic and polar interactions with JH-RE-06, as shown in the above schematic.

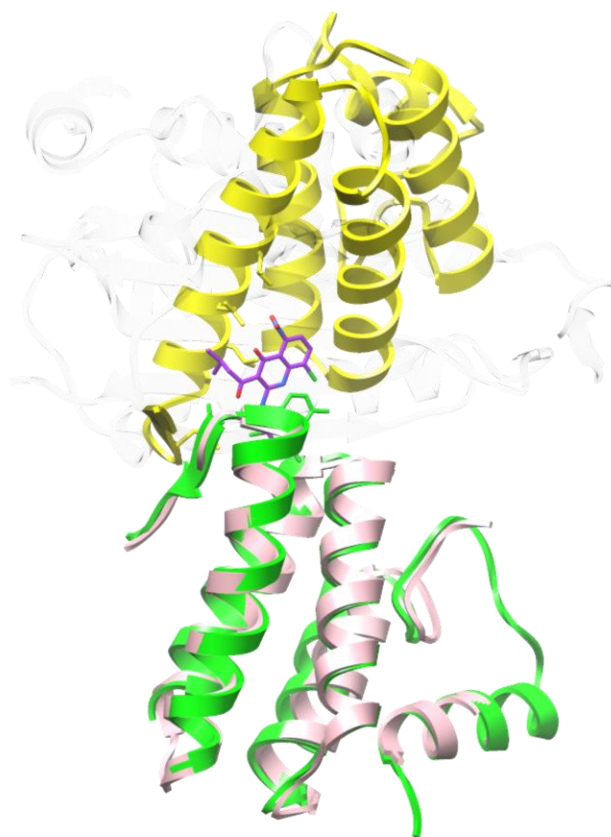


Figure 13: Rev1 Dimerization Blocks Rev7 Interaction.

This superimposition of Rev1 monomer 1 (yellow), monomer 2 (green) and Rev1 in complex with Rev7 (pink with Rev7 faded gray in background) shows that by inducing Rev1 dimerization, JH-RE-06 blocks the interface where normally Rev7 would bind.

3.3 In Vitro Validation of Rev1 Dimer Induction in the Presence of JH-RE-06.

To confirm that the dimer observed in our crystal structure was not an artifact of crystal packing, we tested whether the presence of JH-RE-06 would enhance the Rev1 CTD dimer formation in the presence of a cross-linking agent, disuccinimidyl suberate (DSS) *in vitro*. Our results showed that dimerization was indeed enhanced in the presence of JH-RE-06 (Figure 14).

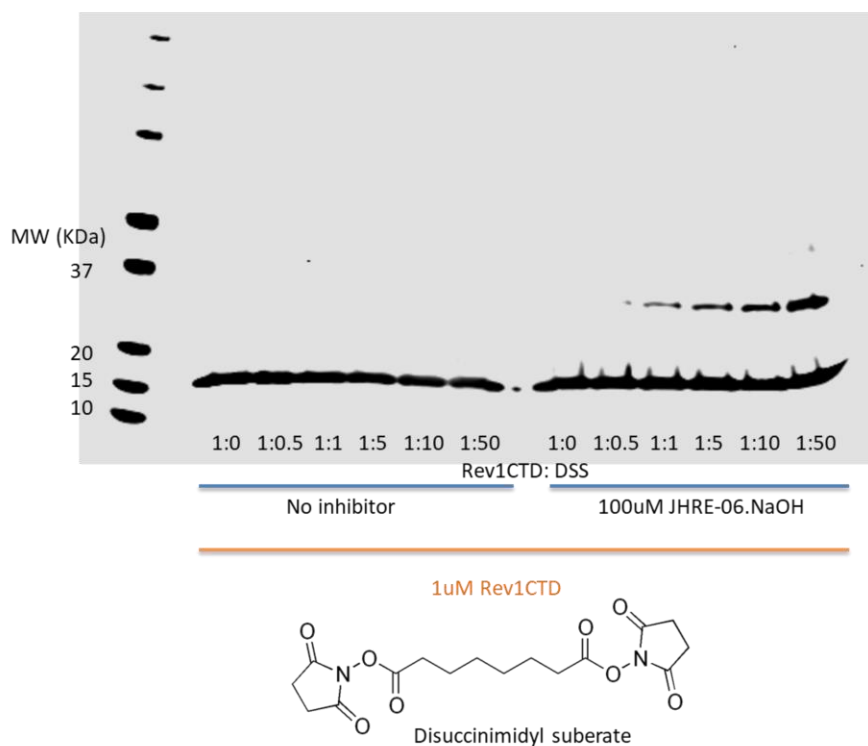


Figure 14: JH-RE-06 Enhances Rev1-CTD Dimerization In Vitro.

In the presence of JH-RE-06, Rev1 dimerization was enhanced with the addition of increasing concentrations of the cross-linking reagent, DSS.

3.4 JH-RE-06 Enhances Tumor Sensitivity to Cisplatin and other DNA-damaging Agents in Tumor Cells and Mouse Xenograft Model.

Next, we investigated whether JH-RE-06 could enhance chemosensitivity of tumor cells to cisplatin. To test this, we exposed various tumor cell lines to cisplatin alone, JH-RE-06 alone, or cisplatin and JH-RE-06 together, and counted surviving colonies. Our results showed that JH-RE-06 enhanced cisplatin cytotoxicity over a variety of tumor cell lines (Figure 15).

Next, we showed that JH-RE-06 suppresses spontaneous and cisplatin-induced mutagenesis by using the HPRT mutagenesis assay. In this assay, spontaneous or treatment-induced mutations that inactivate the hypoxanthine phosphoribosyltransferase (HPRT) gene will prevent cells from incorporating a toxic guanine analog, 6-thioguanine (6-TG), into DNA and allow cells to survive in 6-TG selection medium. As a result, an increase in the number of surviving cells is correlated with enhanced mutagenicity. The ability of HT1080 cells to incorporate 6-TG was measured when treated with cisplatin or JH-RE-06 alone, or cisplatin and JH-RE-06 together. Cells that survived and formed colonies were able to do so as a result of mutagenesis that blocks nucleotide incorporation. Our results showed that not only does JH-RE-06, on its own, suppress background levels of mutation, but also, in conjunction with cisplatin, reduces cisplatin-induced mutagenesis in HT1080 cells (Figure 16).

Moreover, we showed using a luminescence-based cell viability assay that JH-RE-06 was effective in enhancing the cytotoxicity of other DNA-damaging agents besides cisplatin, including the bulky DNA-damaging agent benzo[a]pyrene-7,8-dihydrodiol-9,10-epoxide (BPDE), the UV-mimetic 4-nitroquinolone 1-oxide (4-NQO), and the alkylating agent methyl methanesulfonate (MMS) to *Kras^{mut}P53^{-/-}* cells, which are extremely aggressive and highly resistant to chemotherapy (Figure 17).

Taken together, these results show that JH-RE-06 sensitizes various tumor cells not only to cisplatin but other DNA-damaging agents and suppresses cisplatin-induced mutagenesis in HT1080 cells. This work was done by Dr. Nimrat Chatterjee as a result of our collaboration with the Graham Walker group at MIT.

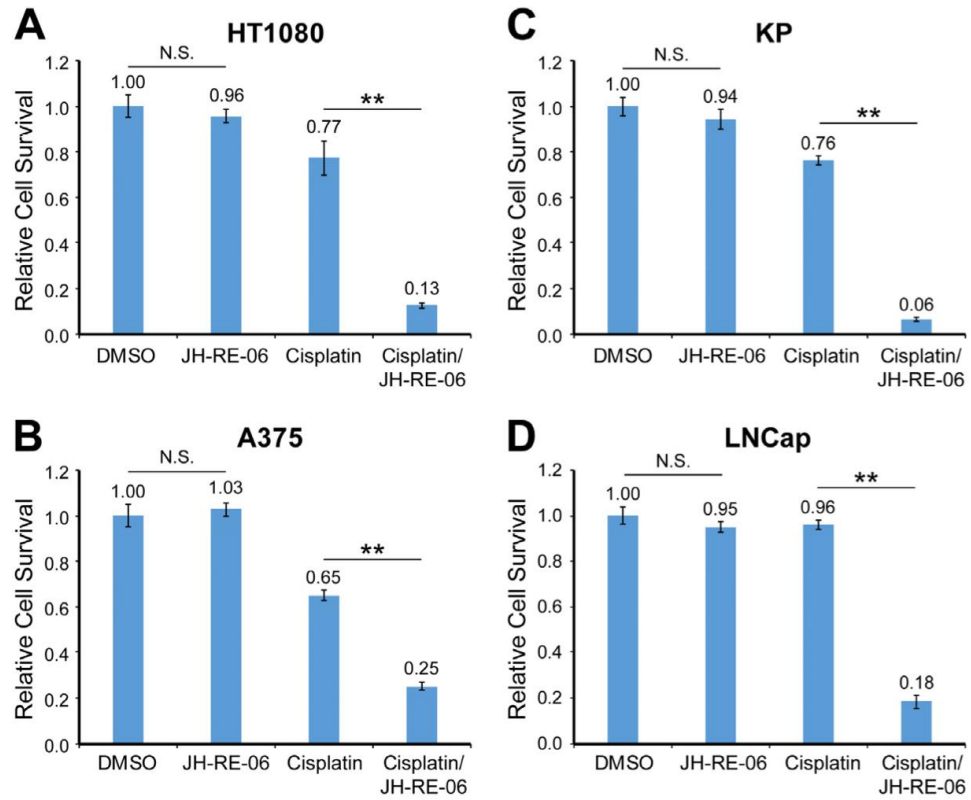


Figure 15: JH-RE-06 Enhances Cisplatin Chemosensitivity in Different Cancer Cell Lines.

Various tumor cell lines (HT1080: human fibrosarcoma, KP: human lung carcinoma, A375: human melanoma, LNCap: human prostate carcinoma) were exposed to cisplatin or JH-RE-06 alone, or cisplatin and JH-RE-06 together. The colony-forming ability of these cells was then measured by staining. Results showed that JH-RE-06 significantly enhances cytotoxicity of cisplatin.

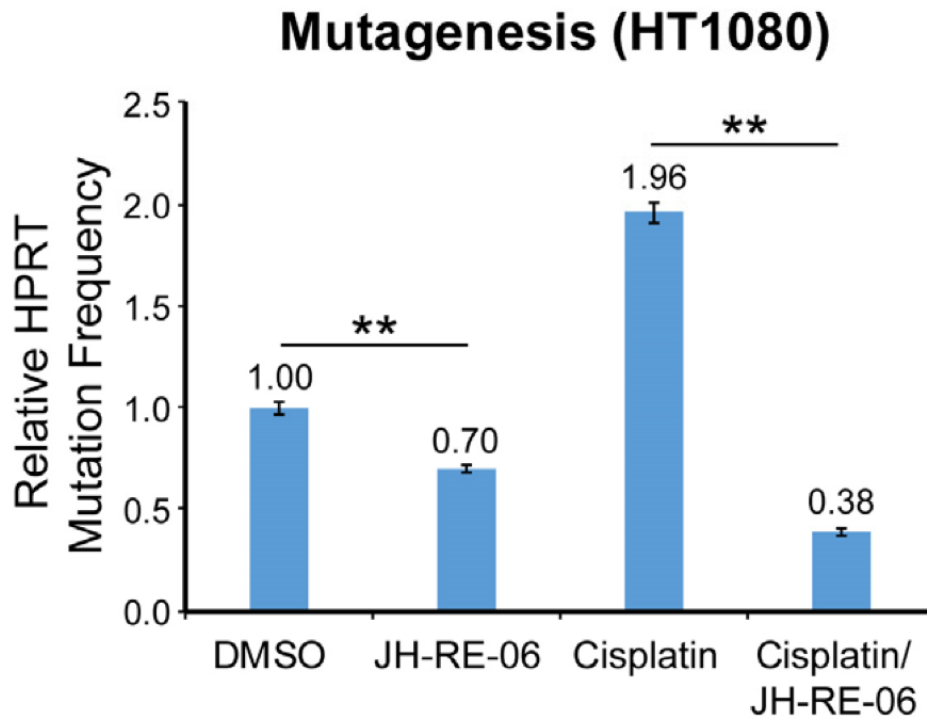


Figure 16: JH-RE-06 Suppresses Cisplatin Induced Mutagenesis in HT1080 Cells

Using the hypoxanthine phosphoribosyl transferase (HPRT) mutagenesis assay, we probed whether JH-RE-06 could suppress mutations caused by cisplatin. HT1080 cells grown in a 6-TG media were treated with cisplatin and/or JH-RE-06. Mutant cells were able to survive on the media. Our results showed that not only does JH-RE-06, on its own, suppress background levels of mutation, but also, together with cisplatin, reduces cisplatin-induced mutagenic activity in HT1080 cells.

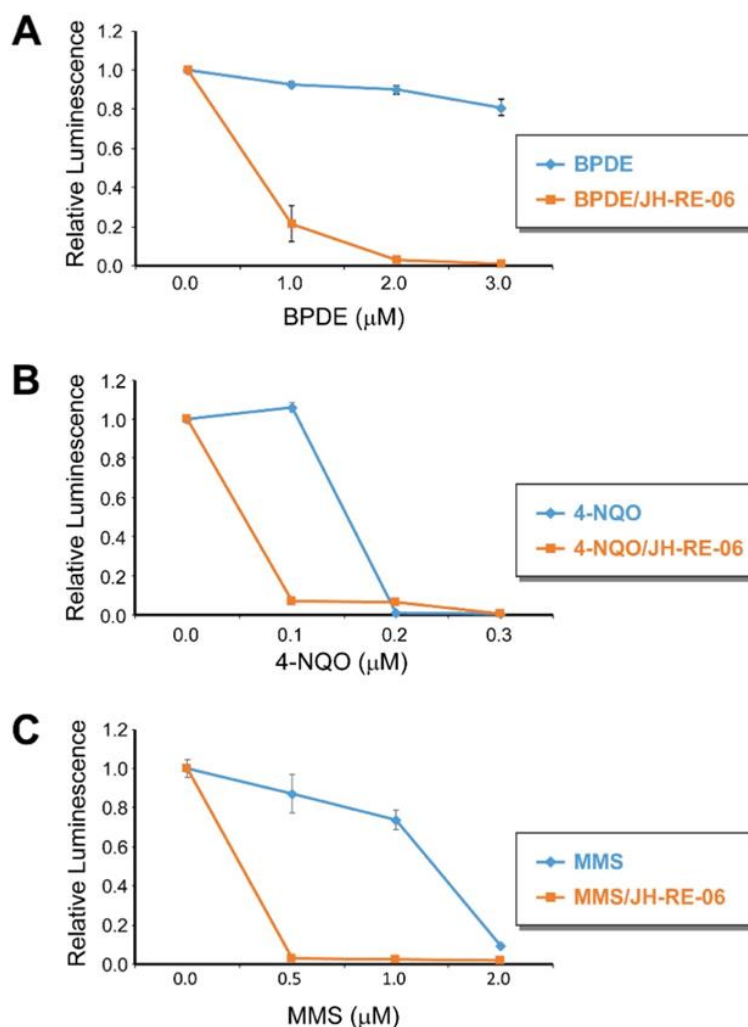


Figure 17: JH-RE-06 Sensitizes *Kras^{mut}P53^{-/-}* Cells to Various DNA-Damaging Agents.

We used the luminescence-based CellTiter-Glo cell viability assay to determine whether JH-RE-06 could enhance the killing of KP cells in the presence of various DNA-damaging agents and found that it did indeed sensitize these cells to methyl methanesulfonate (MMS, which methylates DNA), benzo[a]pyrene-7,8-dihydrodiol-9,10-epoxide (BPDE, which binds to Guanine nucleobases, forming an adduct), and 4-Nitroquinoline 1-oxide (4-NQO, which is a UV-mimetic that causes DSB by inducing reactive oxygen species or ROS)

We next examined whether JH-RE-06 was effective *in vivo* in terms of killing tumor cells. A375 (human melanoma) cells were injected into NCRNU-F (nude) mice to grow xenograft tumors approximately 100 mm³ in size. The mice were randomly distributed into 4 groups to receive twice-weekly injections of saline, cisplatin alone, JH-RE-06 alone, and a JH-RE-06 and cisplatin combination for 5 weeks. Tumors treated with a combination of both shrank to a significant degree. Moreover, mice treated with a combination of both survived longer (Figure 18). This work was done by Nimrat Chatterjee and Azucena Ramos through a collaboration with the Graham Walker and Michael T. Hemann groups at MIT.

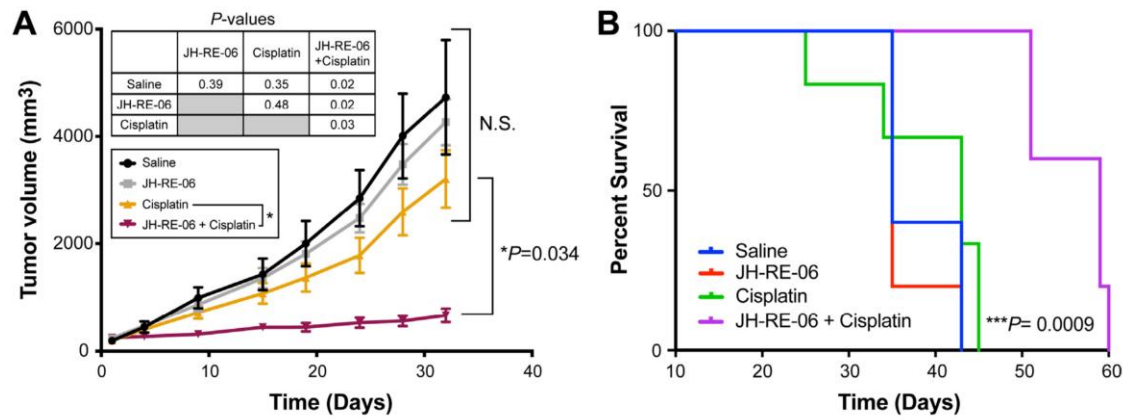


Figure 18: JH-RE-06 Enhances Cisplatin Sensitivity in Murine Xenograft Tumor Model.

Aggressive A375 melanoma cells were injected into mice to form xenograft tumors. These tumors were then injected with either JH-RE-06 or cisplatin alone, or with

both in combination. Combined treated tumors shrank in size significantly relative to tumors that were treated by either alone and mice treated with both survived longer.

3.4 Discussion

Accumulating evidence supports the notion that Rev1 and its interaction with POL ζ via Rev7 plays an essential role in TLS. Suppression of Rev1 or Rev7 expression in tumor cells makes them hypersensitive to chemotherapy. This makes the interface between Rev1 and Rev7 an attractive target for inhibitor development. Protein-protein interfaces are notoriously hard to target, with the large surface area and conformational flexibility involved.⁸⁶ The Rev1-Rev7 interface is no different, with the solvent-accessible interface being $\sim 890 \text{ \AA}^2$ and the solvent-excluded surface area being $\sim 480 \text{ \AA}^2$ (Figure 19). While much of the interaction comes from the smaller, buried surface area, the hydrophobic pocket defined by that interface is shallow and seemingly intractable for small molecule targeting. Additionally, the C-terminal tail of Rev1-CTD is highly flexible, another apparent hindrance to inhibitor targeting. Contrary to what conventional wisdom would dictate, we have now shown that the Rev1-Rev7 interface is suitable for small-molecule inhibitor targeting. JH-RE-06 forces Rev1 to dimerize, effectively doubling the size of the shallow hydrophobic pocket at the interface. The inhibitor is then ensconced in the cavity formed by the two Rev1 monomers. Additionally, the normally disordered C-terminal tails of the two monomers are ordered

into an anti-parallel beta sheet, further stabilizing the structure. As a direct result of this induced dimerization, the Rev7 binding interface is effectively blocked. All these factors lend JH-RE-06 superb specificity and effectiveness in blocking the Rev1-Rev7 binding interface.

Such specificity is translated to potential future therapeutic benefits of JH-RE-06. We show that tumor cell response to cisplatin treatment is significantly improved in the presence of JH-RE-06. Cisplatin-induced mutagenesis is also suppressed in the presence of JH-RE-06. Since cancer cells may respond to DNA damage caused by cisplatin and other chemotherapeutics by upregulating TLS, recruiting TLS proteins (like Rev1 and POL ζ) to the site of the DNA damage, JH-RE-06 has the advantage of being an effective adjuvant to sensitize cancer cells to cisplatin and other DNA-damaging chemotherapeutics and at the same time to suppress the acquisition of new treatment-induced resistance mechanisms in relapsed tumors. The therapeutic potential of translesion synthesis inhibition is strongly supported by the striking *in vivo* data showing that a combination of JH-RE-06 and cisplatin significantly delayed the growth of xenograft tumors in mice and prolonged the animal survival window.

Although our specific example was demonstrated for the Rev1-Rev7 interface in the context of translesion DNA synthesis, ligand induced receptor dimerization may be a general approach that can be applied to many other systems to enable the discovery

and development of novel small molecule modulators targeting protein-protein interfaces, including shallow and flexible ones, that were often considered intractable.

Our future work will focus on other protein-protein interfaces that are involved in the TLS pathway and other inter-connected pathways involved in tumor cell proliferation and resistance to chemotherapy, that can be exploited for drug discovery.

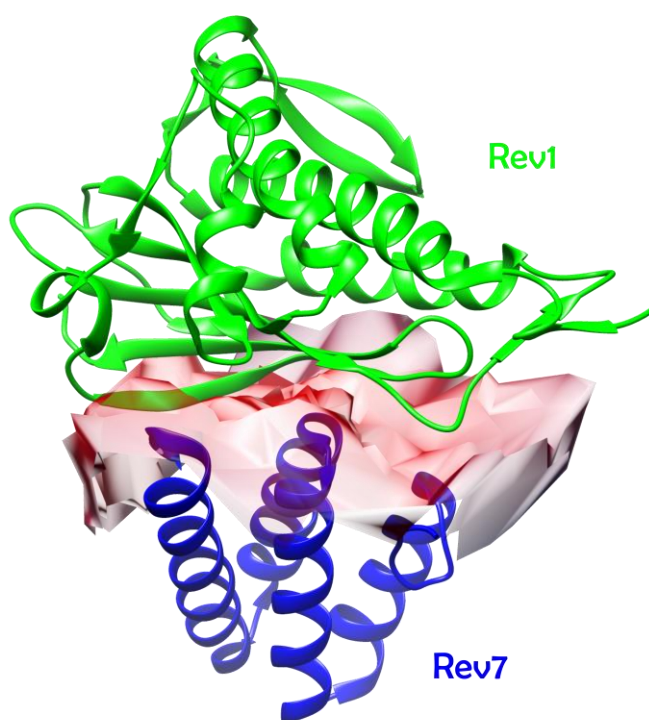


Figure 19: The Rev1-Rev7 Interface.

The interface between Rev-CTD and Rev7 (both solvent-accessible and solvent-excluded) is shown as a red surface. The solvent-excluded interface provides most of the energy of interaction and forms a shallow hydrophobic pocket that we targeted for inhibitor development.

3.5 Methods

3.5.1 Genetic Cloning and Protein Purification

The gene encoding the mouse POL κ RIR (K564-N577), a di-glycine linker, and the mouse Rev1-CTD (F1150-T1249) was synthesized and cloned into an in-house pET15b vector, resulting in an N-terminally His₁₀-GB1-tagged fusion protein, with the tag separated by a TEV protease site. Adding the FLAG tag after the TEV protease site generated the FLAG-tagged chimeric POL κ RIR-Rev1-CTD construct. Both constructs were verified by Sanger sequencing. The chimeric POL κ RIR-Rev1-CTD, as well as the FLAG-tagged POL κ RIR-Rev1-CTD, were purified using Ni-NTA affinity chromatography, the His₁₀-GB1 tag was cleaved using TEV protease, and the cleaved product purified to homogeneity using size-exclusion chromatography. This was first done by Dr. Jessica Wojtaszek and the description has been modified from a manuscript draft.

The His₈-tagged Rev7/3 protein was purified using Ni-NTA affinity chromatography and size-exclusion chromatography as described previously²⁴.

3.5.2 High-throughput ELISA Screen

The ELISA screening assay for potential inhibitors was performed thus: 50 nM His₈-tagged Rev7/3 in 200 μ L phosphate-buffered saline (PBS, Gibco) with 0.2% BSA (Sigma) was added to a Ni-NTA coated 96-well plate (Qiagen) and incubated for 30

minutes. Excess His₈-tagged Rev7/3 was washed away with PBS buffer containing 0.05% Tween-20 (Omnipur). This step was repeated four times. In a separate 96-well plate, 80 nM FLAG-tagged POL κ RIR-Rev1-CTD was incubated with 10 μ M potential small molecule inhibitors in 200 μ L PBS containing 2% DMSO (Thermo) for 30 minutes. This mixture was then transferred to the His₈-Rev7/3 coated wells and incubated for 30 minutes. The wells were then washed with PBS containing 0.05% Tween-20 to remove unbound FLAG-tagged POL κ RIR-Rev1-CTD. 200 μ L of the anti- FLAG HRP-conjugated antibody (Sigma) in PBS containing 0.2% BSA was then added to the wells, and incubated for 1 hour. The antibody was then washed off with PBS containing 0.05% Tween-20. This step was repeated four times. 200 μ L of the The HRP substrate, 3,3',5,5'-tetramethylbenzidine (TMB, Seracare) was added to the wells. After an incubation period of 20-30 minutes, during which a blue color developed, the reaction was quenched with 1 M HCl, resulting in a color change to yellow. A SpectraMax plate reader was used to quantitate the intensity of the yellow color by measuring absorbance at 450 nm.

The ELISA assay was used to screen several compound libraries, including the LOPAC library (Sigma-Aldrich) of 1,280 pharmacologically active compounds, the PRESTWICK library (Prestwick Chemical) of 1,200 FDA-approved drugs, and ~8,000 compounds from the Korea Chemical Bank representative of ~430,000 diverse

compounds. Among several hit compounds, JH-RE-06 was selected for further characterization due to its potency.

The assay was developed by Dr. Jessica Wojtaszek and further optimized by us. The screening was done by Dr. Wojtaszek and Yaohua Xue.

3.5.3 Chemical Synthesis of JH-RE-06

(8-chloro-2-((2,4-dichlorophenyl)amino)-3-(3-methylbutanoyl)-5-nitroquinolin-4(1H)-one), or JH-RE-06, was prepared from the commercially available Meldrum's acid. The synthesis was initiated with the preparation of the acyl Meldrum's acid, which was heated with 2-chloro-5-nitroaniline under reflux. The reaction took place with the release of CO₂ to provide the β -oxo amide, which was subsequently transformed into the acyl(arylcarbamoyl)-ketene dithioacetal by using CS₂ and Me₂SO₄ in the presence of K₂CO₃. Thermal cyclization in 1,2-dichlorobenzene followed by oxidation using H₂O₂ yielded the sulfoxide intermediate. Coupling with 2,4-dichloroaniline completed the synthesis of JH-RE-06. The purity and the chemical identity of the compound were verified by LC/MS and NMR. This description is adapted from a manuscript draft. JH-RE-06 synthesis was done by Dr. Minhee Lee in the Jiyong Hong group at the Duke University Department of Chemistry.

3.5.4 AlphaScreen Assay for Dose-Dependent Inhibition of the Rev1-Rev7 Interaction

FLAG-tagged mouse POL κ RIR-Rev1-CTD was diluted in PBS buffer with 1mM Tris(2- carboxyethyl)phosphine (TCEP, Hampton) and 0.005% TWEEN-20. The final protein concentration in the reaction was 1 nM. Inhibitor solution that had been serially diluted in 50% DMSO was added to the protein solution in individual wells of a 96-well, half-area, white plate (PerkinElmer) to yield final concentrations of 0-25 μ M of inhibitor in the final solution. The final DMSO concentration was 2%. Protein was incubated with the inhibitor for 30 min. Anti-FLAG Donor Beads (PerkinElmer) were added to each well to a final concentration of 20 ng/ μ L and incubated for an hour. His₈-tagged mouse Rev7/3 was subsequently added to the reaction mix to a final concentration of 10 nM and incubated for 30 min. Anti-His₆ Acceptor beads (PerkinElmer) were added to a final concentration of 20 ng/ μ L and incubated for an hour. The plate was read for chemiluminescence with the excitation wavelength of 680 nm and detection wavelength of 615 nm. This was done with a PerkinElmer Enspire Reader.

3.5.5 X-ray Crystallography

Apo POL κ RIR-Rev1-CTD crystals were obtained via sitting-drop vapor diffusion at 20°C by mixing 0.6 mM mouse POL κ RIR-Rev1-CTD in 25 mM HEPES (pH 7.2), 100 mM KCl, 30 mM CHAPS, and 2 mM TCEP with the mother liquor containing

0.1 M sodium acetate, 25% w/v PEG 4000 and 8% w/v isopropanol at a 1:1 drop ratio.

This crystallization condition was optimized by Dr. Jessica Wojtaszek.

The apo protein crystals were used to perform random micro-seed matrix screening. A sample solution containing a mixture of 0.6 mM mouse POL κ RIR-Rev1-CTD and 4 mM JH-RE-06 NaOH salt in a crystallization buffer of 25 mM HEPES (pH 7.0), 100 mM KCl, 16.7% 2-methyl-2,4-pentanediol (MPD) and 0.1% β -mercaptoethanol (BME), was mixed in a 1:1 ratio in the drop with various commercially available mother liquor solutions (Hampton, Qiagen). Diffraction-quality crystals were obtained in a mother liquor solution containing 20% PEG 3350 and 0.2 M magnesium formate. High-quality diffracting crystals were obtained through repeated seeding, in the final condition of 12.5 mM HEPES (pH 7.5), 50 mM KCl, 8.35% MPD, 0.05% BME, 10% PEG3350 and 0.1 M magnesium formate. The crystals were harvested and cryo-protected with the mother liquor containing 15% MPD and 1.88 mM JH-RE-06 NaOH salt.

X-ray diffraction data were collected on the SERCAT 22-ID beamline at Argonne National Laboratory. The datasets were reduced using XDS⁸⁷. The POL κ RIR-Rev1-CTD /JH-RE-06 complex structure was solved by molecular replacement using the molecular coordinates of the mouse Rev1-CTD and POL κ RIR components of the previously reported quaternary translesionsome structure (PDB ID 4FJO). The final coordinates

were built by iterative model building using COOT⁸⁸ and refined using PHENIX⁸⁹. The coordinates were deposited to the Protein Data Bank (PDB) with accession number of 6C8C.

3.5.6 *In Vitro* DSS Cross-linking Experiment

FLAG-tagged POL κ RIR-Rev1 CTD in a buffer containing 25mM HEPES (pH 7.0), 100 mM KCl, and 4 mM TCEP was mixed with either MPD (control, Hampton) or JH-RE-06 NaOH salt in MPD to yield a final solution containing 1 μ M protein, 5% MPD (v/v), and either 0 or 100 μ M compound. DSS (Thermo) was serially diluted in DMSO and added to the reaction mixture to yield DSS-to-protein molar ratios of 0:1, 0.5:1, 1:1, 5:1, 10:1, and 50:1 and a final DMSO concentration of 5% (v/v). The reaction mixture was incubated for 30 min at room temperature and then quenched with 1 M Tris (pH 8.5). SDS-loading dye containing 4 mM TCEP and 10.8 mM iodoacetamide (Thermo) was added to each sample to block free cysteines and for loading onto a 4-20% gradient SDS-PAGE gel (Bio-Rad). After gel electrophoresis, the samples were transferred to a 0.45 micron nitrocellulose membrane (Bio-Rad) for Western blotting. The blots were probed with a mouse monoclonal anti-FLAG primary antibody (Sigma), and a goat-anti-mouse, HRP-conjugated secondary antibody (LI-COR). The membrane was imaged using the LI-COR Odyssey system.

3.5.7 Cell Culturing

HT1080 cells (human fibrosarcoma cells, ATCC) were grown at 37 °C with 5% CO₂ in the following media: RPMI 1640 (Gibco), 10% (v/v) FBS (HyClone), and 1% Penicillin-Streptomycin antibiotic (Corning). MEF (Mouse Embryonic Fibroblasts) wild-type (*Rev1*^{+/+}) and *Rev1* knockout (*Rev1*^{-/-}) cells, A375 cells (human melanoma), and KP cells (mouse *Kras*^{G12D};*p53*^{-/-} lung adenocarcinoma) were grown at 37 °C with 5% CO₂ in the following media: DMEM (Gibco), 10% (v/v) FBS, and 1% Penicillin-Streptomycin antibiotic. LNCap cells (human prostate adenocarcinoma) were also grown at 37 °C with 5% CO₂ in RPMI 1640 (-phenol) (Gibco), 10% (v/v) FBS, and 1% Penicillin-Streptomycin antibiotic. AG01522 cells (human primary cells, Coriell Institute) were grown at 37 °C with 5% CO₂ in MEM (-Glutamine; +Earle's Salts; +Non-Essential Amino Acids) (Gibco) and 20% (v/v) FBS. All cells were trypsinized with 0.25% Trypsin-EDTA (Corning) for passaging.

This work was done by Dr. Nimrat Chatterjee from the Graham Walker group at MIT.

3.5.8 Clonogenic Survival Assay

Cells were plated in triplicate in 6-well plates at 37 °C for 24 hours. Cisplatin was added to the desired wells for 24 hours. Media was then changed, and JH-RE-06 (at 1.5 µM concentration) was incubated with untreated or cisplatin-treated cells for 24 hours. Media was changed and cells were subsequently allowed to recover for 7 days. For

colony staining, media was removed and the fixing reagent (50% methanol and 10% glacial acetic acid) was added. After 10 minutes, 0.02% Coomassie brilliant blue R-250 in methanol, acetic acid and water in a ratio of 46.5:7:46.5 (v/v/v) was added. Colonies that stained blue and contained at least 40 cells were counted. Relative cell survival or colony formation was calculated by dividing colony counts from treated samples by the DMSO or untreated controls.

This work was done by Dr. Nimrat Chatterjee from the Graham Walker group at MIT.

3.5.9 Cell Viability Assay

Relative viability of cells in response to JH-RE-06 and various DNA-damaging agents was assessed with the CellTiter-Glo Luminescence cell viability assay (Promega), which determines the number of metabolically active cells by measuring the relative amount of ATP in the culture. Cells were plated in each well of a 96-well, clear flat bottom plate (Corning). Increasing doses of drugs in various combinations were added to the plates after an incubation period of 24 hours. JH-RE-06 was dissolved in 0.1% DMSO and other drugs were dissolved in solvents recommended by the manufacturer. DMSO controls were run in parallel as control. The relative viability of cells was monitored after 24 hours of treatment by adding CellTiter-Glo Luminescence stain to an equilibrated plate. Luminescence was measured on a Tecan Spark 10M plate reader.

Relative luminescence was calculated by dividing the luminescence of treated samples with DMSO controls.

This work was done by Dr. Nimrat Chatterjee from the Graham Walker group at MIT.

3.5.10 HPRT Mutagenesis Assay

Cells were grown in HAT media (complete media with 100 μ M Hypoxanthine, 0.4 μ M Aminopterin and 16 μ M Thymidine) for 14 days to weed out spontaneous *HPRT* mutants. Cells were then treated with cisplatin (0.5 μ M) and incubated for 24 hours. Then, in fresh media, JH-RE-06 (1.5 μ M) was added to cells. After 24 hours, cells were trypsinized and washed with PBS. While 200-600 cells were plated in complete media in triplicates in 6-well plates to determine clonal efficiency, the rest were plated in complete media to allow the expression of the phenotype for 8 days. 500,000 cells per treatment were plated in sextuplicate in 10 cm dishes in 6-TG media to allow the growth of *HPRT*⁺ cells. Colonies were fixed with 50% methanol and 10% glacial acetic acid, stained with 0.02% Coomassie brilliant blue R-250 in methanol, acetic acid and water in a ratio of 46.5:7:46.5 (v/v/v), and counted after 14-20 days. Relative *HPRT* mutation frequency was calculated as the ratio of the number of *HPRT* colonies in 6-TG media to the number of surviving colonies plated in complete media to determine clonal efficiency.

This work was done by Dr. Nimrat Chatterjee from the Graham Walker group at MIT.

3.5.11 Mouse Xenograft Tumor Model

NCRNU-F (nude) female, 6-8-week-old mice (Taconic Biosciences) were divided into 4 groups (6 animals/group) for saline (control), cisplatin alone (1 mg/kg per animal), JH-RE-06 alone (1.6 mg/kg per animal), and cisplatin and JH-RE-06 combination treatments. Three million A375 (human melanoma) cells mixed in matrigel (Corning) were injected into the flank of each of the 6 mice per group to generate 10-12 xenograft tumors. The tumors were allowed to grow to a total volume of at least 100 mm³, then the drugs or saline (in 10% Ethanol, 40% PEG 400, and 50% saline) were injected directly into the tumor (100 µL injection volume). Treatments were carried out twice per week for 5 weeks. On the dosing day, tumors were measured with calipers, tumor volume calculated, weights were recorded, and then drugs or saline were injected directly into the tumors. The mice were sedated with isofluorane beforehand.

This work was done by Dr. Nimrat Chatterjee and Azucena Ramos from the Graham Walker and Michael T. Hemann groups at MIT.

Chapter 4. Risk of multidrug-resistant Bacterial

Infections in Cancer Patients

Bacterial infections are the most common life-threatening complication of cancer therapy. This is because cancer patients often develop neutropenia, or abnormally low levels of neutrophils, due to chemo and radiotherapy. Hence, many cancer patients are also immunosuppressed, and at an increased risk of bacterial infections. Use of invasive hospital equipment is another cause for increased risk of bacterial infections in cancer patients. The most frequent and serious type of infections are caused by Gram-negative bacteria, both community and hospital acquired.⁹⁰⁻⁹³ The necessary use of prophylactic treatment in cancer patients, along with the emergence of multidrug-resistant strains of Gram-negative pathogens, as well as difficulty in developing novel antibiotics, has significantly elevated the health risks of severe or fatal infections in cancer patients.⁹⁴ For example, 100% of patients with lymphoma or solid tumors who contracted bloodstream infections as a result of a carbapenem-resistant *Klebsiella pneumoniae* outbreak at the US National Institutes of Health Clinical Center died.⁹⁵ Similarly, 69% of patients with hematologic malignant tumors that contracted resistant *Klebsiella pneumoniae* infections at a cancer center died as a result of infection.⁹⁶

As stated above, prophylactic treatment is another cause of drug-resistant infections in cancer patients. Fluoroquinolone prophylaxis has proved effective in high-risk cancer patients but has resulted over time in the emergence of strains of *Escherichia coli* and *Pseudomonas aeruginosa* resistant to fluoroquinolone and other extended-spectrum β -lactam antibiotics.⁹⁷⁻⁹⁹ Yet another multidrug-resistant Gram-negative pathogen, *Acinetobacter baumannii*, which is becoming increasingly common, is mainly passed on to cancer patients due to healthcare exposure (e.g. time under intensive care, or exposure to medical equipment such as dialysis tubing) and has a mortality rate of 55% in general cancer patients, with a staggering mortality rate of 95% due to bloodstream infections in patients undergoing stem cell transplantation.¹⁰⁰⁻¹⁰¹

Thus, clinicians increasingly struggle to treat many bacterial infections in cancer patients, with fewer and fewer drugs remaining effective against a host of multidrug-resistant Gram-negative pathogens. It is clear that therapeutic needs are currently unmet and the best way forward is through the introduction of novel antibiotics to replace or supplement current therapeutic options.

4.1 The Lipid A Biosynthesis Pathway and LpxC in Gram-negative Bacteria

An attractive novel target is the Lipid A biosynthesis pathway, which is essential for the survival of Gram-negative bacteria. Lipid A forms the hydrophobic membrane

anchor of lipopolysaccharide (LPS), which is the major component of the outer leaflet in the outer membrane of Gram-negative bacteria (Figure 20). The Kdo₂-lipid A moiety is the minimal structure of lipid A required for bacterial growth. The biosynthetic pathway for this molecule consists of 9 enzymes in *E. coli* (Figure 21). Most enzymes in the constitutive lipid A biosynthesis pathway are conserved amongst Gram-negative bacteria. LpxA catalyzes the first step in the pathway, adding an acyl chain to the uridine diphosphate- N-acetylglucosamine (UDP-GlcNAc) moiety. This acylation step is unfavorable, therefore the next step, the deacetylation of UDP-3-O-GlcNAc, catalyzed by the enzyme LpxC, is the committing step. Seven more enzymes then complete the pathway to yield Kdo₂-LipidA.¹⁰²⁻¹⁰⁴

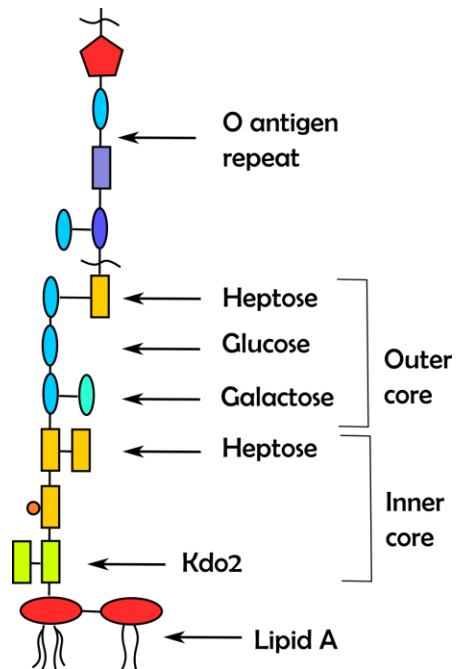


Figure 20: The Structure of Lipopolysaccharide

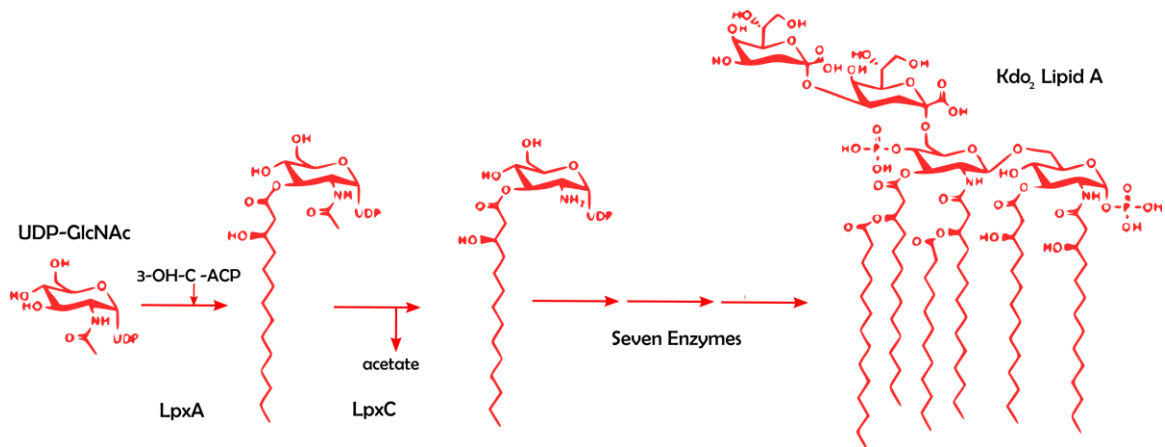


Figure 21: Kdo₂ Lipid A Biosynthesis

LpxC is a Zn^{2+} dependent metalloenzyme, which is important for the viability and virulence of Gram-negative bacteria. The structure of *Aquifex aeolicus* LpxC

(AaLpxC) shows two topologically similar domains, which form a novel four-layer α/β fold. Each domain has a distinct insert region, which combine to form the active site pocket (Figure 22). The Insert II region forms a unique hydrophobic passage to accommodate the acyl-chain of the substrate (as evidenced by a substrate-analog inhibitor bound solution structure and a myristyl-chain bound crystal structure).¹⁰⁵⁻¹⁰⁸

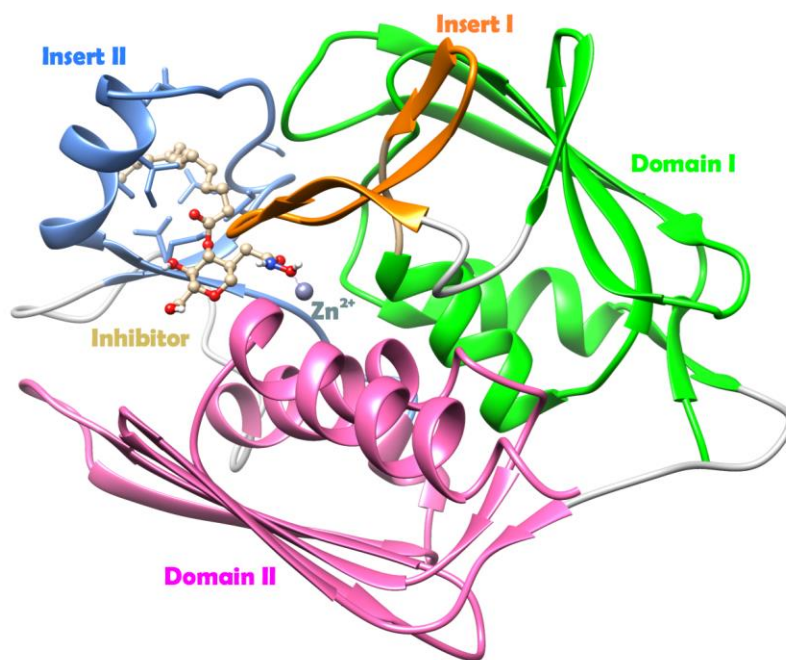


Figure 22: AaLpxC in Complex with Substrate Analog Inhibitor

Solution structure of AaLpxC in complex with TU-514 shows that two domains form a unique α/β fold, with unique insert regions that come together to form the active site. Insert region II forms a hydrophobic passage to bind the substrate acyl chain.

4.2 Targeting LpxC for Antibiotic Development

LpxC is conserved across Gram-negative bacteria, with an invariant HKXXD zinc-binding motif. It is vital for cell viability. Moreover, it has a unique structure and does not show any sequence homology to other classes of enzymes, including human metal deacetylases, making it an excellent target for the development of novel antibiotics

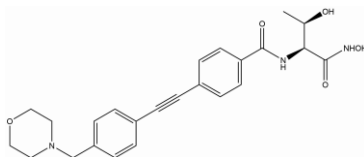
There are many known inhibitors of LpxC, many of which utilize a zinc-binding hydroxamic acid head group. The first reported inhibitor-bound structure of LpxC was with the substrate-analog inhibitor, TU-514. It chelates the catalytic zinc with its hydroxamic acid head group but did not show any antibacterial activity (Figure 23). Other hydroxamic acid inhibitors such as L-161,240 and BB-78485 showed activity against *E. coli* LpxC but not against other orthologs. The first reported inhibitor of LpxC, which showed antimicrobial activity against several orthologs, was CHIR-090.¹⁰⁹⁻¹¹¹ CHIR-090 has a bulky distal phenyl ring (Table 2), which reduces its activity against *Francisella tularensis*, *Acinetobacter baumannii* and *Rhizobium leguminosarum* LpxC orthologs. The hydrophobic passage comprised of Insert II can vary in width depending on the ortholog. We improved the activity of CHIR-090 by employing a narrower chemical scaffold based on the diacetylene group to generate a compound called LPC-011 (Table 2), which showed enhancement over its parent compound by many-fold over a wide variety of orthologs.¹¹²⁻¹¹³

Table 2: Chemical Structures of LpxC Inhibitors

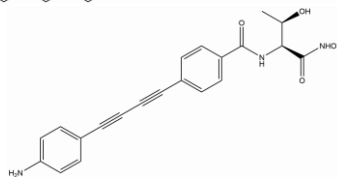
Name

Structure

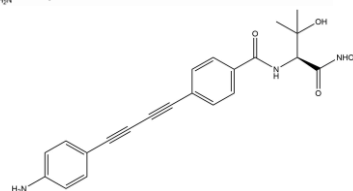
CHIR-090 (Thr)



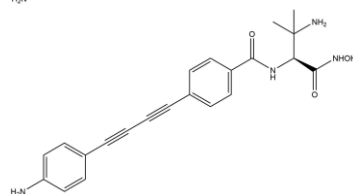
LPC-011 (Thr)



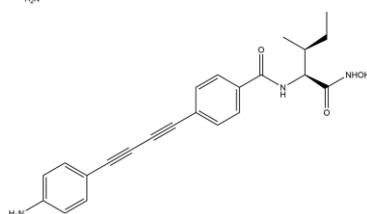
LPC-037 (β-hydroxy-Val)



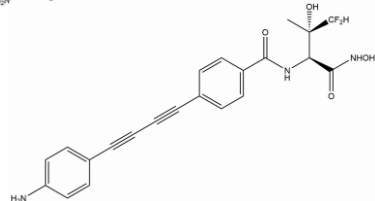
LPC-040 (β-amino-Val)



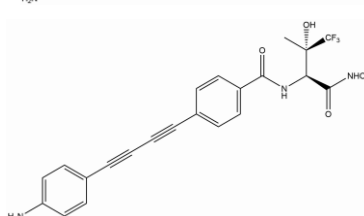
LPC-023 (Ile)



LPC-058



LPC-083



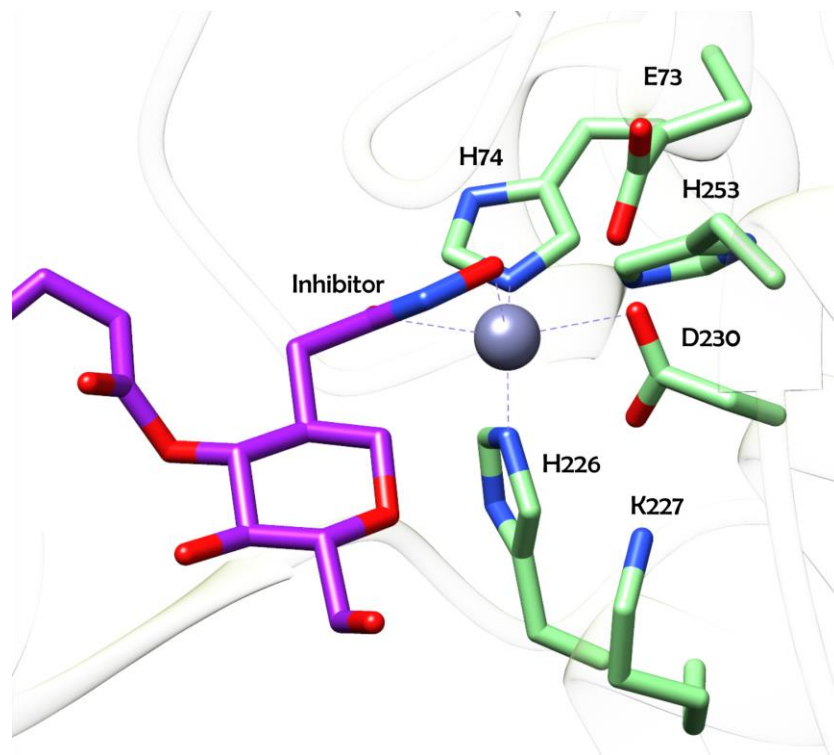


Figure 23: LpxC Inhibitors Often Feature a Hydroxamate Head Group

This view of the conserved active site of LpxC (AaLpxC) shows important residues that are involved in catalysis, coordination of the zinc atom and interacting with the substrate. It also shows the inhibitor TU-514 featuring a hydroxamic acid head group, frequently found in LpxC inhibitors, chelating the zinc atom.

While crystal structures of both the CHIR-090 and LPC-011 bound LpxC molecules exist, the information obtained about protein-ligand interactions through these static models can only be used so far towards further optimizing inhibitors. In reality, both the protein and ligand are dynamic, sampling minor conformations in solution not detectable by crystallography. We propose that this dynamic information

can be gleaned through solution NMR spectroscopy, and in conjunction with information obtained from crystal structures, can be used to further optimize current inhibitors.

Chapter 5. Optimization and Characterization of an LpxC Inhibitor using Static and Dynamic Information

We know from an analysis of the vast database of high-resolution protein structures that amino acid side-chains favor certain rotameric conformations.¹¹⁴ Movement between conformations can happen over a wide range of timescales, happening fast (ns scale) in solvent-exposed residues, and much more slowly (ms) in proteins cores. Movement between rotameric conformations can be approximated to switching or flipping between states.¹¹⁵ High-resolution X-ray crystal structures show the predominant conformation that the side chains or functional groups of a protein or ligand can adopt, but this information is static, and we aimed to discover dynamic information to enhance our understanding of the binding of LpxC inhibitors using solution NMR, so as to design a better inhibitor.

5.1 The χ_1 Angle of the Threonyl Head Group of CHIR-090 and LPC-011 Favors the Trans Conformation but can Sample other Conformations

To determine the dominant conformation of LPC-011 in complex with LpxC, and also to have a reference for our solution studies, we solved the crystal structure of LPC-011 with AaLpxC. The structure showed that the threonyl head group of LPC-011 favors

a *trans* χ^1 angle (180°) (Figure 24). This is surprising as the *trans* conformation is energetically unfavorable, found in only 7% of known protein structures.¹¹⁴

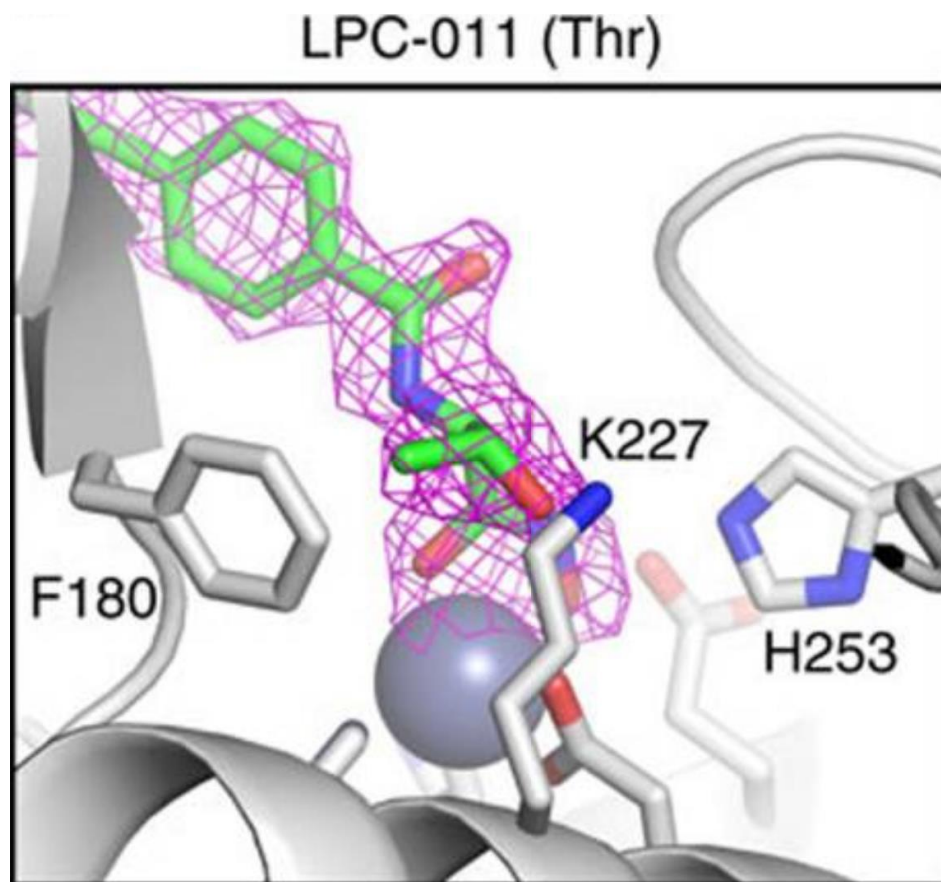


Figure 24: Threonyl Head Group of LPC-011 Features *Trans* χ^1 Angle

The crystal structure of LPC-011 with AaLpxC exhibits an unfavorable, *trans* χ^1 angle of the threonyl headgroup. LpxC shown in ribbon, with important residues and LPC-011 shown in stick model. Purple mesh represents omit map ($2mF_o-DF_c$) at 1.0σ

The unfavorable conformation observed in the crystal structure prompted us to assess whether the inhibitor could access other states in solution. To this end, we aimed

to determine the value of dihedral angles that define side chain conformations by measuring scalar J-coupling values between atoms that bound the three bonds that define the dihedral angle (3-bond J-coupling). Specific dihedral angles have characteristic J-coupling values (Table 3).¹¹⁶ A large $^3J_{\text{NC}\gamma 2}$ or $^3J_{\text{CC}\gamma 2}$ value is associated with a *trans* relationship between the amide nitrogen or carbonyl carbon and the C $\gamma 2$ methyl group of the threonyl head group, corresponding to a *gauche*- χ^1 angle of -60° , whereas a small value is indicative of a *gauche*+ or *gauche*- relationship between the two atoms, corresponding to a *trans* χ^1 angle of 180° or *gauche*+ χ^1 angle of 60° respectively.¹¹⁴ Any value in between can be considered to be a weighted average of the *trans* and *gauche* conformations. Thus a combination of the $^3J_{\text{NC}\gamma 2}$ and $^3J_{\text{CC}\gamma 2}$ scalar coupling measurements can be used to determine the relative populations of all three rotamers of the threonyl head group.

Table 3: Characteristic 3J coupling Values for Threonine Sidechain

3-bond J-coupling	J_{trans}	J_{gauche}
$^3J_{\text{NC}\gamma 2}$	1.9	0.2
$^3J_{\text{CC}\gamma 2}$	3.4	0.4

To measure scalar coupling values, we synthesized isotopically-labelled CHIR-090 and LPC-011 (both have threonyl headgroups). The $^3J_{\text{NC}\gamma 2}$ and $^3J_{\text{CC}\gamma 2}$ coupling values of LPC-011 were 0.58 ± 0.05 Hz and 0.77 ± 0.04 Hz, respectively, corresponding to a preference for the *trans* χ^1 angle (Figure 25a-b). This is consistent with the crystal structure of LPC-011 in complex with AaLpxC (Figure 24). These results additionally showed that the threonyl side chain of LPC-011 can access the *gauche*- and *gauche*+ χ^1 conformations to a smaller degree. CHIR-090 showed a similar distribution of conformational states, predominantly sampling the *trans* χ^1 angle, with two minor conformations in both the *gauche*- and *gauche*+ χ^1 states (Figure 25a-b).

We used this information to optimize LPC-011, by combining the envelope that defines the conformations in the two most populated states (*trans* and *gauche*-) to delineate a new inhibitor envelope (Figure 25c). This strategy indicated that the C β position could accommodate three substitutions. To test this, we added two methyl substitutions at the C β position, with the third, solvent-accessible substitution being one of two hydrophilic groups: hydroxyl (LPC-037) or amino group (LPC-040) (Table 2). The crystal structure of LPC-040 with *Pseudomonas aeruginosa* Lpxc (PaLpxC) confirmed our prediction. The two methyl groups form favorable hydrophobic interactions with conserved residues (F191^{PaLpxC} (F180^{AaLpxC}) and K238^{PaLpxC} (K227^{AaLpxC})). The amino group

forms a water-mediated hydrogen bond with the carbonyl oxygen of F191^{PaLpxC} (F180^{AaLpxC}) (Figure 26).

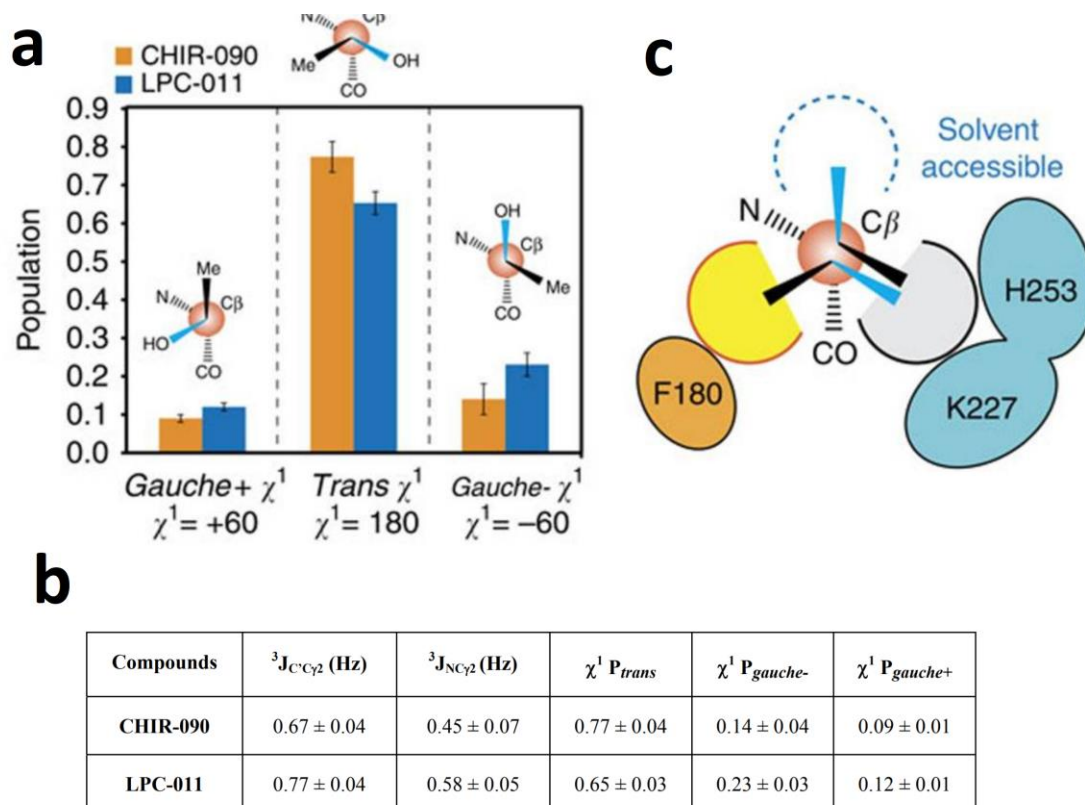


Figure 25: LPC-011 and CHIR-090 Access Minor Conformations in Solution, Defining an Inhibitor Envelope

- (a) Visual representation of the conformations dynamically accessible by LPC-011 and CHIR-090, (b) Specific 3J coupling values, along with population sizes, visually represented in (a), and (c) Combining the two most populated conformations yields a hidden, dynamically accessible inhibitor envelope, suggestive of three substitutions at the C β position.

LPC-040 (β -amino Val)

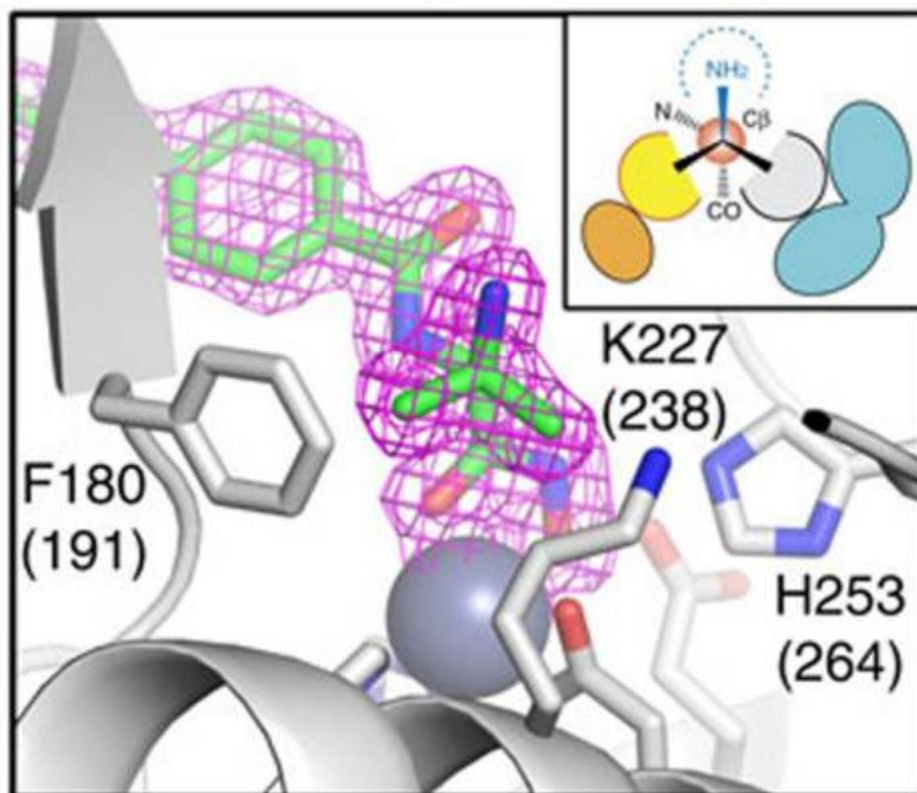


Figure 26: LPC-40 in Complex with PaLpxC

The two methyl substitutions at the C β position form favorable hydrophobic interactions with conserved residues and the amino group substitution forms a water-mediated hydrogen bond with a conserved residue. PaLpxC shown in ribbon, with important residues and LPC-040 shown in stick model. Purple mesh represents omit map ($2mF_o - DF_c$) at 1.0σ . Residue numbers in parentheses, with corresponding AaLpxC residue numbers shown.

5.2 Triple Substitution at C β Position of Threonyl Side-chain Yields Enhanced Inhibitors

We tested the ability of LPC-037 and 040 to inhibit *Escherichia coli* LpxC (EcLpxC) by using an enzymatic assay. CHIR-090 and LPC-011 both exhibit two-step time-dependent binding, with a rapid step leading to a transient “EI” complex, followed by a slowly formed, stable “EI*” complex.¹¹⁰ Therefore, we measured inhibition by measuring K_i^* values, focusing on the formation of the EI* complex. CHIR-090 and LPC-011 have K_i^* values of 153 \pm 8 pM and 26 \pm 1 pM, respectively. The triple- C β -substituted compounds LPC-037 and LPC-040 both showed enhanced LpxC inhibition, with K_i^* values of 14 \pm 1 pM and 12 \pm 1 pM, respectively (~2-fold improvement over LPC-011, ~10-fold improvement over CHIR-090) (Figure 27, Table 5). This is exciting as our elucidation of minor states using solution NMR led to discovery of a space that the inhibitor could

occupy and aided in new substitutions that yielded markedly more potent inhibitors.

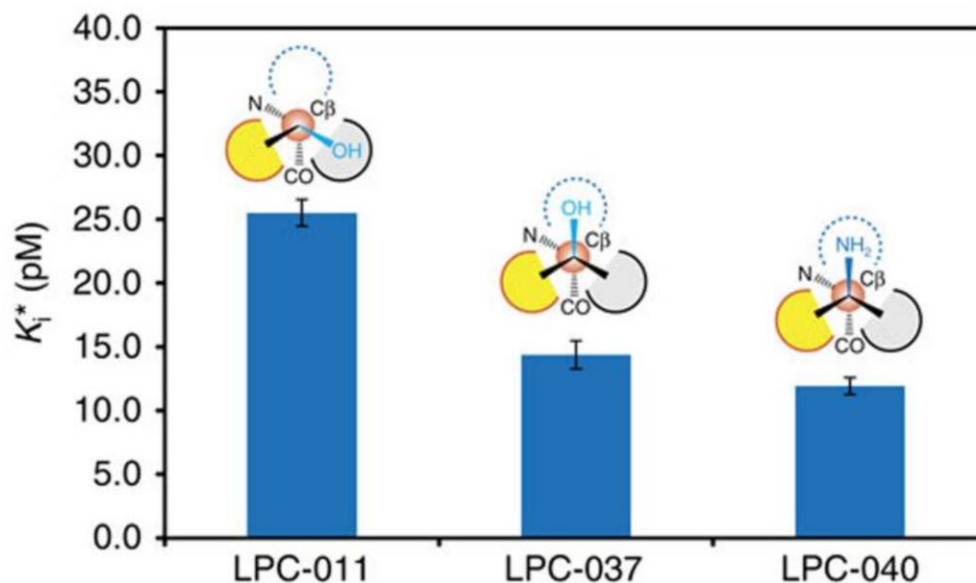


Figure 27: LPC-037 and LPC-040 are Better Inhibitors than LPC-011

The triple substitutions at the C β position yield more potent inhibitors than parent compound

5.3 Expansion of the Inhibitor Envelope is a Successful Strategy for Improving LpxC Inhibitor in the γ Position

After the successful optimization of LpxC inhibitors in the C β position of the threonyl head group using the strategy of delineating a hidden, dynamically accessible inhibitor envelope, we investigated whether the envelope could be further expanded at the γ position. For this we used LPC-023, which contains an isoleucine-hydroxamate head group (Table 2). Isoleucine can be considered as having a threonine scaffold, with a substitution of the O γ 1 group of threonine with the C γ 1-C δ 1 group of isoleucine. We

determined the complex structure of LPC-023 with AaLpxC (Figure 28). We saw two copies of the complex in the asymmetric unit, in one of which the catalytic H253 is flipped outwards, away from the active site. Since such a distorted active site has not been seen previously, we believe it to be a crystallization artifact, and therefore focused our attention on the other protomer. The structure shows that the LPC-023 head group is in a *trans* χ^1 state, similar to the CHIR-090 and LPC-011 threonyl group. The C δ 1 methyl group exhibits a *gauche*⁺ χ^2 conformation relative to the C α atom. Since the *gauche*⁺ χ^2 rotamer is only observed in less than 5% of known protein structure, this rotamer represents a high-energy state of the inhibitor. We therefore tested whether the C δ 1 group could access alternative χ^2 states in solution.

The isoleucine C δ 1 chemical shift is dependent on its χ^2 angle. A downfield shifted chemical shift is indicative of a *gauche*⁺ or *trans* rotamer, and an upfield shifted chemical shift is indicative of the *gauche*⁻ rotamer (Table 4, Figure 28a).¹¹⁷ The LpxC-bound inhibitor has a C δ 1 chemical shift of 15.2 p.p.m., indicating that it exists entirely either in the *trans* or *gauche*⁺ conformation. However, the free inhibitor has a C δ 1 chemical shift of 12.8 p.p.m., which would indicate an averaging between the three possible rotameric states. To determine the exact conformations, we measured the scalar coupling value between the C δ 1 and C α atoms. A *trans* conformation results in a large scalar coupling value of ~3.7 Hz, whereas a *gauche* conformation yields a small coupling

of ~1.5 Hz. Our $^3J_{\text{CaCb1}}$ measurement yields a value of ~2.05 Hz, corresponding to ~75% of the population being in the *gauche*⁺ χ^2 state and ~25% in the *trans* state (Figure 28b). Thus, we concluded that the inhibitor is able to sample both the *gauche*⁺ and *trans* states of the χ^2 rotamers, whereas the *gauche*⁻ state is dynamically inaccessible.

Our NMR studies thus expand the inhibitor envelope, and indicate room for two methyl-sized substitutions to form interactions with the catalytically important histidine and lysine residues. We chose fluorine as a substituent, as its size is comparable to the methyl group, and the fluorine atom is both strongly hydrophilic and lipophilic. This makes it ideal for forming potential hydrophobic interactions with the protonated histidine side chain and the lysine stem, or electrostatic interactions with a protonated histidine imidazole ring and a positively charged lysine side chain ammonium group (Figure 28c). We therefore introduced a di-fluoro substitution to the methyl group of LPC-037 to yield LPC-058 (Table 2). The complex structure of LPC-058 with PaLpxC shows that the inhibitor adopts the expected ligand conformation, with the β -methyl group occupying the hydrophobic pocket, forming van der Waals interactions with F191 (F180^{AaLpxC}), the β -hydroxyl occupying the solvent pocket, forming a water-mediated hydrogen bond with the backbone of F191 (F180^{AaLpxC}), and the difluoromethyl group facing towards the catalytically important H264 (H253A^{aLpxC}) and K238 (K227^{AaLpxC}). One of the fluorine atoms exhibits a *gauche*⁺ rotamer relative to the C α atom and forms a

hydrogen bond with Nε1 atom of the protonated H264, while the second fluorine atom adopts a *trans* rotamer and forms an electrostatic interaction with the ammonium group of K238. Thus the expanded inhibitor envelope elucidated with our NMR studies yields an inhibitor that forms optimal and favorable interactions with the active site residues of LpxC (Figure 29).

Table 4: Cδ1 Chemical Shift, Depending on χ^2 Rotameric Angle

<i>Trans</i>	<i>gauche</i> ⁺	<i>gauche</i> ⁻
	>14.8	<9.3

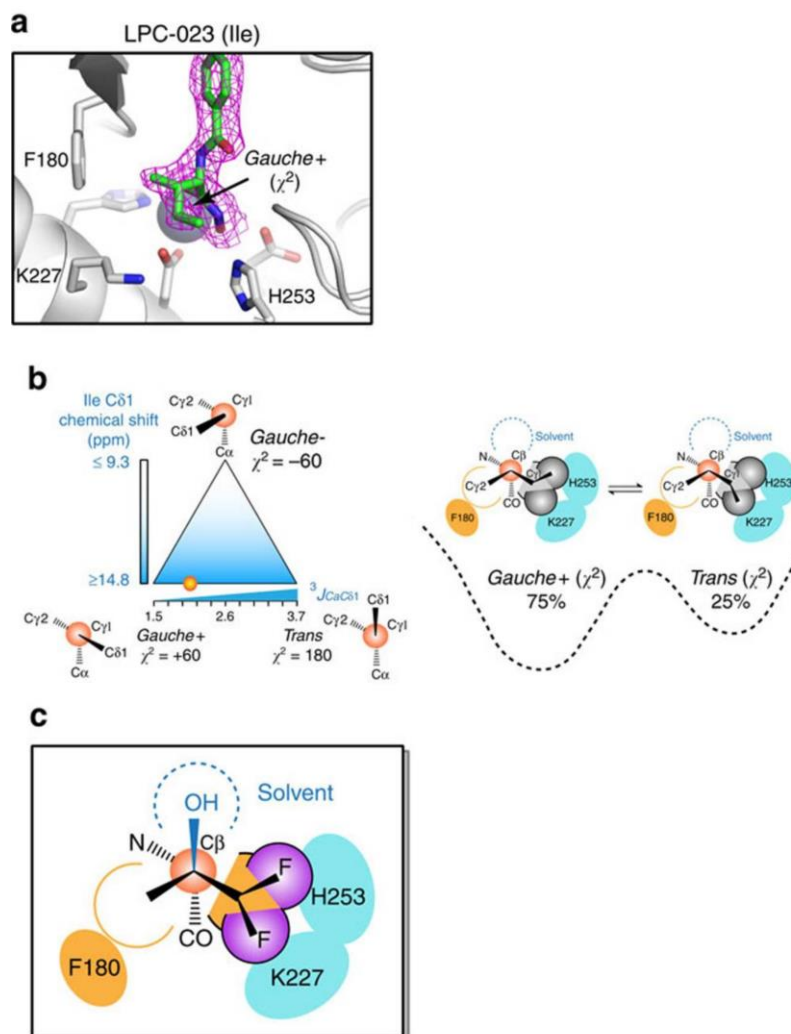


Figure 28: Optimization of LPC-023 with Help of Extended Inhibitor Envelope

Crystal structure of AaLpxC in complex with LPC-023 exhibits a *gauche+* χ^2 rotamer. AaLpxC shown in ribbon, with important residues and LPC-023 shown in stick model. Purple mesh represents omit map ($2mFo-DFc$) at 1.0σ . **(b)** $C\delta 1$ chemical shift and $3J_{CaC\delta 1}$ coupling measurements of protein-bound of LPC-023 reveal a dynamic equilibrium between *gauche+* and *trans* χ^2 rotameric states (75 and 25% respectively), and **(c)** Delineation of hidden inhibitor envelope and suggested substitutions.

LPC-058
(β -difluoromethyl-L-*allo*-threonine)

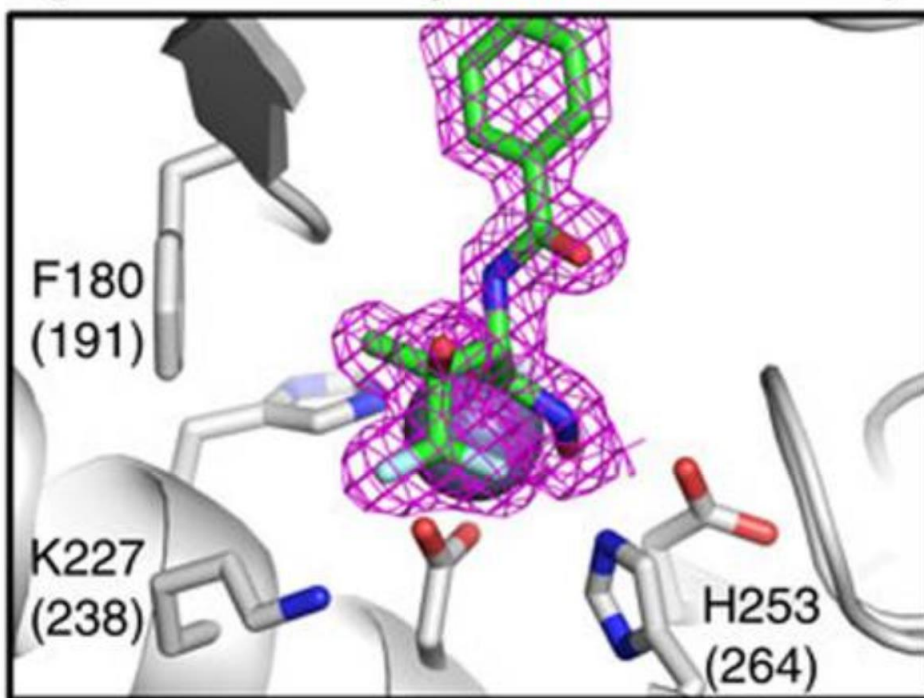


Figure 29: LPC-058 Forms Optimal Interactions with LpxC Active Site Residues

LPC-058 optimally occupies the PaLpxC binding pocket (residue numbers in parentheses, with corresponding AaLpxC residue numbers shown). PaLpxC shown in ribbon, with important residues and LPC-058 shown in stick model. Purple mesh represents omit map (2mFo-DFc) at 1.1 σ .

5.4 LPC-058 Exhibits Enhanced Inhibition and Antibiotic Activity in Comparison to LPC-011 and CHIR-090

To examine whether the added interactions as a result of the expanded envelope translate into a better inhibitor, we measured the kinetics of LPC-058 binding to EcLpxC. LPC-058 is a staggeringly potent inhibitor. Similar to LPC-011 and CHIR-090, it displayed slow-binding kinetics consistent with the fast step of the formation of an initial encounter complex (EI) followed by a slow isomerization to the EI* complex, with an inhibition constant (K_i^*) of 3.5 ± 0.2 pM. This is 7-fold more potent than LPC-011 and 44-fold more potent than CHIR-090 (Table 5).

We also measured the minimum inhibitory concentration (MIC) values of LPC-058 against a range of Gram-negative pathogens to see how it compares in antibiotic activity with LPC-011 and CHIR-090. LPC-058 showed improvement against all Gram-negative bacterial strains tested, with an enhancement of 2- to 25-fold compared to LPC-011 and 5- to 128-fold relative to CHIR-090 (Figure 30). Of special note is the antibiotic activity of LPC-058 against *Acinetobacter baumannii* (MIC=0.39 $\mu\text{g ml}^{-1}$), making it the first reported LpxC inhibitor with an MIC value below 1 $\mu\text{g ml}^{-1}$ against this clinically important pathogen *in vitro*.

5.5 Discussion

It is well known that proteins are not static molecules and residues and even entire chains and secondary and tertiary structures can have dynamic movements and sample different conformations. On the contrary, the conformational dynamics of small molecules bound to proteins has been rarely investigated and certainly not exploited for drug design. In this work we show that small molecule inhibitors of LpxC are able to access alternative, minor configurations in solution, using which information we have been able to define a dynamically accessible inhibitor envelope not seen in crystal structures. This expanded inhibitor envelope provides new insights and suggests molecular substitutions to optimize inhibitors. For LpxC inhibitors, we have shown that the expansion of the inhibitor envelope yields an extraordinarily potent inhibitor, LPC-058, which exhibits enhancement over its parent compounds LPC-011 in terms of inhibition (7-fold improvement) and antibiotic activity (2- to 25-fold improvement) with just three additional substitutions. This makes LPC-058 the most potent LpxC inhibitor *in vitro* and with the most broad-spectrum antibiotic characteristics *in vitro*. This highlights the therapeutic potential of LPC-058 as a broad-spectrum antibiotic against many clinically relevant Gram-negative bacteria.

It can be argued that some features of the inhibitor envelope can be intelligently guessed from the structural information available of the CHIR-090 and LPC-011 bound

LpxC complex structures, such as the hydrophilic substitution in the solvent-accessible pocket at the C β position. Indeed, inhibitors with head groups similar to LPC-037 and LPC-040 have been previously reported.¹¹⁸⁻¹¹⁹ However, the delineation of two methyl-sized pockets at the O γ 1 position of the threonyl head group could have not been predicted based on the analysis of the crystal structure alone. In fact, the most widely used substitution of a pro-*R*-methyl group is the CF₃ group, in contrast to the CF₂ group employed in LPC-058. A compound with the CF₃ substitution (LPC-083, Table 2) was a worse inhibitor than LPC-037 by ~9-fold, and by ~5-fold than LPC-011. It is also a worse antibiotic than LPC-011 by ~2.5-fold in *E.coli*. (Figure 31).

This work highlights the potential of drug optimization with the use of dynamic information, which can reveal a hidden, dynamically accessible inhibitor envelope. This is unique from the singular use of static information obtained from crystallographic structures for inhibitor optimization. This strategy can be used in various systems for lead drug optimization, especially with peptide or peptidomimetic inhibitors.

This work also highlights the therapeutic potential of LpxC inhibitors and their ability to fill the void of antibiotics for current and future therapeutic needs for multi-drug resistant infections. Future work will include optimization efforts for the tail group of LpxC, so as to aid in the development of better broad-spectrum antibiotic properties, and optimization to enhance inhibitor solubility, stability, and to decrease toxicity.

Future work will also focus on the development of substrate-analog inhibitors of LpxC, which will serve the dual purpose of providing more concrete evidence for the catalytic mechanism of LpxC and of elucidating a new class of LpxC inhibitors.

Table 5: Inhibition Constants for LpxC Inhibitors

Compound	Ki*(pM)
CHIR-090	152 ± 8
LPC-011	26 ± 1
LPC-037	14 ± 1
LPC-040	12 ± 1
LPC-058	3.5 ± 0.2
LPC-083	1254

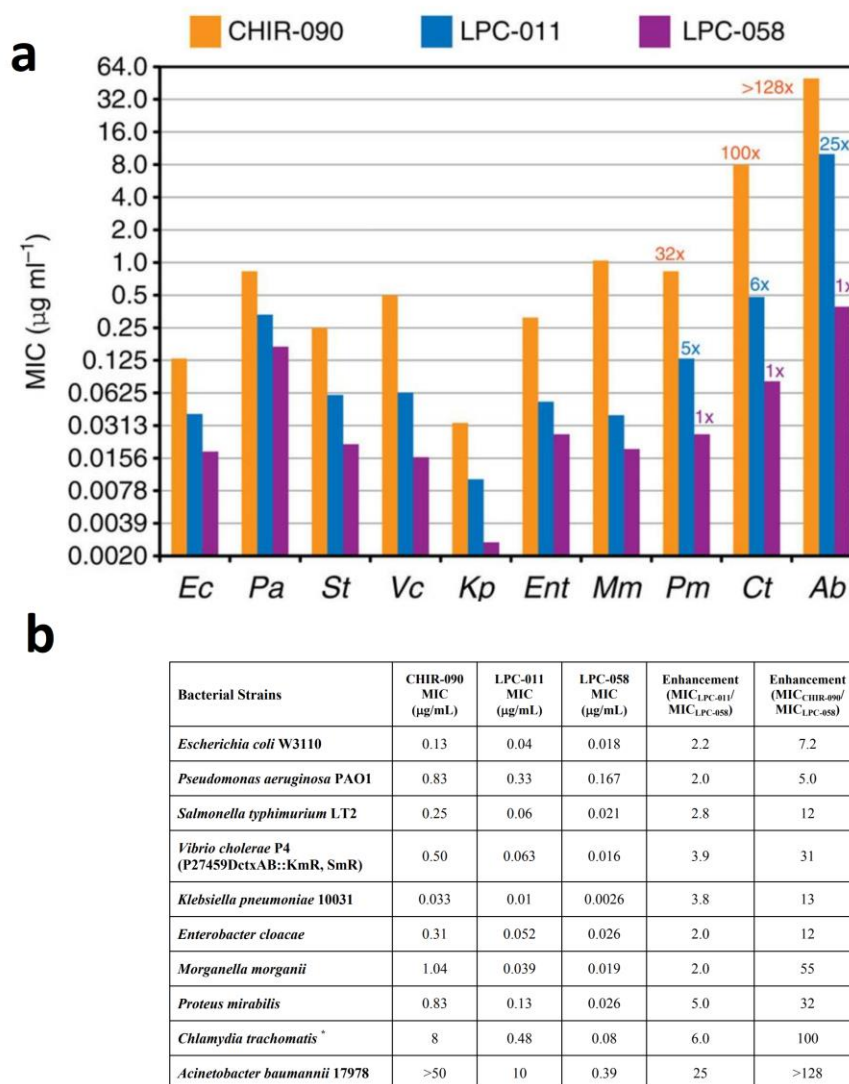


Figure 30: LPC-058 is a Better Antibiotic at a Broad Spectrum Level than CHIR-090 and LPC-011

*Minimum chlamydicidal concentration (MCC) measured

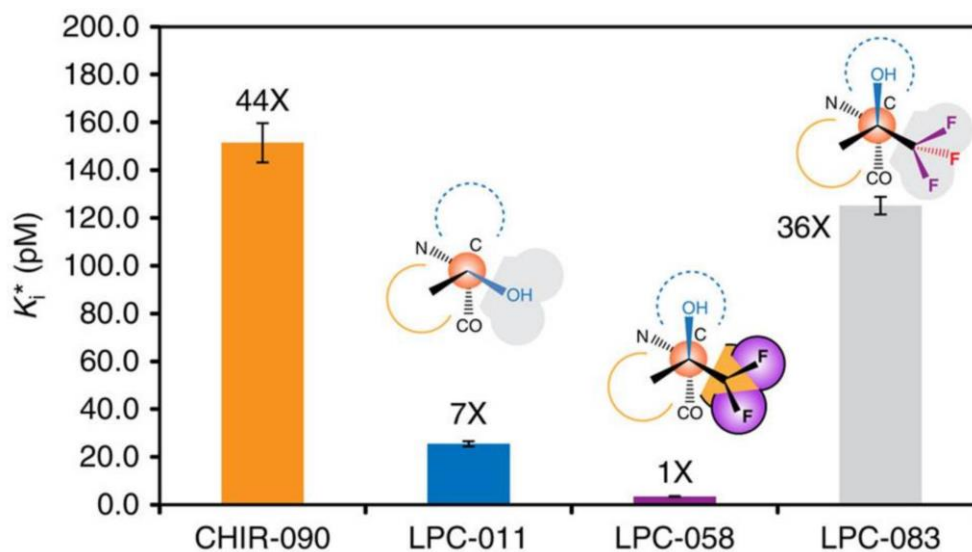


Figure 31: LPC-058 is a Potent Inhibitor Compared to Parent Compound

The difluoro-substituted LPC-058 is a much more potent inhibitor than its parent compound LPC-011, and grandfather compound, CHIR-090. In contrast, the trifluoro-substituted LPC-083 is worse than both LPC-058 and LPC-011.

5.6 Methods

5.6.1 Crystallographic Studies

Protein samples of AaLpxC and PaLpxC were prepared as described previously¹¹¹. To prepare the crystallographic samples, inhibitors dissolved in DMSO were mixed to four-fold excess with 8 mg ml⁻¹ AaLpxC (1-275, C181A) in the following buffer: 100 mM potassium chloride, 2 mM dithiothreitol (DTT) and 25 mM HEPES (pH 7.0) or 12 mg ml⁻¹ PaLpxC (1-299, C40S) in the following buffer: 50 mM sodium chloride, 2 mM TCEP and 25 mM HEPES (pH 7.0), respectively. For PaLpxC, 10 mM zinc sulfate was added as a crystallization additive. The protein-inhibitor mixture was

incubated at room temperature for 30 min. Sitting-drop vapor diffusion trays were incubated at 20 °C. Crystallization trials were done with commercially available screens (Hampton, Qiagen). The protein-inhibitor sample was mixed 1:1 with the mother liquor solution in the drop well. The crystal screening yielded microcrystals for the AaLpxC/LPC-011 complex (mother liquor: 0.1 M HEPES (pH 7.0) and 15% PEG 8000) and for the AaLpxC/LPC-023 complex (mother liquor: 0.18 M ammonium chloride, 11.8% PEG3350 and 4% 1,3-propanediol). The microcrystals were used to prepare micro-seeding stocks by the Seed-Bead protocol (Hampton). Diffraction quality crystals were obtained by using streak-seeding with a fine streaking wand (Hampton) The final crystallization reservoirs were as follows: 0.05 M ammonium acetate and 10% PEG3350 (AaLpxC/LPC-011) and 0.18 M ammonium chloride, 11.8% PEG3350 and 10% 1,3-propanediol (AaLpxC/LPC-023). Diffraction-quality crystals of the PaLpxC/LPC-040 and PaLpxC/LPC-058 complexes were obtained in the following mother liquor: 0.1 M sodium acetate trihydrate (pH 4.8–5.1) and 2.4–2.6 M ammonium nitrate. Crystals were cryoprotected using the respective mother liquor solutions with 30% MPD (AaLpxC/LPC-011), 30% ethylene glycol (AaLpxC/LPC-023) or 10% glycerol (PaLpxC/LPC-040 and LPC-058), before flash-freezing.

Data sets of the PaLpxC/inhibitor complexes were collected in-house at the X-ray core facility with a Rigaku MicroMax-007 HF rotating anode generator and R-Axis IV++

detector. Data sets of the AaLpxC/inhibitor complexes were collected at the SER-CAT 22-ID beamline at the Advanced Photon Source at Argonne National Laboratory. The X-ray diffraction data were reduced using HKL2000¹¹⁷ or XDS⁸⁶. The crystal structures were solved by molecular replacement with Phaser⁸⁰ using previously known LpxC structures for the AaLpxC/inhibitor complexes (PDBID 3P3C) and PaLpxC/inhibitor complexes (PDBID: 3P3E). Iterative model building and refinement was carried out using COOT⁸⁷ and PHENIX⁸⁸. The 2mFo-DFc omit maps were generated using PHENIX. X-ray data are summarized in Table 6. The coordinates for the X-ray structures have been deposited to the PDB with accession codes of 5DRO (AaLpxC/LPC-011), 5DRQ (PaLpxC/LPC-040), 5DRP (AaLpxC/LPC-023) and 5DRR (PaLpxC/LPC-058).

The PaLpxC/inhibitor complex structures were determined by Dr. Chul-jin Lee.

Table 6: X-ray data collection and refinement statistics for LpxC inhibitors

	AaLpxC/ LPC-011	PaLpxC/ LPC-040	AaLpxC/ LPC-023	PaLpxC/ LPC-058
Data collection				
Space group	P 21 21 21	P 21 21 21	P1	P 21 21 21
Cell dimensions				
a,b,c (Å)	54.8, 74.8, 135.9	52.4, 74.0, 88.6	45.7 50.4 61.7	52.8, 73.9, 88.2
α, β, γ (°)	90, 90, 90	90, 90, 90	80.3, 71.7, 88.9	90, 90, 90
Resolution (Å)	67.94-2.01 (2.08-2.01)	50.00-1.63 (1.66-1.63)	50.00-1.84 (1.87-1.84)	28.32-1.59 (1.68-1.59)
<i>R_{sym}</i> or <i>R_{merge}</i>	11.9 (51.3)	5.4 (40.3)	5.3 (31.1)	4.7 (42.4)
Mean <i>I</i> / σ <i>I</i>	21.67 (5.05)	16.56 (4.25)	24.5 (3.2)	15.01 (2.45)
Completeness (%)	97.2 (92.1)	99.7 (99.6)	97.7 (96.5)	97.7 (94.5)
Redundancy	14.4 (11.1)	6.3 (6.6)	4.4 (4.4)	5.0 (4.8)
Unique reflections	36885 (3708)	43373 (4171)	40342 (3995)	46039 (4405)
Refinement				
<i>R_{work}</i> / <i>R_{free}</i>	0.156/0.186	0.170/0.203	0.156/0.192	0.179/0.210
No. of atoms	4840	2742	4619	2690
Protein	4370	2332	4296	2328
Ligand/ion	70	147	64	101
Water	400	263	259	261
Avg. B-factors	21.9	26.6	34.9	26.5
Protein	20.8	24.8	34.5	25.5
Ligand/ion	70	37.2	37.3	31.8
Water	31.9	36.6	40.9	33.7
R.m.s. deviation				
Bond length (Å)	0.002	0.009	0.006	0.004
Bond angle (°)	0.69	1.16	0.99	0.8
Ramachandran				
Favored (%)	96.8	97.4	97	97.7
Outliers (%)	0	0	0	0

parentheses values are for high resolution shells

5.6.2 NMR Measurements

Deuterated AaLpxC was expressed and purified as described previously¹⁰⁷. The AaLpxC-inhibitor solutions were prepared by adding inhibitor to the purified protein in 5% deuterated DMSO in a 1:2 protein-inhibitor molar ratio, and incubated initially at room temperature and then at 45 °C. Samples were concentrated and exchanged into NMR buffer (25 mM sodium phosphate pH 7.0, 100 mM KCl, 5% deuterated DMSO and 100% D₂O). The NMR sample concentration was ~1 mM.

The scalar coupling measurements (³JC'Cγ2 and ³JNCγ2) for the AaLpxC-CHIR-090/LPC-011 complexes were obtained on a Bruker 700 MHz NMR spectrometer at 45 °C, using J-modulated 1H–13C constant-time HSQC experiments^{122,123}. The reference and scalar coupling-modulated CT-HSQC spectra were recorded in an interleaved manner (constant-time delay (2T) = 57.4 ms, 13C maximum evolution time = 12.1 ms). Data were processed using NMR pipe¹²⁴ with eightfold zero-filling in the ¹³C (indirect) dimension. The peak intensities were measured using Sparky 3¹²⁵, and the ³JC'Cγ2 and ³JNCγ2 couplings were calculated from the reference spectrum (I_{ref}) and the J-modulated spectrum (I_{mod}) according to equation (1):

$$\frac{I_{mod}}{I_{ref}} = \cos(2\pi JT) \quad (1)$$

Rotameric populations were calculated using the three-site jump model¹¹⁵ using self-consistent parameterization of 3J coupling values¹¹⁶.

The scalar coupling value ($^3J_{CaC\delta 1}$) for the AaLpxC/LPC-023 complex was obtained with an Agilent 800 MHz NMR spectrometer at 37 °C using a J-modulated constant-time ^{13}C HSQC experiment using selective Ile-C α inversion pulses. The $^3J_{CaC\delta 1}$ coupling was calculated using equation (1). Since the C $\delta 1$ chemical shift of LPC-023 (15.2 p.p.m.) excludes the *gauche*- χ^2 rotamer, the remaining rotamers were calculated from $^3J_{CaC\delta 1}$ based on the two-site jump model between the *gauche*+ and *trans* configurations¹¹⁷.

The NMR study was done by Dr. Qinglin Wu and the description is adapted from our published manuscript¹²⁶.

5.6.3 Enzymatic Assays

The radio-labelled substrate for the LpxC enzymatic assays, [α - ^{32}P] UDP-3-O-[(R)-3-hydroxymyristoyl]-N-acetylglucosamine, and the un-labelled carrier substrate were prepared as described previously¹²⁷. The assays were performed with 5 μ M substrate at 30 °C in the following buffer: of 25 mM HEPES (pH 7.4), 100 mM KCl, 1 mg ml⁻¹ BSA and 2 mM DTT. Inhibitors serially diluted in DMSO were added to the reaction mixture with a 10-fold dilution. LpxC protein was added to the reaction mixture with 1:4 dilution to the final concentration as specified below.

The K_M value was determined by varying substrate concentrations (0.4- 50 μM) with 0.2 nM of LpxC. To study the slow, tight-binding inhibition, LpxC activity was measured in the presence of varying inhibitor concentrations. The product conversions were determined from 15 s up to 2 h after addition of 0.2 nM enzyme for CHIR-090 and LPC-011 in the presence of 5 μM substrate. LPC-058 inhibition was assayed in the presence of 30 μM substrate and 0.1 nM enzyme such that k_{obs} (rate of transition from EI to EI*) can be extracted under the slow, but not tight-binding conditions¹²⁸. Equation (2), defined by t (time), v_s (steady-state rate), v_i (initial rate), k_{obs} (rate of transition from EI to EI*) and c (baseline constant), was used to fit the data:

$$[P] = v_s t + \frac{v_i - v_s}{k_{\text{obs}}} [1 - e^{-k_{\text{obs}} t}] + c \quad (2)$$

The K_i^* was determined by studying the rate of product accumulation after the EI* complex formation. IC₅₀ curves for were determined in the presence of 20 pM the enzyme and varying inhibitor concentrations. The Morrison's quadratic equation (3), defined by $[E]_T$ (total enzyme concentration) and $[I]_T$ (total inhibitor concentration), was used to determine K_i^{app} :

$$\frac{v_i}{v_0} = 1 - \frac{[E]_T + [I]_T + K_i^{\text{app}} - \sqrt{([E]_T + [I]_T + K_i^{\text{app}})^2 - 4[E]_T[I]_T}}{2[E]_T} \quad (3)$$

The inhibition constant K_i^* is extracted from K_i^{app} using the following equation (4):

$$K_i^* = K_i^{app} / (1 + \frac{[S]}{K_M}) \quad (4)$$

For two-step slow-binding inhibition, kinetic parameters (k_5 , k_6 and K_i) were calculated from curve fitting of experimental k_{obs} values to inhibitor concentrations based on equations (5 and 6).

$$k_{obs} = k_6 + \frac{k_5[I]}{K_i^{app} + [I]} = k_6 + \frac{k_5[I]}{K_i(1 + [S]/K_M) + [I]} \quad (5)$$

$$K_i = K_i^* (1 + k_5/k_6) \quad (6)$$

The enzymatic assays were done by Dr. Jinshi Zhao and the description is adapted from the published manuscript¹²⁶.

5.6.4 Minimum Inhibitory Concentration (MIC) Measurements

The MIC assay protocol was adapted for 96-well plates from methods described in National Committee for Clinical Laboratory Standards (NCCLS)¹²⁹. Bacteria were grown in the Mueller–Hinton medium with 5% DMSO at 37 °C in the presence of varying concentrations of inhibitors. To obtain more accurate readings of the MICs, three series of two-fold serial dilutions of inhibitors were used. The starting concentrations of the three series are different by factors of 1.33 and 1.67, respectively. MICs were reported as the lowest compound concentration that inhibited bacterial growth.

The MIC measurements were done by Dr. Jinshi Zhao and the description is adapted from our published manuscript¹²⁶.

Chapter 6. Conclusions

Structural biochemistry has evolved exponentially over the years, with almost 150,000 structures available in the Protein Data Bank and growing every day. The information obtained from these structures has been used to address important biological needs, including the advancement of therapeutics through structure-aided design of novel compounds.

However, there are certain roadblocks that can hinder the development of highly selective (non-toxic) and bioavailable inhibitors. Our current vision is often limited by the static and reductionist picture that is available to us with current rational drug design techniques, such as lack of information on dynamics or protein-protein interaction networks. These challenges arise due to the difficulty of translating protein or ligand dynamics information to medicinal chemistry and the complexity of selectively and potentially targeting protein-protein interaction networks due to our still limited understanding of the behavior of protein-protein interfaces. My thesis work illustrates through two very different examples, that information that may not be visible in crystal structures can be useful in providing additional information for designing novel therapeutics.

In the first example of inhibitor-induced dimerization, we illustrate that receptor dimerization that can block protein-protein interfaces may be useful as a general

principle to design inhibitors that target “intractable” large, shallow and dynamic protein interfaces. It is one of the few examples of successful inhibitor-induced PPI stabilization. One of the ways in which this can be incorporated in *ab initio* drug discovery campaigns is by targeting known protein-protein interaction domains. For example, researchers utilized the knowledge that the fungal natural product fusicoccin stabilizes interaction between a plant ATPase with proteins containing the 14-3-3 protein-protein interaction domain to design a screen aimed at complex stabilization. They identified a pyrrolidone compound, which they then optimized and validated by crystallography. This compound was significantly more potent than its parent compound and shows that PPI stabilizers can be identified with screens targeting a specific known interaction and optimized with conventional chemical optimization techniques.¹³⁰⁻¹³¹ It should be noted that in the case of Rev1-CTD dimerization, JHRE-06 stabilized a conformation that is not found in nature, so PPI stabilizers may be used even in cases where the PPI is not found in physiological conditions, as such a stabilization would almost certainly be disruptive to target function. It is conceivable that new dynamics measurements may capture the low population states of dimerized receptors and enable rational prediction of the feasibility of inhibitor-induced receptor dimerization in such cases.

Another way to screen for PPI stabilizers could be by including products with naturally derived or symmetric scaffolds in chemical libraries. It is encouraging that natural product libraries are growing and emerging. Despite this development, since most libraries contain conventional “drug-like chemicals,” *in silico* screening may also be used in docking experiments and has been shown to be a successful strategy in at least one instance.⁵⁹

A target that we are interested in is Rev7, the accessory subunit of POL ζ . Rev7 is interesting because it is implicated in double-stranded break repair, not just through TLS via its interaction with Rev3 and Rev1, but also by non-homologous end-joining (NHEJ) via its interaction with SHLD3 (also known as RINN1) of the shieldin complex.¹³² Both pathways can get upregulated to promote resistance to chemotherapeutic agents.^{133,79} Additionally, Rev7 is involved in spindle assembly during mitosis via its interactions with p31^{comet} and Mad2, and all three proteins have been shown to be important for cell cycle progression, as well as been implicated in tumorigenesis and resistance to anti-mitotic cancer drugs.¹³⁴⁻¹³⁶ Importantly, Rev7 function in these three pathways (TLS, NHEJ and mitotic spindle assembly) via the crucial HORMA (Hop1, Rev7, Mad2) domain, a known protein-protein interaction domain also found in p31^{comet} and Mad2.¹³⁷ The HORMA domain is a structurally conserved domain that is known to dimerize. It is composed of a “core domain” which is involved in dimerization, and a C-terminal

“safety belt” domain, which can have an open or closed configuration. In the open state, the safety belt folds into two β -strands that lie over one side of the core β -sheet. In the closed state, the safety belt engulfs the core domain. This allows a peptide from a binding partner to interact with the HORMA domain core; and is completely wrapped around by the safety belt.¹³⁸⁻¹³⁹ HORMA domain dimerization is required for conformational switching between open and closed states, and is essential for the proper functioning of HORMA proteins.¹⁴⁰⁻¹⁴² There is strong evidence to suggest that two copies of Rev7 bind to one unit of Rev3 which tuck it underneath the seatbelt region, and that Rev7 dimerization is required for proper TLS.^{141,143} Rev7 likely binds to SHLD3 in a manner similar to its interaction with Rev3. Mutation of a conserved residue in the Rev7 seatbelt region abrogates SHLD3-Rev7 binding, and SHLD3 has two N-terminal Rev3-like RBM motifs and predicted structural folds.¹⁴² Since conformational switching between open and closed states is likely required for the interaction between Rev7 and Rev3 (TLS) and Rev7 and SHLD3 (NHEJ), the idea of an inhibitor that locks Rev7 in a closed conformation is an attractive one. Additionally, Rev7, Mad2 and p31^{comet} interact with each other during mitotic spindle assembly with their HORMA domains, and a stabilized Rev7 dimer would prevent such an interaction from occurring. To screen for a compound that could stabilize a Rev7 dimer, an assay similar to that used by Rose and colleagues¹³⁰ to find a PPI stabilizer could be used: monitoring the binding of green

fluorescent protein (GFP) fused protein A with-immobilized glutathione S-transferase (GST) tagged protein B against a large compound library. Since it is known that Rev7 and SHLD3 rapidly accumulate at sites of DNA damage, a functional screen to identify a compound that blocks Rev7 and SHLD3 interaction could be the assessment of SHLD3 recruitment to sites of induced DSBs in the presence of a candidate compound. DSB recruitment assays are well developed and one was recently used to characterize Rev7-mediated recruitment of SHLD2 (another component of the shieldin complex) to DSBs.¹⁴⁴ The likelihood of an identified compound being a PPI stabilizer could be enriched by employing one of the available naturally-derived product libraries, such as Reaxys or Chinese Natural Product Database.¹⁴⁵

In the second-example of the delineation of a dynamically-accessible inhibitor envelope, we demonstrate one of the first examples of successful incorporation of ligand dynamics information in iterative structure-based drug optimization. This strategy can be used to aid in rapid lead compound optimization, particularly with peptide or peptidomimetic inhibitors. Examples of where this strategy can be particularly useful is with peptides or peptidomimetics that disrupt PPI. A drawback of these inhibitors is their low selectivity for their targets unless they are expanded in size with linkers, in which case they exhibit poor solubility and bioavailability. Additionally, current peptide inhibitors exhibit low proteolytic stability, with rapid targeting for cleavage by

endogenous proteases. Successful optimization with the substitution of appropriate functional groups to side chains and backbone has the potential of addressing all those issues: improved selectivity, stability and bioavailability.¹⁴⁶ An example of inhibitors that could be improved with this strategy are peptide inhibitors of the caspase-9/XIAP complex mentioned previously. Many inhibitors are non-specific and have been reported to have toxic side-effects.⁵⁰⁻⁵¹ Another example is the peptide inhibitor of HIV envelope protein gp41 (enfuvirtide), which suffers from rapid clearance from renal cells and low bioavailability.¹⁴⁷ Improvement of side chain functional groups with ligand dynamics as illustrated by our example could be used to enhance the potency of this drug. Additionally, the part of gp41 being targeted by enfuvirtide is only exposed transiently, and a highly selective and tight-binding inhibitor would have the advantage of being able to potentially stabilize the “vulnerable” conformation of the target.

In summary, with today's growing and urgent needs for the development of novel therapeutics, these two examples break new ground in illustrating how to innovate the strategy for structure-guided drug design, which may find further applications in other bio-medically relevant systems.

References

1. Mellor J, Fulton SM, Dobson MJ, Wilson W, Kingsman SM, Kingsman AJ. A retrovirus-like strategy for expression of a fusion protein encoded by yeast transposon Ty1. *Nature*. 1985 January 17;313(5999):243-6.
2. Toh H, Ono M, Saigo K, Miyata T. Retroviral protease-like sequence in the yeast transposon Ty 1. *Nature*. 1985 June 20; 315: 691–691
3. Miller M, Jaskólski M, Rao JK, Leis J, Wlodawer A Crystal structure of a retroviral protease proves relationship to aspartic protease family. *Nature*. 1989 Feb 9;337: 576–579 23.
4. Navia MA, Fitzgerald PMD, McKeever BM, Leu C-T, Heimbach JC, Herber WK, Sigal IS, Darke PL, Springer JP. Three-dimensional structure of aspartyl protease from human immunodeficiency virus HIV-1. *Nature*. 1989 Feb 16; 337: 615–620 24.
5. Blundell T, Pearl L. A second front against AIDS. *Nature*. 1989 Feb 16;337: 596–597 25.
6. Lapatto R, Blundell T, Hemmings A, Overington J, Wilderspin A, Wood S, Merson JR, Whittle PJ, Danley DE, Geoghegan KF (1989) X-ray analysis of HIV-1 proteinase at 2.7 Å resolution confirms structural homology among retroviral enzymes. *Nature*. 1989 Nov 16;342: 299–302
7. Freed EO. HIV-1 assembly, release and maturation. *Nat Rev Microbiol*. 2015 August 01;13(8):484-96.
8. Altschul SF, Madden TL, Schäffer AA, Zhang J, Zhang Z, Miller W, Lipman DJ (1997) Gapped BLAST and PSI-BLAST: a new generation of protein database search programs. *Nucleic Acids Res*. 1997 Sep 1;25: 3389–3402
9. Terstappen GC, Schlupen C, Raggiaschi R, Gaviraghi G. Target deconvolution strategies in drug discovery. *Nat Rev Drug Discov*. 2007 November 01;6(11):891-903.
10. Dias MH, Kitano ES, Zelanis A, Iwai LK. Proteomics and drug discovery in cancer. *Drug Discov Today*. 2016 February 01;21(2):264-77

11. Fields S, Song O. A novel genetic system to detect protein- protein interactions. *Nature*. 1989 Jul 20; 340, 245-246.
12. Krogan NJ, Cagney G, Yu H, Zhong G, Guo X, Ignatchenko A, et al. Global landscape of protein complexes in the yeast *Saccharomyces cerevisiae*. *Nature*. 2006 March 30;440(7084):637-43.
13. Shim JS, Lee J, Park HJ, Park SJ, Kwon HJ. A new curcumin derivative, HBC, interferes with the cell cycle progression of colon cancer cells via antagonization of the Ca²⁺/calmodulin function. *Chem Biol*. 2004 October 01;11(10):1455-63.
14. Athanasios A, Charalampos V, Vasileios T, Ashraf GM. Protein-protein interaction (PPI) network: Recent advances in drug discovery. *Curr Drug Metab*. 2017 Jan;18(1):5-10.
15. Berman HM, Westbrook J, Feng Z, Gilliland G, Bhat TN, Weissig H, Shindyalov IN, Bourne PE. The Protein Data Bank. *Nucleic Acids Research*. 2000;28: 235-242.
16. Dorsey B, Levin RB, McDaniel SL, Vacca JP, Guare, JP, Darke PL, Zugay JA, Emmini EA, and Schleif WA. L-735,524: the design of a potent and orally bioavailable HIV protease inhibitor. *J. Med. Chem*. 1994 Oct 14;37, 3443–3451.
17. Sledz P, and Caflisch A. Protein structure-based drug design: from docking to molecular dynamics. *Curr. Opin. Struct. Biol*. 2017 Nov 14;48, 93–102.
18. Marchand JR, Lolli G, Caflisch A. Derivatives of 3-Amino-2-methylpyridine as BAZ2B Bromodomain Ligands: In Silico Discovery and in Crystallo Validation. *J Med Chem*. 2016 November 10;59(21):9919-27
19. Malhotra S, Thomas SE, Ochoa MB, Blundell TL. Structure-guided, target-based drug discovery - exploiting genome information from HIV to mycobacterial infections. *Popstepy Biochem*. 2016;62(3):262-272
20. Trabuco G, Villa E, Mitra K, Frank J, and Schulten K. Flexible fitting of atomic structures into electron microscopy maps using molecular dynamics. *Structure*. 2008;16, 673–683.
21. Jukic M, Konc J, Gobec S, and Janezic, D. Identification of conserved water sites in protein structures for drug design. *J. Chem. Inf. Model*. 2017;57, 3094–3103.

22. Scapin G, Potter CS, Carragher B. Cryo-EM for Small Molecules Discovery, Design, Understanding, and Application. *Cell Chem Biol*. 2018 November 15;25(11):1318-25.
23. Tordai H, Leveles I, Hegedus T. Molecular dynamics of the cryo-EM CFTR structure. *Biochem Biophys Res Commun*. 2017 September 30;491(4):986-93
24. Jhoti H, Cleasby A, Verdonk M, Williams G. Fragment-based screening using X-ray crystallography and NMR spectroscopy. *Curr Opin Chem Biol*. 2007 October 01;11(5):485-93
25. Agrawal P. NMR Spectroscopy in Drug Discovery and Development. *Mater Methods*. 2013;4:599
26. Szymanski P, Markowicz M, Mikiciuk-Olasik E. Adaptation of high-throughput screening in drug discovery-toxicological screening tests. *Int J Mol Sci*. 2012;13(1):427-52
27. Devor DC, Singh AK, Frizzell RA, et al. Modulation of Cl⁻ secretion by benzimidazolones. I. Direct activation of a Ca(2⁺)-dependent K⁺ channel. *Am J Physiol Lung Cell Mol Physiol*. 1996;271:L775–L784
28. Gossert AD, Jahnke W. NMR in drug discovery: A practical guide to identification and validation of ligands interacting with biological macromolecules. *Prog Nucl Magn Reson Spectrosc*. 2016 November 01;97:82-125
29. Zhou H, Aguilar A, Chen J, Bai L, Liu L, Meagher JL, et al. Structure-based design of potent Bcl-2/Bcl-xL inhibitors with strong in vivo antitumor activity. *J Med Chem*. 2012 July 12;55(13):6149-61
30. Park CM, Bruncko M, Adickes J, Bauch J, Ding H, Kunzer A, et al. Discovery of an orally bioavailable small molecule inhibitor of prosurvival B-cell lymphoma 2 proteins. *J Med Chem*. 2008 November 13;51(21):6902-15
31. Wylie AA, Schoepfer J, Jahnke W, Cowan-Jacob SW, Loo A, Furet P, et al. The allosteric inhibitor ABL001 enables dual targeting of BCR-ABL1. *Nature*. 2017 March 30;543(7647):733-7

32. Sugiki T, Furuita K, Fujiwara T, Kojima C. Current NMR Techniques for Structure-Based Drug Discovery. *Molecules*. 2018 January 12;23(1):10.3390/molecules23010148
33. Hollenstein K, Dawson RJ, Locher KP. Structure and mechanism of ABC transporter proteins. *Curr Opin Struct Biol*. 2007 August 01;17(4):412-8
34. Szewczyk P, Tao H, McGrath AP, Villaluz M, Rees SD, Lee SC, et al. Snapshots of ligand entry, malleable binding and induced helical movement in P-glycoprotein. *Acta Crystallogr D Biol Crystallogr*. 2015 March 01;71(Pt 3):732-41
35. Teague SJ. Implications of protein flexibility for drug discovery. *Nat Rev Drug Discov*. 2003 July 01;2(7):527-41
36. Cheng JW, Lepre CA, Moore JM. ¹⁵N NMR Relaxation Studies of the FK506 Binding Protein: Dynamic Effects of Ligand Binding and Implications for Calcineurin Recognition. *Biochemistry*. 1994 April;33(14):4093-4100
37. Eisenmesser EZ, Bosco DA, Akke M, Kern D. Enzyme dynamics during catalysis. *Science*. 2002 February 22;295(5559):1520-3
38. Namanja AT, Peng T, Zintsmaster JS, Elson AC, Shakour MG, Peng JW. Substrate recognition reduces side-chain flexibility for conserved hydrophobic residues in human Pin1. *Structure*. 2007 March 01;15(3):313-27
39. Peng JW. Communication breakdown: protein dynamics and drug design. *Structure*. 2009 March 11;17(3):319-20
40. Mauldin RV, Carroll MJ, Lee AL. Dynamic dysfunction in dihydrofolate reductase results from antifolate drug binding: modulation of dynamics within a structural state. *Structure*. 2009 March 11;17(3):386-94
41. Zintsmaster JS, Wilson BD, Peng JW. Dynamics of ligand binding from ¹³C NMR relaxation dispersion at natural abundance. *J Am Chem Soc*. 2008 October 29;130(43):14060-1
42. Ofra Y, Rost B. Protein-protein interaction hotspots carved into sequences. *PLoS Comput Biol*. 2007 July 01;3(7):e119

43. Scott DE, Bayly AR, Abell C, Skidmore J. Small molecules, big targets: drug discovery faces the protein-protein interaction challenge. *Nat Rev Drug Discov.* 2016 August 01;15(8):533-50
44. Moreira IS, Koukos PI, Melo R, Almeida JG, Preto AJ, Schaarschmidt J, et al. SpotOn: High Accuracy Identification of Protein-Protein Interface Hot-Spots. *Sci Rep.* 2017 August 14;7(1):2
45. Jubb H, Blundell TL, Ascher DB. Flexibility and small pockets at protein-protein interfaces: New insights into druggability. *Prog Biophys Mol Biol.* 2015 October 01;119(1):2-9
46. Braisted AC, Oslob JD, Delano WL, Hyde J, McDowell RS, Waal N, et al. Discovery of a potent small molecule IL-2 inhibitor through fragment assembly. *J Am Chem Soc.* 2003 April 02;125(13):3714-5
47. Arkin MR, Randal M, DeLano WL, Hyde J, Luong TN, Oslob JD, et al. Binding of small molecules to an adaptive protein-protein interface. *Proc Natl Acad Sci U S A.* 2003 February 18;100(4):1603-8
48. Blundell TL, Sibanda BL, Montalvao RW, Brewerton S, Chelliah V, Worth CL, et al. Structural biology and bioinformatics in drug design: opportunities and challenges for target identification and lead discovery. *Philos Trans R Soc Lond B Biol Sci.* 2006 March 29;361(1467):413-23
49. Oost TK, Sun C, Armstrong RC, Al-Assaad AS, Betz SF, Deckwerth TL, et al. Discovery of potent antagonists of the antiapoptotic protein XIAP for the treatment of cancer. *J Med Chem.* 2004 August 26;47(18):4417-26
50. Huang JW, Zhang Z, Wu B, Cellitti JF, Zhang X, Dahl R, et al. Fragment-based design of small molecule X-linked inhibitor of apoptosis protein inhibitors. *J Med Chem.* 2008 November 27;51(22):7111-8
51. Wu H, Tschopp J, Lin SC. Smac mimetics and TNFalpha: a dangerous liaison? *Cell.* 2007 November 16;131(4):655-8
52. Keskin O, Gursoy A, Ma B, Nussinov R. Principles of protein-protein interactions: what are the preferred ways for proteins to interact? *Chem Rev.* 2008 April 01;108(4):1225-44

53. Andrei SA, Sijbesma E, Hann M, Davis J, O'Mahony G, Perry MWD, et al. Stabilization of protein-protein interactions in drug discovery. *Expert Opin Drug Discov.* 2017 September 01;12(9):925-40
54. Kobayashi M, Tanaka J, Katori T, Kitagawa I. Marine natural products. XXIII. Three new cytotoxic dimeric macrolides, swinholides B and C and isoswinholide A, congeners of swinholide A, from the Okinawan marine sponge *Theonella swinhoei*. *Chem Pharm Bull (Tokyo)*. 1990;38:2960–2966
55. Bubb MR, Spector I, Bershadsky AD, Korn ED. Swinholide A is a microfilament disrupting marine toxin that stabilizes actin dimers and severs actin filaments. *J Biol Chem.* 1995;270:3463–3466
56. Klenchin VA, King R, Tanaka J, Marriott G, Rayment I. Structural Basis of Swinholide A Binding to Actin. *Chem Biol.* 2005;12:287–291.
57. Graves B, Thompson T, Xia M, Janson C, Lukacs C, Deo D, et al. Activation of the p53 pathway by small-molecule-induced MDM2 and MDMX dimerization. *Proc Natl Acad Sci U S A.* 2012 July 17;109(29):11788-93
58. Classen S, Olland S, Berger JM. Structure of the topoisomerase II ATPase region and its mechanism of inhibition by the chemotherapeutic agent ICRF-187. *Proc Natl Acad Sci.* 2003;100:10629–10634
59. Nemetski SM, Cardozo TJ, Bosch G, Weltzer R, O'Malley K, Ejigiri I, et al. Inhibition by stabilization: targeting the *Plasmodium falciparum* aldolase-TRAP complex. *Malar J.* 2015 August 20;14:9
60. Oecking C, Piotrowski M, Hagemeyer J, Hagemann K. Topology and target interaction of the fusicoccin-binding 14-3-3 homologs of *Commelina communis*. *Plant J.* 1997;12:441–453
61. Bray F, Ferlay J, Soerjomataram I, Siegel RL, Torre LA, Jemal A. Global cancer statistics 2018: GLOBOCAN estimates of incidence and mortality worldwide for 36 cancers in 185 countries. *CA Cancer J Clin.* 2018 November 01;68(6):394-424.
62. Manova V, Gruszka D. DNA damage and repair in plants - from models to crops. *Front Plant Sci.* 2015 October 23;6:885.

63. Nonnekens J, Hoeijmakers JH. After surviving cancer, what about late life effects of the cure? *EMBO Mol Med*. 2017 January 01;9(1):4-6.
64. Postel-Vinay S, Vanhecke E, Olaussen KA, Lord CJ, Ashworth A, Soria JC. The potential of exploiting DNA-repair defects for optimizing lung cancer treatment. *Nat Rev Clin Oncol*. 2012 February 14;9(3):144-55.
65. Ghosal G, Chen J. DNA damage tolerance: a double-edged sword guarding the genome. *Transl Cancer Res*. 2013;2(3):107-29.
66. Pan ST, Li ZL, He ZX, Qiu JX, Zhou SF. Molecular mechanisms for tumour resistance to chemotherapy. *Clin Exp Pharmacol Physiol*. 2016 August 01;43(8):723-37.
67. Zahreddine H, Borden KL. Mechanisms and insights into drug resistance in cancer. *Front Pharmacol*. 2013 March 14;4:28.
68. Ohmori H, Friedberg EC, Fuchs RP, Goodman MF, Hanaoka F, Hinkle D, Kunkel TA, Lawrence CW, Livneh Z, Nohmi T, Prakash L, Prakash S, Todo T, Walker GC, Wang Z, Woodgate R. The Y-family of DNA polymerases. *Molecular Cell*. 2001 July;8(1):7-8.
69. Yang K, Weinacht CP, Zhuang Z. (2013). Regulatory role of ubiquitin in eukaryotic DNA translesion synthesis. *Biochemistry* 52:3217–28.
70. Makarova AV, Burgers PM. (2015). Eukaryotic DNA polymerase ζ . *DNA Repair* 29:47–55.
71. Boiteux S, Jinks-Robertson S. (2013). DNA repair mechanisms and the bypass of DNA damage in *Saccharomyces cerevisiae*. *Genetics* 193:1025–64.
72. Guo C, Kosarek-Stancel JN, Tang TS, Friedberg EC.(2009). Y-family DNA polymerases in mammalian cells. *Cell Mol Life Sci* 66:2363–81.
73. Sale JE, Lehmann AR, Woodgate R. Y-family DNA polymerases and their role in tolerance of cellular DNA damage. *Nat Rev Mol Cell Biol*. 2012 February 23;13(3):141-52.
74. Vaisman A, Woodgate R. Translesion DNA polymerases in eukaryotes: what makes them tick? *Crit Rev Biochem Mol Biol*. 2017 June 01;52(3):274-303

75. Huang Y, Huang YH, Liang Y, Qiu S, Li W, Zheng Y, Han Z, Yuan R. Elevated expression of REV1 is a predictor of unfavorable prognosis in patients with prostate cancer. *International Journal of Clinical and Experimental Medicine*. 2018;11(8):8412-20.
76. He X, Ye F, Zhang J, Cheng Q, Shen J, Chen H. REV1 genetic variants associated with the risk of cervical carcinoma. *Eur J Epidemiol*. 2008;23(6):403-9.
77. Lin X, Okuda T, Trang J, Howell SB. Human REV1 modulates the cytotoxicity and mutagenicity of cisplatin in human ovarian carcinoma cells. *Mol Pharmacol*. 2006 May 01;69(5):1748-54.
78. Doles J, Oliver TG, Cameron ER, Hsu G, Jacks T, Walker GC, et al. Suppression of Rev3, the catalytic subunit of Pol{zeta}, sensitizes drug-resistant lung tumors to chemotherapy. *Proc Natl Acad Sci U S A*. 2010 November 30;107(48):20786-91.
79. Xie K, Doles J, Hemann MT, Walker GC. Error-prone translesion synthesis mediates acquired chemoresistance. *Proc Natl Acad Sci U S A*. 2010 November 30;107(48):20792-7.
80. Niimi K, Murakumo Y, Watanabe N, Kato T, Mii S, Enomoto A, et al. Suppression of REV7 enhances cisplatin sensitivity in ovarian clear cell carcinoma cells. *Cancer Sci*. 2014 May 01;105(5):545-52.
81. Zafar MK, Eoff RL. Translesion DNA Synthesis in Cancer: Molecular Mechanisms and Therapeutic Opportunities. *Chem Res Toxicol*. 2017 November 20;30(11):1942-55.
82. Kikuchi S, Hara K, Shimizu T, Sato M, Hashimoto H. Structural basis of recruitment of DNA polymerase zeta by interaction between REV1 and REV7 proteins. *J Biol Chem*. 2012 September 28;287(40):33847-52.
83. Yang W. An overview of Y-Family DNA polymerases and a case study of human DNA polymerase eta. *Biochemistry*. 2014 May 06;53(17):2793-803.
84. Wojtaszek J, Lee CJ, D'Souza S, Minesinger B, Kim H, D'Andrea AD, et al. Structural basis of Rev1-mediated assembly of a quaternary vertebrate translesion polymerase complex consisting of Rev1, heterodimeric polymerase (Pol) zeta, and Pol kappa. *J Biol Chem*. 2012 September 28;287(40):33836-46.

85. Wojtaszek J, Liu J, D'Souza S, Wang S, Xue Y, Walker GC, et al. Multifaceted recognition of vertebrate Rev1 by translesion polymerases zeta and kappa. *J Biol Chem*. 2012 July 27;287(31):26400-8.
86. Zinzalla G, Thurston DE. Targeting protein-protein interactions for therapeutic intervention: a challenge for the future. *Future Med Chem*. 2009 April 01;1(1):65-93
87. Kabsch W. Xds. *Acta Crystallogr D Biol Crystallogr*. 2010 February 01;66(Pt 2):125-32.
88. Emsley P, Cowtan K. Coot: model-building tools for molecular graphics. *Acta Crystallogr D Biol Crystallogr*. 2004 December 01;60(Pt 12 Pt 1):2126-32.
89. Adams PD, Grosse-Kunstleve RW, Hung LW, Ioerger TR, McCoy AJ, Moriarty NW, et al. PHENIX: building new software for automated crystallographic structure determination. *Acta Crystallogr D Biol Crystallogr*. 2002 November 01;58(Pt 11):1948-54.
90. Lustberg MB. Management of neutropenia in cancer patients; Clinical advances in hematology & oncology. 2012 Dec;10(12):825-6.
91. Thom KA, Kleinberg M, Roghmann MC. Infection prevention in the cancer center. *Clin Infect Dis*. 2013 August 01;57(4):579-85
92. Mehrad B, Clark NM, Zhanel GG, Lynch JP. Antimicrobial resistance in hospital-acquired gram-negative bacterial infections. *Chest*. 2015 May 01;147(5):1413-21.
93. Cornejo-Juarez P, Vilar-Compte D, Garcia-Horton A, Lopez-Velazquez M, Namendys-Silva S, Volkow-Fernandez P. Hospital-acquired infections at an oncological intensive care cancer unit: differences between solid and hematological cancer patients. *BMC Infect Dis*. 2016 June 10;16:1.
94. Perez F, Adachi J, Bonomo RA. Antibiotic-resistant gram-negative bacterial infections in patients with cancer. *Clin Infect Dis*. 2014;59 Suppl 5(Suppl 5):S335-9.
95. Snitkin ES, Zelazny AM, Thomas PJ, et al. Tracking a hospital outbreak of carbapenem-resistant *Klebsiella pneumoniae* with whole-genome sequencing. *Sci Transl Med*. 2012;4 148ra16

96. Satlin MJ, Calfee DP, Chen L, et al. Emergence of carbapenem-resistant Enterobacteriaceae as causes of bloodstream infections in patients with hematologic malignancies. *Leuk Lymphoma*. 2013;54:799–806
97. Freifeld A, Sepkowitz K. The conundrum of fluoroquinolone prophylaxis. *Nat Clin Pract Oncol*. 2006;3:524–5
98. Johnson JR, Johnston B, Clabots C, Kuskowski MA, Castanheira M. *Escherichia coli* sequence type ST131 as the major cause of serious multidrug-resistant *E. coli* infections in the United States. *Clin Infect Dis*. 2010;51:286–94
99. Cattaneo C, Antoniazzi F, Casari S, et al. *Pseudomonas aeruginosa* bloodstream infections among hematological patients: an old or new question? *Ann Hematol*. 2012;91:1299–304
100. Fukuta Y, Muder RR, Agha ME, et al. Risk factors for acquisition of multidrug-resistant *Acinetobacter baumannii* among cancer patients. *Am J Infect Control*. 2013;41:1249–52
101. Kim SB, Min YH, Cheong JW, et al. Incidence and risk factors for carbapenem- and multidrug-resistant *Acinetobacter baumannii* bacteremia in hematopoietic stem cell transplantation recipients. *Scand J Infect Dis*. 2014;46:81–8
102. Raetz CR, Guan Z, Ingram BO, Six DA, Song F, Wang X, et al. Discovery of new biosynthetic pathways: the lipid A story. *J Lipid Res*. 2009 April 01;50 Suppl:103.
103. Raetz CR, Reynolds CM, Trent MS, Bishop RE. Lipid A modification systems in gram-negative bacteria. *Annu Rev Biochem*. 2007;76:295-329.
104. Raetz CR, Whitfield C. Lipopolysaccharide endotoxins. *Annu Rev Biochem*. 2002;71:635-700.
105. Jackman J. E., C. R. H. Raetz, and C. A. Fierke. 1999. UDP-3-O-(R-3-hydroxymyristoyl)-N-acetylglucosamine deacetylase of *Escherichia coli* is a zinc metalloenzyme. *Biochemistry*. 38 1902–1911

106. Whittington DA, Rusche KM, Shin H, Fierke CA, Christianson DW. Crystal structure of LpxC, a zinc-dependent deacetylase essential for endotoxin biosynthesis. *Proc Natl Acad Sci U S A*. 2003 July 08;100(14):8146-50.
107. Coggins BE, Li X, McClerren AL, Hindsgaul O, Raetz CR, Zhou P. Structure of the LpxC deacetylase with a bound substrate-analog inhibitor. *Nat Struct Biol*. 2003 August 01;10(8):645-51.
108. Coggins BE, McClerren AL, Jiang L, Li X, Rudolph J, Hindsgaul O, et al. Refined solution structure of the LpxC-TU-514 complex and pKa analysis of an active site histidine: insights into the mechanism and inhibitor design. *Biochemistry*. 2005 February 01;44(4):1114-26.
109. Lee CJ, Liang X, Gopalaswamy R, Najeeb J, Ark ED, Toone EJ, et al. Structural basis of the promiscuous inhibitor susceptibility of *Escherichia coli* LpxC. *ACS Chem Biol*. 2014 January 17;9(1):237-46.
110. Barb AW, Jiang L, Raetz CR, Zhou P. Structure of the deacetylase LpxC bound to the antibiotic CHIR-090: Time-dependent inhibition and specificity in ligand binding. *Proc Natl Acad Sci U S A*. 2007 November 20;104(47):18433-8.
111. McClerren AL, Endsley S, Bowman JL, Andersen NH, Guan Z, Rudolph J, et al. A slow, tight-binding inhibitor of the zinc-dependent deacetylase LpxC of lipid A biosynthesis with antibiotic activity comparable to ciprofloxacin. *Biochemistry*. 2005 December 20;44(50):16574-83.
112. Liang X, Lee CJ, Chen X, Chung HS, Zeng D, Raetz CR, et al. Syntheses, structures and antibiotic activities of LpxC inhibitors based on the diacetylene scaffold. *Bioorg Med Chem*. 2011 January 15;19(2):852-60.
113. Lee CJ, Liang X, Chen X, Zeng D, Joo SH, Chung HS, et al. Species-specific and inhibitor-dependent conformations of LpxC: implications for antibiotic design. *Chem Biol*. 2011 January 28;18(1):38-47.
114. Lovell SC, Word JM, Richardson JS, Richardson DC. The penultimate rotamer library. *Proteins*. 2000 August 15;40(3):389-408.
115. Hennig M, Bermel W, Spencer A, Dobson CM, Smith LJ, Schwalbe H. Side-chain conformations in an unfolded protein: chi1 distributions in denatured

- hen lysozyme determined by heteronuclear ^{13}C , ^{15}N NMR spectroscopy. *J Mol Biol.* 1999 May 14;288(4):705-23.
116. Perez C, Lohr F, Ruterjans H, Schmidt JM. Self-consistent Karplus parametrization of 3J couplings depending on the polypeptide side-chain torsion χ_1 . *J Am Chem Soc.* 2001 July 25;123(29):7081-93.
 117. Hansen DF, Neudecker P, Kay LE. Determination of isoleucine side-chain conformations in ground and excited states of proteins from chemical shifts. *J Am Chem Soc.* 2010 June 09;132(22):7589-91.
 118. ZhongBo F, Weiyong K, Huaimin W, Jianbiao P, Feng S, Yueyan Y, Joginder B, Xinglong. A Scalable Synthesis of a Hydroxamic Acid LpxC Inhibitor. *Org. Process Res. Dev.* 2012 Jul 4;16(8):1436–1441.
 119. Mansoor UF, Vitharana D, Reddy PA, Daubaras DL, McNicholas P, Orth P, et al. Design and synthesis of potent Gram-negative specific LpxC inhibitors. *Bioorg Med Chem Lett.* 2011 February 15;21(4):1155-61.
 120. Otwinowski Z., Minor W. Processing of X-ray diffraction data collected in oscillation mode. *Methods Enzymol.* 1997; 276:307–326.
 121. McCoy A. J. et al. Phaser crystallographic software. *J. Appl. Crystallogr.* 2007; 40: 658–674.
 122. Grzesiek S., Vuister GW., Bax A. A simple and sensitive experiment for measurement of JCC couplings between backbone carbonyl and methyl carbons in isotopically enriched proteins. *J. Biomol. NMR.* 1993 July; 3 (4): 487–493
 123. Vuister G. W., Wang AC., Bax A. Measurement of three-bond nitrogen-carbon J couplings in proteins uniformly enriched in ^{15}N and ^{13}C . *J. Am. Chem. Soc.* 1993 June; 115 (12): 5334–5335.
 124. Delaglio F., Grzesiek S., Vuister GW., Zhu G., Pfeifer J., Bax A. NMR Pipe: a multidimensional spectral processing system based on UNIX pipes. *J. Biomol. NMR.* 1995 November; 6 (3): 277–293.
 125. Goddard TD., Kneller DG. Sparky 3. University of California. 2008.

126. Lee CJ, Liang X, Wu Q, Najeeb J, Zhao J, Gopalaswamy R, et al. Drug design from the cryptic inhibitor envelope. *Nat Commun.* 2016 February 25;7:10638.
127. Jackman JE., Raetz CRH., Fierke C. A. Site-directed mutagenesis of the bacterial metalloamidase UDP-(3-O-acyl)-N-acetylglucosamine deacetylase (LpxC). Identification of the zinc binding site. *Biochemistry.* 2001;40 (2):514–523.
128. Zhang R, Windsor WT. In vitro kinetic profiling of hepatitis C virus NS3 protease inhibitors by progress curve analysis. *Methods Mol Biol.* 2013;1030:59-79.
129. National Committee for Clinical Laboratory Standards. Approved Standard M7-A1: Methods for dilution antimicrobial susceptibility test for bacteria that grow aerobically. Clinical and Laboratory Standards Institute, Wayne, PA, USA. 1997.
130. Rose R, Erdmann S, Bovens S, Wolf A, Rose M, Hennig S, et al. Identification and structure of small-molecule stabilizers of 14-3-3 protein-protein interactions. *Angew Chem Int Ed Engl.* 2010 June 01;49(24):4129-32
131. Richter A, Rose R, Hedberg C, Waldmann H, Ottmann C. An optimised small-molecule stabiliser of the 14-3-3-PMA2 protein-protein interaction. *Chemistry.* 2012 May 21;18(21):6520-7
132. Ghezraoui H, Oliveira C, Becker JR, Bilham K, Moralli D, Anzilotti C, et al. 53BP1 cooperation with the REV7-shieldin complex underpins DNA structure-specific NHEJ. *Nature.* 2018 August 01;560(7716):122-7
133. Francica P, Rottenberg S. Mechanisms of PARP inhibitor resistance in cancer and insights into the DNA damage response. *Genome Med.* 2018 December 28;10(1):8
134. Bhat A, Wu Z, Maher VM, McCormick JJ, Xiao W. Rev7/Mad2B plays a critical role in the assembly of a functional mitotic spindle. *Cell Cycle.* 2015;14(24):3929-38
135. Habu T, Matsumoto T. p31(comet) inactivates the chemically induced Mad2-dependent spindle assembly checkpoint and leads to resistance to anti-mitotic drugs. *Springerplus.* 2013 October 25;2:562. eCollection 2013

136. Sotillo R, Hernando E, Diaz-Rodriguez E, Teruya-Feldstein J, Cordon-Cardo C, Lowe SW, et al. Mad2 overexpression promotes aneuploidy and tumorigenesis in mice. *Cancer Cell*. 2007 January 01;11(1):9-23
137. Rosenberg SC, Corbett KD. The multifaceted roles of the HORMA domain in cellular signaling. *J Cell Biol*. 2015 November 23;211(4):745-55
138. Aravind L, Koonin EV. The HORMA domain: A common structural denominator in mitotic checkpoints, chromosome synapsis and DNA repair. *Trends Biochem. Sci*. 1998;23:284–286. doi:10.1016/S0968-0004(98)01257-2
139. Muniyappa K, Kshirsagar R, Ghodke I. The HORMA domain: an evolutionarily conserved domain discovered in chromatin-associated proteins, has unanticipated diverse functions. *Gene*. 2014 July 25;545(2):194-7
140. West AMV, Komives EA, Corbett KD. Conformational dynamics of the Hop1 HORMA domain reveal a common mechanism with the spindle checkpoint protein Mad2. *Nucleic Acids Res*. 2018 January 09;46(1):279-92
141. Rizzo AA, Vassel FM, Chatterjee N, D'Souza S, Li Y, Hao B, et al. Rev7 dimerization is important for assembly and function of the Rev1/Polzeta translesion synthesis complex. *Proc Natl Acad Sci U S A*. 2018 August 28;115(35):E8200.
142. Mariani L, Chiroli E, Nezi L, Muller H, Piatti S, Musacchio A, et al. Role of the Mad2 dimerization interface in the spindle assembly checkpoint independent of kinetochores. *Curr Biol*. 2012 October 23;22(20):1900-8.
143. Tomida J, Takata K, Lange SS, Schibler AC, Yousefzadeh MJ, Bhetawal S, et al. REV7 is essential for DNA damage tolerance via two REV3L binding sites in mammalian DNA polymerase zeta. *Nucleic Acids Res*. 2015 January 01;43(2):1000-11
144. Findlay S, Heath J, Luo VM, Malina A, Morin T, Coulombe Y, et al. SHLD2/FAM35A co-operates with REV7 to coordinate DNA double-strand break repair pathway choice. *EMBO J*. 2018 September 14;37(18):10.15252/emboj.2018100158. Epub 2018 Aug 28

145. Gu J, Gui Y, Chen L, Yuan G, Lu HZ, Xu X. Use of natural products as chemical library for drug discovery and network pharmacology. PLoS One. 2013 April 25;8(4):e62839
146. Wojcik P, Berlicki L. Peptide-based inhibitors of protein-protein interactions. Bioorg Med Chem Lett. 2016 February 01;26(3):707-13
147. Yi HA, Fochtman BC, Rizzo RC, Jacobs A. Inhibition of HIV entry by targeting the envelope transmembrane subunit gp41. Current HIV Research. 2016;14(3):283-94

Biography

I attended Dawood Public School from nursery school till my Ordinary ('O') levels (1992 to 2006), and Karachi Grammar School for my Advanced ('A') levels (2006 to 2008). I completed my undergraduate degree (AB in Molecular Biology) from Princeton University in June 2012. I matriculated at the Duke University Department of Biochemistry in August 2012. I have been a graduate research assistant in the Pei Zhou laboratory since 2013. I was a speaker at the "Diffraction Methods" Gordon Research Seminar in 2016. A list of my publications is as follows:

1. Jessica L. Wojtaszek*, Nimrat Chatterjee*, Javaria Najeeb*, Azucena Ramos, Minhee Lee, Ke Bian, Yaohua Xue, Deyu Li, Michael T. Hemann, Jiyong Hong, Graham C. Walker, and Pei Zhou. Small molecule adjuvant disrupting Rev1-Pol ζ mediated mutagenic translesion synthesis improves chemotherapy. Manuscript submitted 2018.
2. Nadine Lemaître, Xiaofei Liang, Javaria Najeeb, Chul-jin Lee, Marie Titecat, Emmanuelle Leteurtre, Michel Simonet, Eric J. Toone, Pei Zhou, Florent Sebbane, Curative Treatment of Severe Gram-Negative Bacterial Infections by a New Class of Antibiotics Targeting LpxC, MBio 2017
3. Chul-jin Lee*, Xiaofei Liang*, Qinglin Wu*, Javaria Najeeb*, Jinshi Zhao, Ramesh Gopalaswamy, Marie Titecat, Florent Sebbane, Nadine Lemaître, Eric J. Toone, Pei Zhou, Drug design from the cryptic inhibitor envelope, Nat. Commun. 2016.
4. Chul-jin Lee, Xiaofei Liang, Ramesh Gopalaswamy, Javaria Najeeb, Eugene D. Ark, Eric J. Toone, Pei Zhou, Structural basis of the promiscuous inhibitor susceptibility of Escherichia coli LpxC, ACS Chem. Biol. 2014

5. Javaria Najeeb, Mechanistic Analysis of the Dsl1 Tethering Complex, AB Molecular Biology thesis, Princeton University, Princeton NJ 2012.